Tailoring Functional Protein Brushes into Precision Nanosystems

MASTER THESIS

submitted in partial fulfilment
of the requirements for the degree

- Master of Science Biomedical Chemistry -

by

Julius Gemen

born 25.05.1995 (Thuine/Emsland)

2713230

Mainz, March 2019

MAX-PLANCK-INSTITUT
FÜR POLYMERFORSCHUNG

JOHANNES GUTENBERG
UNIVERSITÄT MAINZ

JG|U

<u>Declaration of Originality</u>

I, Julius Gemen, enrolment number 2713230, hereby declare that the submitted thesis is my own unaided work. All direct or indirect sources used are acknowledged as references. This applies also to all texts, graphics and images included in the thesis.

<table>
<tr><td>_____</td><td></td><td>_____</td></tr>
<tr><td>- Place and Date -</td><td></td><td>- Signature -</td></tr>
</table>

This master thesis was conducted at the Max Planck Institute for Polymer Research from September 2018 till March 2019 under supervision of Prof Dr. Tanja Weil.

First referee: Prof. Dr. Tanja Weil

Second referee: Prof. Dr. Pol Besenius

Delivered: 01.03.2019

Deutsche Zusammenfassung

Proteine besitzen eine unerreichte, komplexe und perfekt definierte molekulare Architektur, die sie zu hochinteressanten Vorstufen präziser Nanosysteme macht. Indem Aminosäurereste des Polypeptidgrundgerüstes spezifisch chemisch verändert werden, können Wissenschaftler physikalische Strukturen und chemische Funktionen dieser Materialen entsprechend der jeweils gewünschten Anwendung modifizieren.

In dieser Arbeit wird die Synthese von Polymer-Protein-Hybridbürsten vorgestellt, die neben ihrem hochdefinierten Aufbau und modulierbaren Grundgerüst auch selbst eine katalytische Funktion besitzen. Um dies zu erreichen, wird das Metalloprotein Cytochrom *c* aus *Saccharomyces cerevisiae* in ein Polypeptid-Rückgrat umgewandelt, von dem aus thermoresponsive Polymere wachsen können. Es wird gezeigt, dass das resultierende Hybridmaterial, das durch die kontrollierte, radikalische Polymerisationsmethode AGET ATRP hergestellt wird, seine ursprüngliche katalytische Aktivität konserviert. Weiterhin wird gezeigt, dass die modifizierten Metalloproteine selbst auch ATRP katalysieren können, was sie zu einem weiteren Beispiel bereits beschriebener ATRPasen macht.

Insgesamt wird ein Ansatz zur Entwicklung neuartiger, intelligenter Biomaterialien, die unter Verwendung von systematisch entwickelten chemischen Modifikationen und von Polymeren hergestellt werden, vorgestellt.

Abstract

Proteins possess an unrivalled, complex, but molecularly defined nanoscale architecture, which makes them highly interesting as precursors to construct precision nanosystems. By performing specific chemical modifications of amino acid side residues on the monodisperse polypeptide scaffold, nanoscale engineers are provided with a platform to customize both physical structures and chemical functions according to a desired application. In this present work, we report the design of polymer-protein brushes that are, besides their highly-defined and tailorable scaffold, able to carry out catalytic function. To achieve this, the metalloprotein cytochrome *c* from *Saccharomyces cerevisiae* was converted into a polypeptide backbone where thermoresponsive polymers can be grafted from. First, by harnessing controlled/living radical polymerization by AGET ATRP, we demonstrate the precise design of the hybrid material, for which the catalytic activity of the protein is shown to be preserved. In addition, we show that the modified metalloprotein derivatives themselves are able to catalyze polymerizations *via* ATRP, which further expands the list of known ATRPases. Collectively, we present the use of systematically developed chemical modifications and polymers to integrate non-intrinsic functions as a concept towards developing a novel category of smart biomaterials.

Abbreviations

CytC	cytochrome *c*
cCytC	cationized CytC
PEG-cCytC	PEGylated cCytC
PEG-dcCytC-fluo	denaturated PEG-cCytC with fluorescent label
PEG-dcCytC-fluo-Br	PEG-dcCytC-fluo with ATRP initiators
PEG-CytC	PEGylated CytC
cCytC-Br	cCytC with ATRP initiators
PEG-cCytC-Br	PEG-cCytC with ATRP initiators
CytC-BiotinPEG	CytC with PEG-Biotin label

$\varnothing$, σ	average, standard deviation
#	amount
δ	chemical shift
λ_{ex}, λ_{em}, λ_{abs}	wavelength of excitation, emission, absorbance
3D	three-dimensional
AFM	atomic force microscopy
A(R)GET	activators (re-)generated by electron transfer
a.u.	arbitrary unit
ABTS	2,2'-azino-bis(3-ethylbenzothiazoline-6-sulphonic acid)
AscA, NaAsc	ascorbic acid, sodium ascorbate
ATP	adenosine triphosphate
ATRP	atom transfer radical polymerization
BiB	2-bromoisobutanoic acid
C, Cys	cysteine
CD	circular dichroism
(comp./incomp.) conv.	(complete/incomplete) conversion
D	diffusion coefficient
D$_2$O	deuterium oxide
(k)Da	(kilo)dalton
DLS	dynamic light scattering
(P)DMAA	(poly)dimethylacrylamide
DMF	dimethylformamide
DMSO	dimethyl sulfoxide
DNA	deoxyribonucleic acid
DOSY	diffusion-ordered spectroscopy
DSS	4,4-dimethyl-4-silapentane-1-sulfonic acid
EDA	ethylenediamine
EDC	1-ethyl-3-(3-dimethylaminopropyl)carbodiimide
EDTA	ethylenediaminetetraacetic acid
Fe	iron
eq.	equivalents

et al.	et alii
g, mg	gram, milligram
GPC	gel permeation chromatography
h, d	hour, day
H, His	histidine
Hb	hemoglobin
HRP	horseradish peroxidase
HSA	human serum albumin
LCST	lower critical solution temperature
M, mM	molar concentration, millimolar concentration
M, Met	methionine
MALDI-ToF	matrix assisted laser desorption/ionization time of flight
Me	metal
MI	maleimide
mL, µL	milliliter, microliter
M_n	number average molar mass
MQ	Milli-Q
m/z	mass-to-charge ratio
MS	mass spectrometry
MW(CO)	molecular weight (cutoff)
NHS	*N*-hydroxysuccinimide (ester)
(P)NIPAM	(poly)*N*-isopropylacrylamide
NMR	nuclear magnetic resonance
(P)OEG(M)A	(poly)oligo(ethylene glycol) methyl ether (meth)acrylate
PBS	phosphate-buffered saline
PDB ID	Protein Data Bank Identifier
PDI	polydispersity index
PEG$_{2000}$	polyethylene glycol with M_n 2000 g/mol
prot.	protein
R_0	hydrodynamic radius
RGT	reaction rate temperature
rt/r.t.	room temperature
SDS-PAGE	sodium dodecyl sulfate polyacrylamide gel electrophoresis
SSA	sodium 4-styrenesulfonate
T	temperature
t	time
TBA	tributylamine
TDA	tris(3,6-dioxaheptyl)amine
TEM	transmission electron microscopy
TPMA	tris(2-pyridylmethyl)amine
TPP	triphenyl phospine
UV-VIS	ultraviolet-visible

Table of Content

X

1 Introduction

1.1 Metalloproteins: how evolution harnessed metal's unique properties

1.1.1: Proteins: nature's working horses

Proteins are biological macromolecules constructed from a set of 20 different building blocks – the amino acids. Instead of randomly forming undefined and inconsistent 3D structures, noncovalent interaction of side residues gives rise to complex structures and specific nanoscale architecture. During the course of evolution, nature has transposed their protein's primary structure repeatedly, tailoring superstructure and function to an optimum. Those individuals, which were able to adapt their nanostructures to changing habitat conditions, succeeded in the competition of evolution.[1]

The majority of polypeptides in living organisms are structural proteins. By repeated assembly to specific shapes, macroscopic structures can evolve. A common example for the illustration of the connection between nanoscale interaction and macroscopic structure and function is keratin. In the human body, keratin is leading by far the most abundant protein and forms a range of entirely different macroscopic structures like hairs or nails.[2]

Another major subgroup of proteins are the biological catalysts, called enzymes. Enzymes are responsible for catalyzing nearly all metabolic reactions in living cells. Through evolutionary optimization of enzyme function, some of these enzymes are described as 'perfect'. In these cases, reaction speed is not limited by reaction kinetics anymore, but only by diffusion of substrates. Examples for enzymes with 'kinetic perfection' are acetylcholinesterase or carbonic anhydrase.[1]

Obviously, a library of 20 building blocks constitutes an intrinsic limitation regarding nanoscale function. This is circumvented by interacting with other molecules, which do not necessarily consist of amino acids, thus expanding the room of functionality. Non-protein compounds, that assist enzymes, are called cofactors (***Figure 1***).[2]
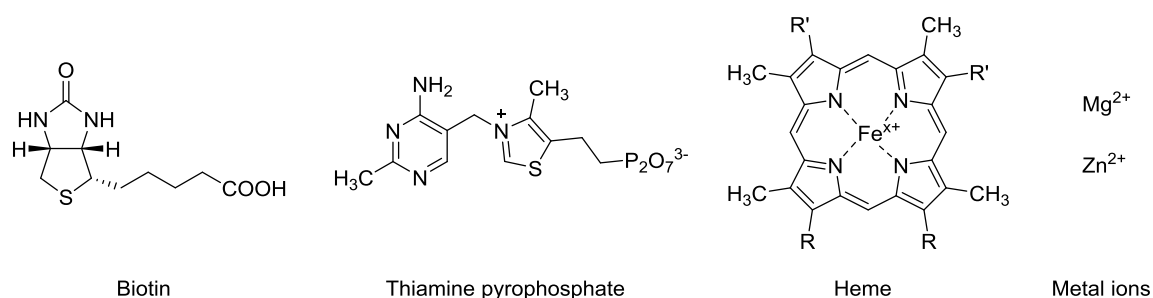

Biotin   Thiamine pyrophosphate   Heme   Metal ions

Figure 1: *Selection of common protein cofactors.*

1 INTRODUCTION

A functional 'holoenzyme' consists of the polypeptidic apoenzyme (the protein component) and its cofactor. In literature, these cofactors are often divided in three major groups: metal ions, coenzymes and prosthetic groups.[3]

While metal ions and coenzymes temporarily interact with given enzymes, prosthetic groups are tightly bound to and therefore permanent part of their respective enzymes. This binding can be covalent; a common example is the heme in cytochrome *c*, which serves as a single electron carrier. Non-covalent binding can for example be observed for biotin, which is responsible for CO_2 transfer in a variety of carboxylase enzymes.[2]

1.1.2: Metalloproteins: important examples from nature

Among different proteins in the biosphere, it is estimated that over 50% of them can be classified under the term 'metalloprotein'.[4] Here, the metal ions do not necessarily have to contribute to the catalytic activity of an enzyme. In many cases, cations (esp. Ca^{2+} or Zn^{2+}) balance charges of repulsive side residues and facilitate correct folding of the protein to its tertiary or quaternary structure.[2]

As the metalloproteome – the entire set of metalloproteins that is expressed by an organism – is very diverse, many ways of metal-protein binding can be observed. The most common ligands for those cations are amines (particularly histidine), carboxylates (particularly aspartate) and sulfur-containing moieties (cysteine, methionine). Furthermore, a large range of prosthetic groups is able to bind and stabilize metal ions.[5]

About 30 different elements from the periodic system have been found to fulfil a task in nature. While some of them only appear in very specific systems, others play a key role in most known organisms. Apart from the fundamental building blocks of organic chemistry (C, H, O, N, S, P, Cl) and ubiquitous alkaline (earth) metals (Na, K, Mg, Ca), transition metals like iron (Fe), copper (Cu), zinc (Zn), manganese (Mn) or molybdenum (Mo) are essential for many living things.[4]

Carbonic anhydrase (see ***Figure 2***) is an example for a metalloenzyme. In its catalytic core, a Zn^{2+} cation is complexed by three histidine side residues. The fourth ligand is a water molecule that is activated by the Lewis acid Zn^{2+}. With its increased nucleophilicity, water can now react with CO_2 to form hydrogen carbonate. Under standard conditions, this reaction is kinetically inhibited.[5] In humans, carbonic anhydrase plays an important role and participates in many processes such as lung and kidney function or acid production in the stomach.
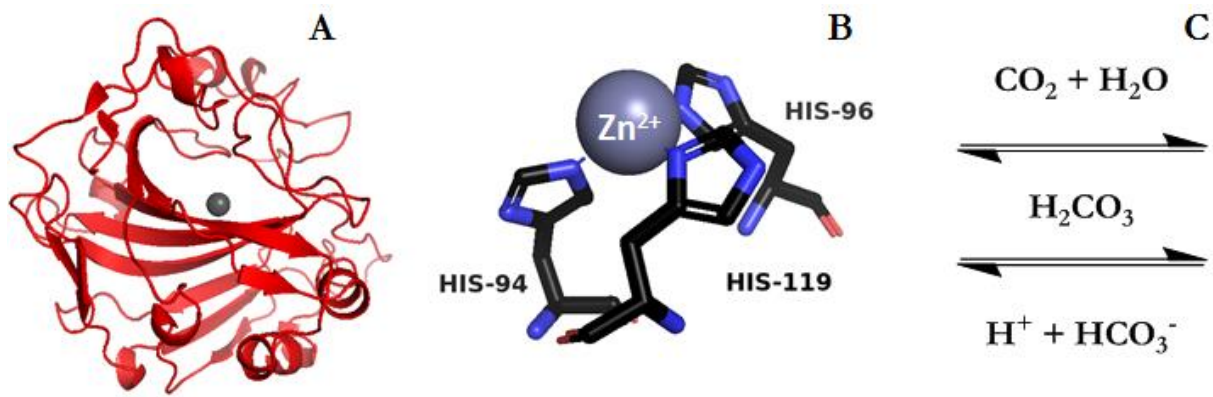
Figure 2: Carbonic anhydrase: tertiary structure (**A**), catalytic Zn^{2+} core (**B**) and catalyzed reaction (**C**) [PDB ID 1AZM].

An example for a metalloprotein that does not catalyze biological reactions is cytochrome *c*. Cytochrome *c* is an electron transfer agent and is highly conserved between a diverse range of organisms from unicellular organisms to *Homo sapiens*. In fact, the conservation is so high, that cytochrome *c* extracted from wheat still reacts with human cytochrome *c* oxidase.[1] Transfer of single electrons is possible due to binding of a Fe^{3+} cation. In contrast to carbonic anhydrase, cytochrome *c* does not bind the metal cation with its amino acid side residues. Instead, the prosthetic group heme *c* is covalently bound to its primary structure (conserved binding motif CXXCH) with two thioether bonds. Histidine and methionine serve as axial ligands and tailor the heme accessibility and the electric potential between Fe^{3+} and Fe^{2+}.[6]
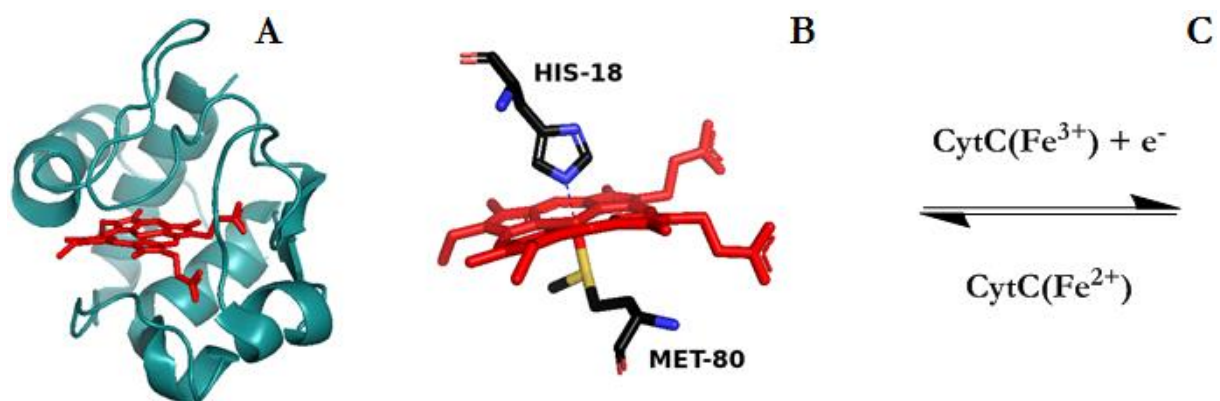
Figure 3: Cytochrome c: tertiary structure (**A**), catalytic heme (**B**) and catalyzed reaction (**C**) [1CHH].

Cytochrome *c* acts as a single electron carrier in the electron transport chain of the cell and is a key tool in producing energy (ATP) out of reduced biological compounds. Furthermore, it also plays an important role in the complex process of apoptosis and can serve as an antioxidizing agent.[1]

3

1.1.3: Optimized architecture: how the protein scaffold affects the catalytic core

In most cases, biological catalysis takes place at defined and spatially limited positions of an enzyme. These active sites, where substrates are converted into their products, represent only one segment of the overall protein structure.[2] The rest of the polypeptide chain, that is not directly responsible for catalysis, fulfils a variety of tasks and can be seen as the 'protein scaffold'.

The outer sphere of the 3D protein structure constitutes its interaction with other cell components. The highly predetermined alignment of positive and negative charges and specific and conserved amino acid sequences on the surface serve as protein fingerprints. These unique surface structures can be recognized by other biological macromolecules and are the basis of synergistic processes between molecules in cells resulting in what we consider as life. [7]

But the protein scaffold and catalytic core cannot be seen as two exclusive compartments of a protein. The 3D structure of the enzyme has a high impact on its catalytic activity and this way tailors and determines its biological function.

To illustrate this, the above-mentioned hemeproteins can serve as an example. Hemeproteins are a large class of metalloproteins that all bind a heme as a prosthetic group. While this might lead to the assumption that their biological functionality is limited, they actually undertake broad-ranging tasks. In vertebrates, hemeproteins for example serve as oxygen transporters (hemoglobin), oxidoreductases (cytochrome *c* oxidase), single electron carriers (cytochrome *c*), signaling cascade elements (guanylate cyclase) or as parts of the innate immune system (catalase).[8]

With its coplanar nitrogen atoms as electron donors, the tetradentate porphyrin ligand occupies four out of six potential coordination sites of the iron cation. As the ligands in axial positions are amino acid side residues, the polypeptide architecture has a distinct impact on the electronic properties of the iron cation. Cytochromes are not catalytically active and contain a low-spin six-coordinate iron core, where bis-histidine and histidine-methionine are by far the most common ligation states (see ***Figure 4***).[9] Studies by *Sligar et al.* have shown that interchanging axial ligands using site-directed mutagenesis has a distinct impact on the cytochrome's reduction potential and ligand binding.[10]
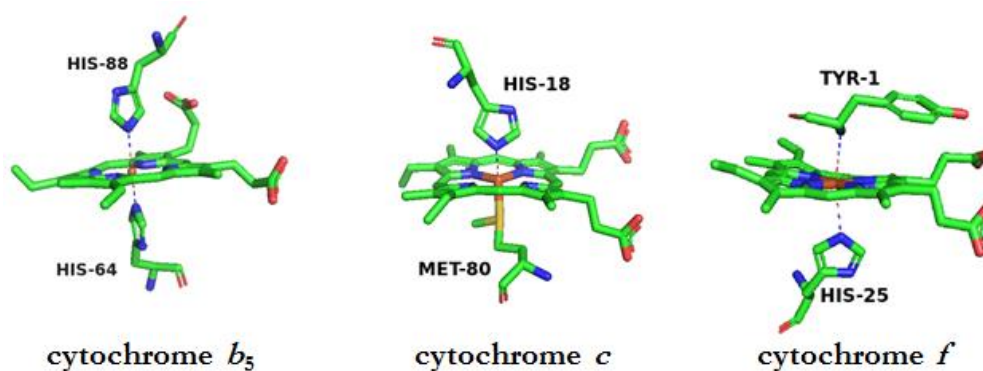
Figure 4: *Heme ligation in cytochrome b₅ [2I96],*
cytochrome c [1CHH] and cytochrome f [1CFM].

Metalloenzymes are intrinsically not ligated by two axial amino acid residues, as their function requires a free coordination position for substrate binding. This way, these hemeproteins are generally high-spin and five-coordinate, with an open coordination site or with water as an exchangeable ligand (***Figure 5***).[5]
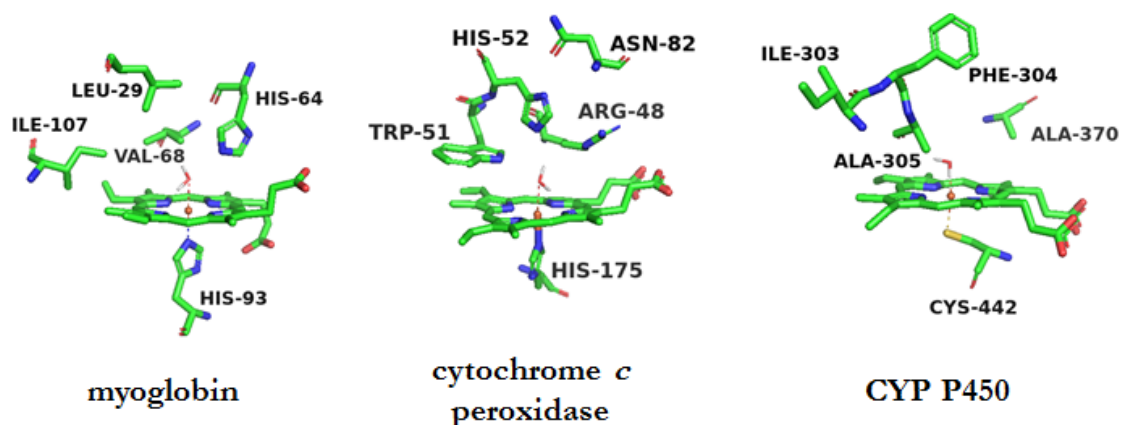
Figure 5: *Heme ligation of metalloenzymes: myoglobin [3RGK],*
cytochrome c peroxidase [1A2F] and CYP P450 [1TQN].

Gray et al. reported that replacing the axial ligand methionine in cytochrome *c* by the non-ligating alanine yielding the mutagenic Ala80 cytochrome *c* results in hemoglobin-like behavior.[11]

In summary, varieties in the protein scaffold surrounding the invariable heme center have a decisive impact on the metalloprotein's function. This way, tailoring the scaffold architecture on a nanoscale level can result in significant differences regarding catalytic activity. Thus, apart from their basic function in nature, (modified) metalloproteins are also of exceptional interest for scientists working in the field of organic catalysis or nanoscale engineering.

1.2 Metalloproteins as polymerization catalysts

1.2.1: ATRP: controlled/living radical polymerization

335 million tons of plastic have been industrially produced in the year 2016.[12] It is estimated that nearly 50% of these polymers have been synthesized harnessing radical polymerization processes.[13] In contrast to other polymerization methods, especially ionic polymerization, free radical polymerization provides distinct benefits: polymerization in water or ionic liquids is possible, monomer scope is comparably large and many different functional groups are tolerated.[14]

However, as termination reactions between two radicals are thermodynamically highly favored and occur at diffusion-controlled rates, control on the nanoscale structure is quite low. In the last decade of the 20th century, the term 'controlled/living radical polymerization' has been coined and different approaches towards elevated polymerization control have been introduced. In all these cases, the aim was to minimize the number of active radicals. As polymer propagation is a process of first order kinetics and termination of radicals represents second order kinetics, low radical concentrations lead to less disperse macromolecules.[15]

One of the most promising and successful methods is the 'Atom Transfer Radical Polymerization', short ATRP. This transition metal-based system has been introduced in 1995 simultaneously by both, *Sawamoto* und *Matyjaszewski*.[16-17] Traditional ATRP requires highly air-sensitive metal cations (especially Cu^+), which intrinsically limits possible application towards in biology or industry. Therefore, different modifications and improvements of ATRP have been introduced and published. Out of different approaches, the focus in this present work is on the 'Activators Generated by Electron Transfer' (AGET) ATRP. [18]

In AGET ATRP, the active metal cation (here: Cu^+) is prepared by reducing air-stable metal cations (here: Cu^{2+}) through the addition of reducing agents. Homolytic cleavage of the C-Br bond of a bromine-containing initiator by oxidation of the copper leads to occurrence of radical species. Polymer chains can now propagate, in most cases (meth)acylates, (meth)acrylamides or styrenes are harnessed as monomers. Here, the key element is reversibility of the homolytic cleavage/oxidation reaction that leads to 'dormant' radical species and limits the number of free radicals (*Figure 6*).

$$
\begin{array}{ll}
k_{act} & = k(\text{activation}) \\
k_{deact} & = k(\text{deactivation}) \\
k_t & = k(\text{termination}) \\
k_p & = k(\text{propargation}) \\
k_{ATRP} & = k_{act}/k_{deact}
\end{array}
$$
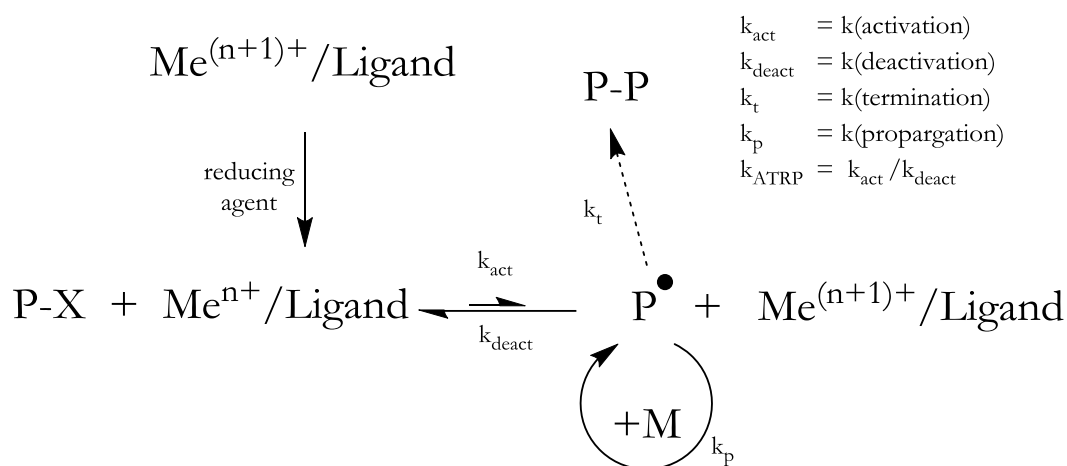
Figure 6: *Mechanism of AGET ATRP.[19]*

1.2.2: Iron in ATRP: a pathway towards more sustainable polymer chemistry?

Whilst a range of transition metals like for example Mo, Fe, Ru, Os or Ni have been described to be able to serve as ATRP catalysts, copper is markedly the most-established and most-studied transition metal for ATRP (see **Figure 7**). Main advantages of copper catalyst systems are their robustness, their monomer compatibility and their easy procurement.

On the other hand, copper systems also implicate certain drawbacks. As copper is known to be toxic, implementation of copper ATRP in industrial production of everyday objects or even biomedical application is limited. Therefore, especially iron-mediated ATRP has emerged growing interest in the last years.[20]
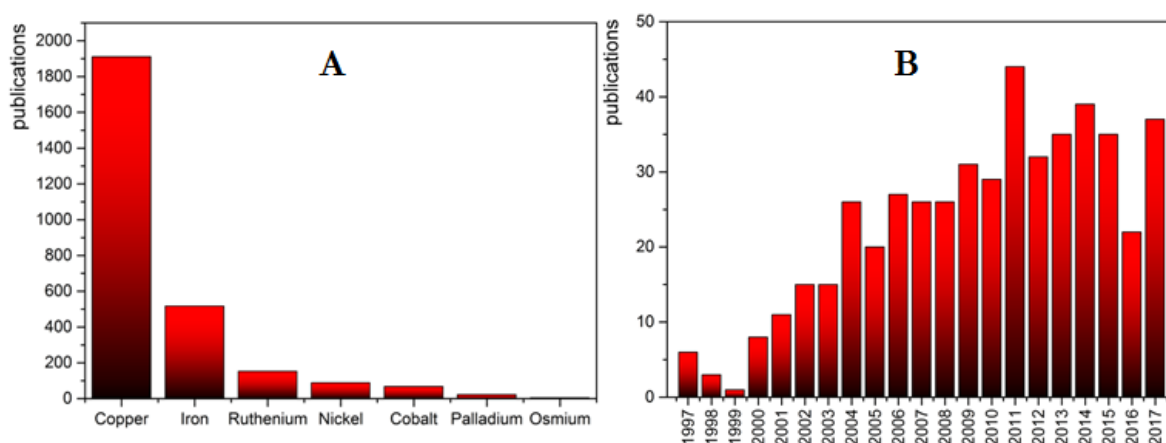
Figure 7: *(A): Results of SciFinder search 'Atom Transfer Radical Polymerization "metal"'. (B): Results of SciFinder search 'Atom Transfer Radical Polymerization iron' sorted by publishing year.*

1 INTRODUCTION

The advantages of iron are obvious. As it is by far the most abundant transition metal in the earth crust, employment of iron in polymer synthesis even at industrial scales is cheap and straightforward. Additionally, its key role in many processes in biological systems (3–5 g of iron per human body)[21] implies a high level of biocompatibility. Finally, iron complexes are well-implemented in organic chemistry and are already described in a wide range of catalysis applications.[22]

Different examples of iron-catalyzed AGET ATRP can be found in literature. In most cases, hydrophobic organic ligands like tributylamine (TBA) or triphenyl phosphine (TPP) allow the solubility of $FeCl_3$ in organic solvents like toluene or even in bulk. While applying high temperatures (often ≥100 °C), polydispersities down to 1.1 – 1.2 can be achieved.[20]

The work published by *Zhu et al.* is a rare example for successful AGET ATRP with iron conducted in aqueous media. The group polymerized the water-soluble monomer OEGMA at 90 °C using ascorbic acid as the reducing agent and tris(3,6-dioxaheptyl) amine (TDA) as a ligand.[23]

In view of high temperatures to be applied and lacking examples of polymerizations in aqueous media, this traditional AGET ATRP approach has significant room for improvement regarding biocompatibility. As a consequence, introduction of enzymes or enzyme-related substructures as ATRP catalysts described in the following subchapter can be seen as another distinct step towards 'greener' polymer chemistry.

1.2.3: ATRPases: advantages and limitations

In 2011, both *Bruns et al.* and *di Lena et al.* simultaneously came up with a new concept of iron-containing ATRP catalysts.[24-25] Instead of exploiting metal complexes by mixing inorganic iron salts with synthetic amine ligands, they harnessed existing hemeproteins like horseradish peroxidase (HRP) or catalase. Both groups showed that even though these polypeptides were completely taken out of their biological context, implementation in polymerizations was possible. For proteins that are able to serve as ATRP catalysts, *Bruns et al.* coined the term 'ATRPase'.

In their first communication, *Bruns et al.* showed successful polymerization of *N*-isopropylacrylamide (NIPAM) in an ARGET ATRP-like reaction setup. In an aqueous solution containing the initiator, NIPAM, HRP and ascorbic acid, they showed successful synthesis of the thermoresponsive polymer PNIPAM. Catalyst ratios lower than 5% gave rise

to polymers with acceptable quality (PDIs down to 1.44). Catalytic enzymes were successfully recovered afterwards and their structural integrity was shown to be preserved.[24]

In a subsequent publication, *Bruns et al.* also introduced hemoglobin as an ATRPase and even proved the potential use of human blood for ATRP catalysis.[26] Here, different water-soluble polymers were synthesized with catalysts ratios even lower than 1%. Quality of obtained macromolecules was still capable of improvement and was shown to be very pH dependent.

Meanwhile, *Matyjaszewski et al.* simplified the ATRPase system by removing the heme from its protein scaffold and chemically optimizing it.[27] After hydrogenation of vinyl moieties, PEGylation for elevated water solubility and addition of bromine ligands, the system was able to yield polyacrylates with low dispersity (PDIs around 1.2).

These studies demonstrated that the use of non-toxic ATRPases, which are intrinsically biodegradable, can be applied in very low catalytic concentrations. This way, they represent an interesting example on the pathway towards 'green chemistry'. While their formation of polymers with predictable size and dispersity still leaves a lot of room for improvement, ATRPases can be seen as an innovative concept for future plastic production.

1.3 Modified proteins as building blocks for precision nanosystems

1.3.1: Optimization of proteins for introduction in nanosystems

While native proteins are unrivalled designer catalysts in nature, their intrinsic specialization within their domain is often a hindrance towards their direct use in synthetic chemistry. Simply put, proteins generally do not possess both form and function within a synthetic context. Nonetheless, proteins provide a host of chemical modification possibilities allowing scientists to manipulate and control organization and architecture of matter at molecular or submolecular levels.[28] Because of their intrinsic monodispersity and defined tertiary structure, biomacromolecules often play an irreplaceable role in state-of-the-art nanosystems. While DNA can be folded into a range of desired 3D structures, proteins are able to serve as versatile scaffolds for a variety of desired applications.[29-30] Other advantages of proteins as building blocks are the robustness of the peptide bonds and their easy expression and procurement as products from biological systems.

The proteins exploited for nanoscale engineering do not necessarily have to maintain their predetermined biological structure. Scientists, from both biology and protein chemistry, are

able to tailor protein properties by modifying the polypeptide structure. The motivations behind these modifications are broad and range from enhanced cellular uptake, customized stability and bioactivity to directed nanoscale assembly and therapeutics.[31-32] The scientific work from *Frances Arnold*, chemistry Nobel Prize laureate of 2018, is a striking example of how mutagenic exchanges of amino acids affect protein's properties like function, structure or thermostability.[33]

Another approach of tailoring the properties of a protein is the chemical modification of amino acid side residues. These side residues with reactive groups like amines, carboxylates and thiols can be converted to other functional groups to engineer the protein's capabilities according to target application (***Figure 8***).[34-37]
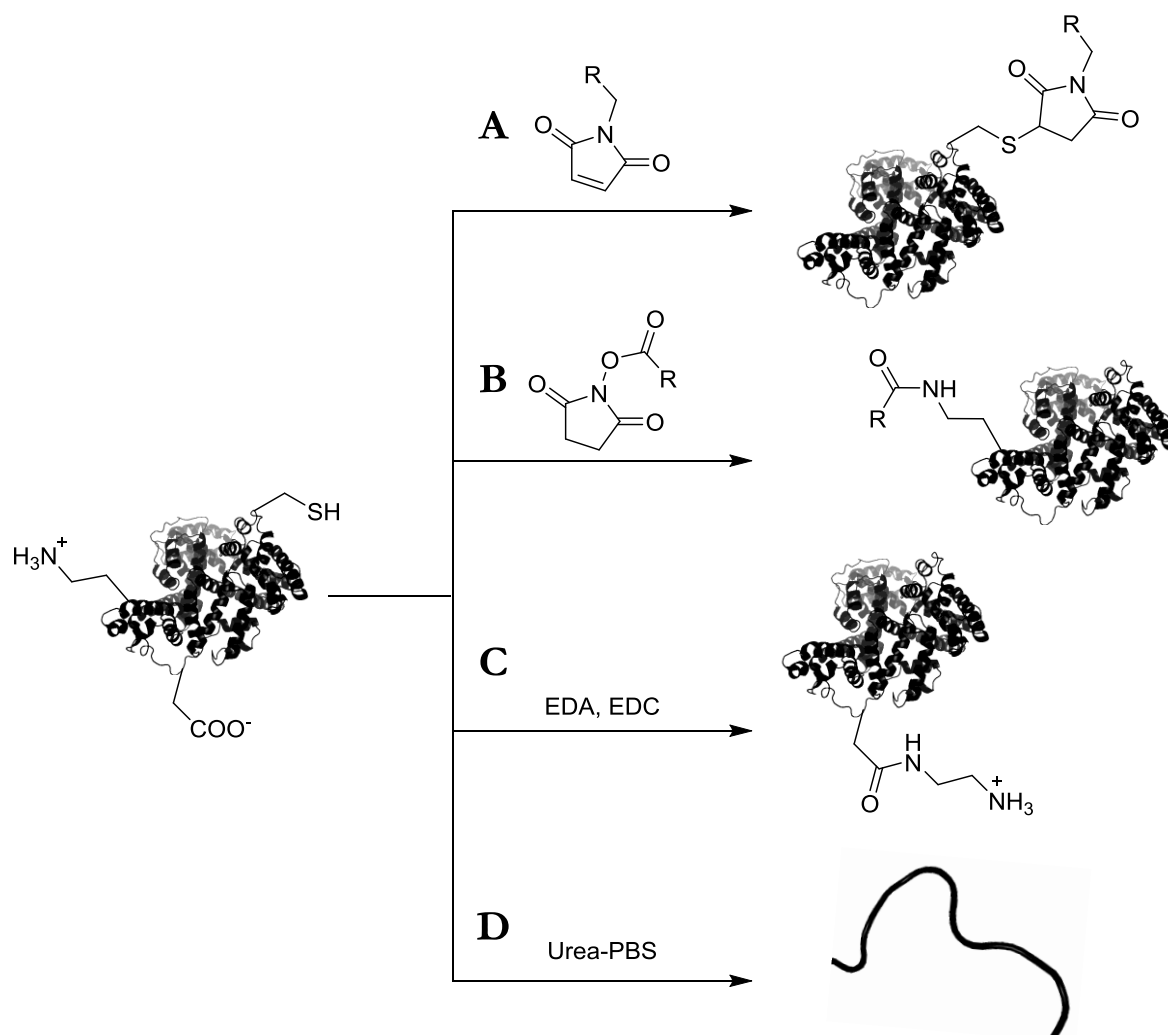

Figure 8: *Different examples for chemical protein modification: thiol modification harnessing maleimide compounds (**A**), lysine functionalization harnessing NHS activated ester (**B**), cationization with ethylenediamine (**C**) and denaturation in urea buffer (**D**).*

1.3.2: Denatured proteins as nanoscale building blocks: a chemist's viewpoint

Apart from protein's intrinsic biocompatibility and biodegradability, it's their absolutely exceptional predetermined construction that makes them ideal backbones for protein-polymer hybrids. As such, absolute positioning of synthetic polymers on the polyvalent surface of the protein is possible. Physical, chemical and biological properties of the resulting material can be tailored by changing features like monomeric constituents, polymer length or total amount of conjugated macromolecules.[38] Here, denaturation of the globular protein to a more strand-like and elongated shape allows enhanced accessibility of potential modification sites.

By combining denatured polypeptide backbones and synthetic polymers to yield a hybrid nanoscale scaffold, material scientists are able to design bimodular building blocks with synergistic properties. Choosing functional polymers responsive to heat[39-40], light[41] or chemical triggers[42] allows the fabrication of stimuli-responsive state-of-the-art nanoscale frameworks.

Two major ways are described for the connection of synthetic polymer and polypeptide backbone. Following the *grafting to*-procedure, presynthesized polymers bearing reactive moieties like maleimides or active esters (see **1.3.1**) are linked to specific reactive amino acid side residues (see ***Figure 9,*** **A**). The amount of grafted polymers can be tailored by the ratio of protein backbone to activated polymer moiety.

In a *grafting from*-polymerization reaction, initiators for radical polymerization are covalently attached to the modified protein to yield a macroinitiator. Here, polymers of tailorable size can be grown form these specific sites by adjusting the macroinitiator with the desired monomer (see ***Figure 9***, **B**). Standard polymerization techniques exploited here are ATRP (see **1.2.1**) or RAFT polymerization.[43]
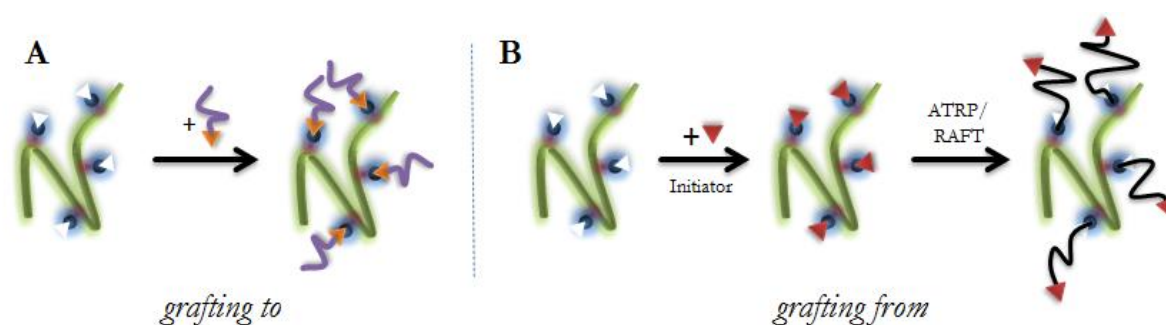
Figure 9: *Linkage of denatured protein backbone and polymer in a grafting to (**A**) or grafting from (**B**) procedure.*

The resulting semi-synthetic materials are not only of theoretical interest in fundamental research. Modified proteins already serve as approved biopharmaceuticals in medical therapy since 1990.[44] Here, modification of proteins can overcome certain drawbacks of native proteins as therapeutics such as biodegradation, fast renal excretion or immune cell activation. Polymer structures on the protein's surface can generate materials with 'stealth'-like properties hardly detectable by endogenous defense mechanisms.[43]

But utilization of this unlimited library of protein-polymer conjugates is not restricted to pharmaceuticals only. The list of applications ranges from catalysis in bioreactors to protein isolation and is expected to be greatly expanded in future.[45]

2 Motivation

In this present work, the metalloprotein cytochrome *c* from *Saccharomyces cerevisiae* (see **3.1**) was chosen as the starting material to design thermoresponsive polymer-protein brushes as precision nanosystems where each component, even the scaffold itself, would provide a function. We envision that in the resulting hybrid material, diverse and desirable features like highly-defined protein architecture, heme-based catalytic activity and polymers sensitive to external triggers can be integrated within one macromolecule. By controlling these features with their respective chemistry, functional polymer-protein brushes based on a denatured metalloprotein backbone can be seen as a polyvalent and multidimensional platform to further expand the toolbox of chemical engineers to create intelligent nanomaterials.

First, we describe the protein modification strategies due to its importance in engineering the protein architecture by exploiting the sequence definition of its polypeptide backbone. Here, analogous to other modified proteins developed in our group, the globular metalloprotein cytochrome *c* can be converted into a strand-like polypeptide macroinitiator by undergoing the reaction sequence *cationization – PEGylation – denaturation and labeling – initiator addition* (see **3.2**). Exploiting copper-catalyzed ATRP of NIPAM using the *grafting from* approach, polymer-protein brushes with tailorable sizes, polymer/protein ratios and thermoresponsiveness can be synthesized (see **3.3**).
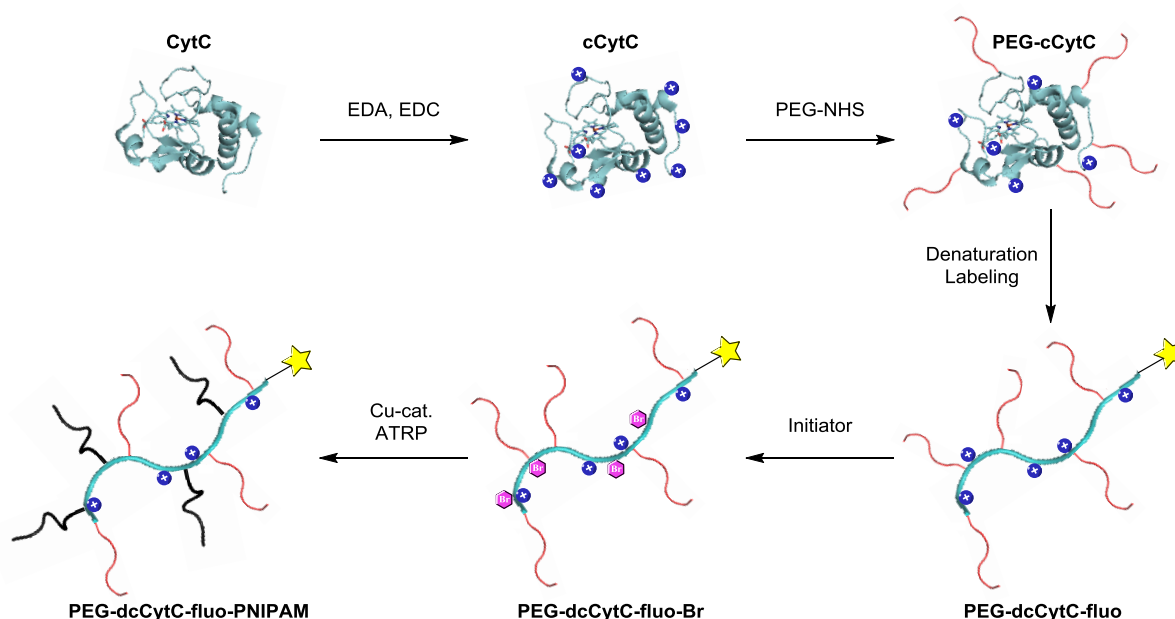
Figure 10: *Synthesis scheme to convert cytochrome c into a functional protein brush.*

The obtained protein brushes can then be analyzed regarding their physical, chemical and biological properties. Harnessing different methods like NMR, MALDI-ToF MS or gel electrophoresis allows deeper insight into the structural composition of the hybrid material. Here, the effect of temperature on the framework's architecture is of special interest. If the activity of the heme can be shown to be conserved, the thermoresponsivity of the brushes might result in unique and unusual catalytic properties upon temperature switching (see **3.4**). Additionally, expanding the scope of monomers to be linked to the polypeptide backbone demonstrates the engineering capacity and broad applicability of the platform.

As the surface-initiated ATRP is the key step in the above-mentioned brush synthesis and that in fact different metalloenzymes are known to serve as ATRPases, it's an evident question whether cytochrome *c*'s heme activity can be harnessed to catalyze polymerizations (see **3.5**) or even to graft polymers from the protein's own surface (see **3.6**). Since the ATRPase functionality is not described for cytochrome *c* yet, its potential to enable formation of linear polymers in aqueous solution has to be investigated in advance. The successful application of cytochrome *c* or synthesized derivatives as ATRP catalysts would further expand the list of biodegradable, non-toxic and thus sustainable ATRPase metalloproteins.

3 Results and Discussion

3.1 Introducing cytochrome *c* from *Saccharomyces cerevisiae*

3.1.1: Background: selection of the metalloprotein

The target of this present work was the synthesis and analysis of hybrid materials containing a polypeptide backbone based on cytochrome *c* from *Saccharomyces cerevisiae*. In this respect, it was possible to reference on a variety of experience gained in the WEIL group in modifying protein-based materials. The reaction scheme to modify cytochrome *c*'s surface and structure was derived and optimized from previous studies within our group.[35-36] In our previous work, human serum albumin (HSA) was converted to a strand-like macroinitiator allowing the growth of polymers from its surface exploiting the *grafting from* polymerization method. A polymer-protein brush with properties customizable by monomer choice, number of polymer chains or polymer length was obtained. Moving on, we envision that the switch in scaffold from purely structural (HSA) to a functional/catalytic one (cytochrome *c*) would be a natural step to develop the next generation of polymer-protein hybrids:

- Cytochrome *c* (12.6 kDa, 109 amino acids) is a comparably small protein. This allows a more precise modification of different side residues. Additionally, it also eases protein analysis exploiting methods like MALDI-ToF MS and/or gel electrophoresis that might be limited in high molecular weight regions (e.g. HSA: 66.4 kDa, 585 amino acids).

- The biological function of the metalloprotein cytochrome *c* is to carry single electrons. To fulfill this task, a redox-active heme is covalently bound to its primary structure as a prosthetic group.[1] This raises the question whether – besides serving as a polypeptide scaffold – the modified protein could also undertake a catalytic function in a nanosystem.

- The major advantage of using a natural polypeptide as a macroinitiator over other possible macromolecules like synthetic polymers is their perfectly defined structure (see **1.3.2**). Cytochrome *c* from *Saccharomyces cerevisiae* was chosen as it contains a single free cysteine in its primary structure. This is not the case for the far more frequently harnessed cytochrome *c* from equine heart. As precise thiol modification by maleimide chemistry is well-known in literature, monofunctionalization at a defined position (C-108) is possible.[46] Synthetic modification of macromolecules at designated and limited sites might be a key tool for scientists aiming for more precise nanosystems to enable a better understanding. Here, nature itself is the role model with its fascinating abilities of site selective chemical modifications of different substrates using enzymes as optimized catalysts.[2]

3.1.2: Cytochrome *c*'s primary structure

Cytochrome *c* from *Saccharomyces cerevisiae* is built up from the following amino acids:[47]

MTEFKAGSAK KGATLFKTRC LQCHTVEKGG PHKVGPNLHG IFGRHSGQAE

GYSYTDANIK KNVLWDENNM SEYLTNPKKY IPGTKMAFGG LKKEKDRNDL

ITYLKKACE
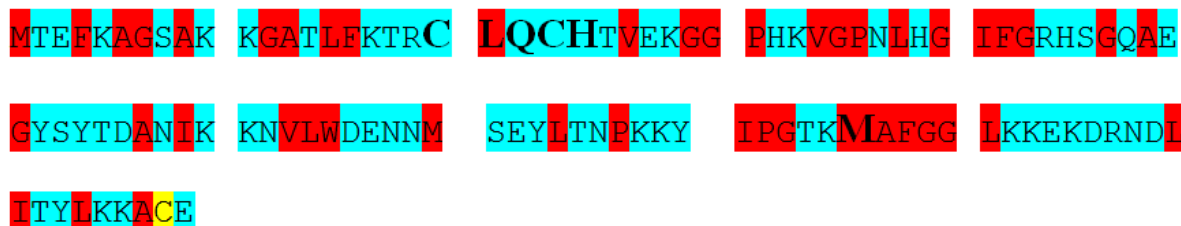
Figure 11: *Primary structure of cytochrome c from Saccharomyces cerevisiae. Amino acids highlighted in blue are hydrophilic, red-highlighted residues are hydrophobic. The cysteine in position 108 (yellow) is free for monofunctionalization.*

In contrast to other cytochromes, cytochrome *c* is a very water-soluble polypeptide, which can be seen by the relatively high amount of hydrophilic amino acids (blue) in its primary structure (see *Figure 11*). Also the CXXCH (bold letters) heme binding motif, which is highly conserved between cytochromes of different species, can be found.[48] In this motif, the cysteines C-20 and C-23 and the vinyl chains of the heme *c* are forming the covalent bond between protein and prosthetic group (see *Figure 12*). The histidine H-24 serves as one axial ligand, while methionine M-86 is situated on the other side of the complexed iron core.
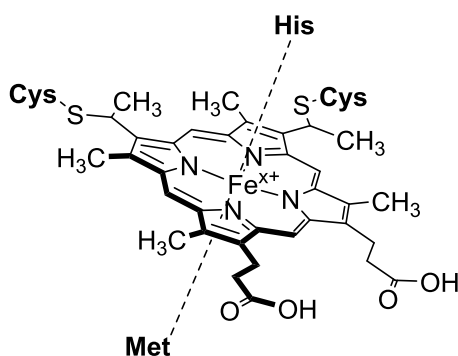
Figure 12: *Chemical structure of heme c within the metalloprotein cytochrome c.*

The cysteine C-108 (yellow) close to the C-terminus of the protein is the only 'free' cysteine in the primary structure.

3.2 Synthesis of the polypeptide macroinitiator

3.2.1: Cationization of native cytochrome *c*

Cationization of carboxylates often is the first step in the chemical modification of proteins in the WEIL group to increase the density of amino groups which will be subsequently transformed into other reactive handles. In this step, side residues with negative charges (aspartate and glutamate) are converted to amines using carbodiimide chemistry. Here, the high electrophilicity of 1-ethyl-3-(3-dimethylaminopropyl)carbodiimide (EDC) is exploited to connect the carboxylates with excess ethylenediamine (EDA) in a condensation reaction. This reaction yields an amide with a new, primary amine in a position accessible for further functionalization (***Figure 13***):
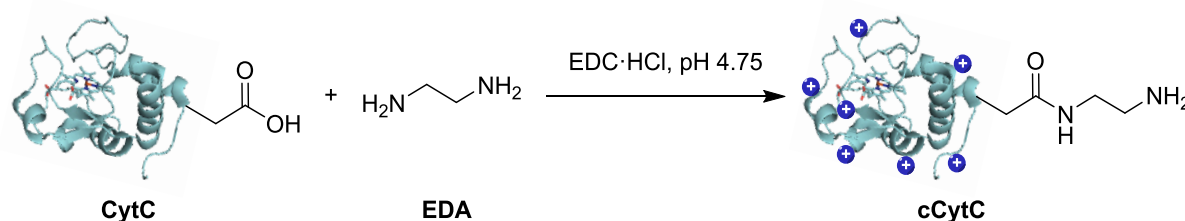
Figure 13: *Condensation reaction between a carboxylate side residue and EDA.*

Stoichiometrically, the aim was to push the system to the maximum of converted carboxylates by using high excess of both EDC and EDA. In total, cytochrome *c* consists of 14 carboxylic moieties, including seven glutamates, four aspartates, its C-terminus and two more COO$^-$ groups as part of the heme.

Different reaction setups led to the finding that >25 equivalents of EDC·HCl and overnight reaction is needed for reproducible conversion rates of the carboxylates. After lyophilization, the product cCytC (average mass ~13.4 kDa according to MALDI-ToF MS) was obtained as a pale red, fluffy and well water-soluble solid. The low mass of a single EDA molecule in comparison to the protein weight doesn't allow determination of carboxylate conversion by MALDI-ToF MS.

The effects of cationization on the protein was characterized by circular dichroism spectroscopy, which in contrast to NMR or crystallography, is an easy method to determine the secondary structural composition of a protein. Amino acids absorb right/left-handed polarized light to a different extent depending on their chiral environment. Exploiting this, CD spectroscopy allows drawing conclusions on the number of α-helices and β-sheets in the protein's structure.[49] Aspartate and glutamate both significantly prefer α-helices over

β-sheets and their conversion to cationic primary amines should fundamentally change their behavior in interacting with neighboring amino acids.[50] For this reason, one might draw the conclusion that a high conversion rate of those residues should involve significant reduction of α-helices in the proteins tertiary structure. Indeed the amount of α-helices was observed to decrease by CD spectroscopy to an extent much higher than expected (see **_Figure 14_**). On the contrary, previous studies in the WEIL group did not show that much of impact of cationization on proteins like HSA.[51]
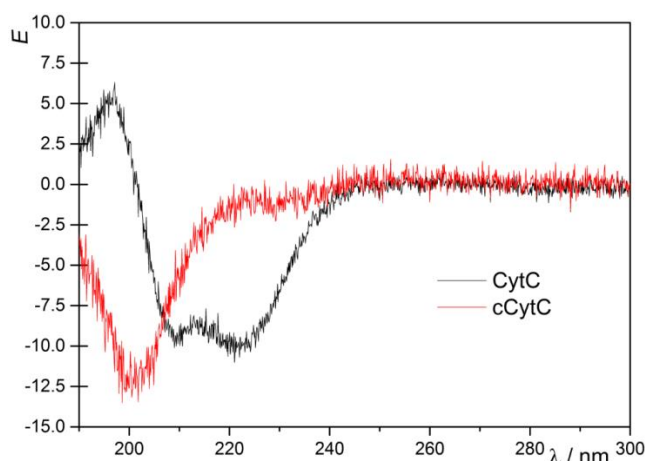
Figure 14 : _Circular dichroism spectra of native cytochrome c and cCytC._

3.2.2: PEGylation of cationized cytochrome _c_

The next step in the reaction scheme is the PEGylation of the protein exploiting the _grafting to_ strategy. PEG_{2000}-coupled NHS active esters serve as reactive moieties quickly converting lysine amino residues of the proteins to amides. In this present work, full conversion of the 14 carboxylates to primary amines during the previous conversion of native cytochrome _c_ to cCytC was assumed (see **3.2.1**). Thus, the amount of reactive positions for addition of compounds coupled with NHS active esters was calculated as follows (**_Table 1_**):

Table 1: _Number of primary amines in the structure of cCytC._

What?	#
Lysine residues in the primary structure of CytC	16
Carboxylic acids converted to primary amines	14
N-terminus	1
Total	**31**

PEGylation is a required step to keep proteins water-soluble after modification and denaturation. The necessity of PEGylation of cCytC was illustrated by its reaction with the ATRP initiator 2-bromoisobutanoic acid N-hydroxysuccinimide ester (BiB-NHS) to yield the potential macroinitiator cCytC-Br (***Figure 15***):
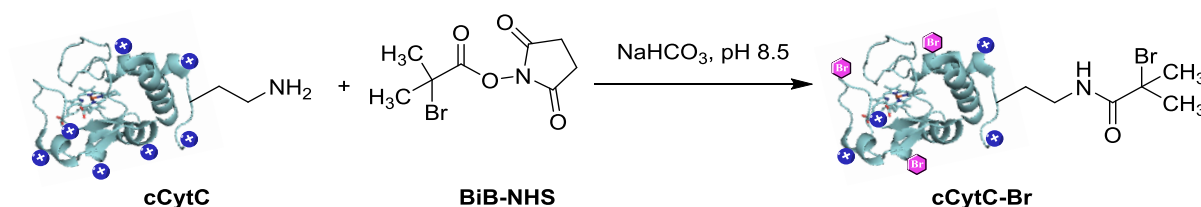
Figure 15: *Functionalization of cCytC with the ATRP initiator BiB-NHS yielding the water-insoluble macroinitiator cCytC-Br.*

With only 10 equivalents of BiB-NHS to the protein (cCytC) without PEGylation, the red solution became turbid after some minutes. The resulting pale red solid obtained after lyophilization was not water-soluble anymore.

In contrast to that, addition of $4-7$ PEG$_{2000}$ chains to the surface of the protein allowed full coverage with an excess of the hydrophobic ATRP initiator mentioned above and yielded a well water-soluble compound (***Figure 16***):
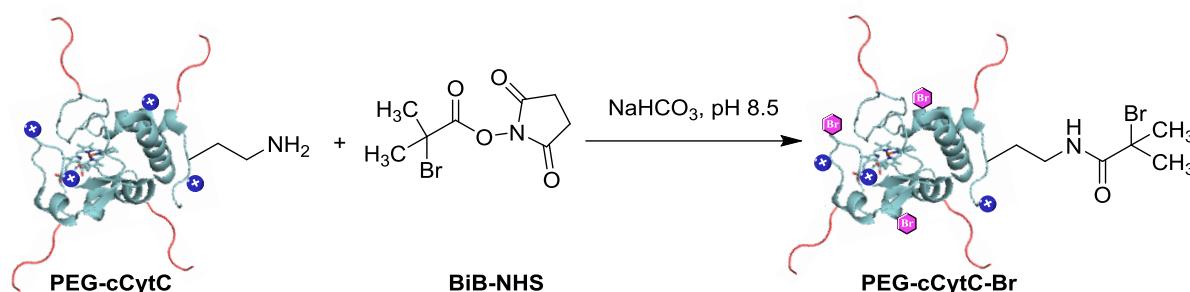
Figure 16: *Functionalization of PEG-cCytC with BiB-NHS yielding PEG-cCytC-Br.*

With stirring overnight, the reaction of cCytC and PEG$_{2000}$-NHS was allowed to reach completion. By standardizing the reaction time, the amount of PEG$_{2000}$ chains on the protein's surface can be tailored by the stoichiometric ratio of the substrates.

Besides easier handling due to increased molecular sizes, a high amount of grafted PEG$_{2000}$ chains would also guarantee high water solubility after denaturation and modification of the enzyme. 'OverPEGylation' on the other hand increases the bulkiness of the protein brush and might lead to lower accessibility for subsequent reactions. In addition, a high amount of PEG$_{2000}$ would also mean a lower amount of free amino groups that can subsequently be

functionalized with the BiB-NHS initiator. To face the question of optimized enzyme/PEG$_{2000}$-NHS stoichiometry, a fixed amount of cCytC was treated with different amounts of PEG$_{2000}$-NHS (***Figure 17***):
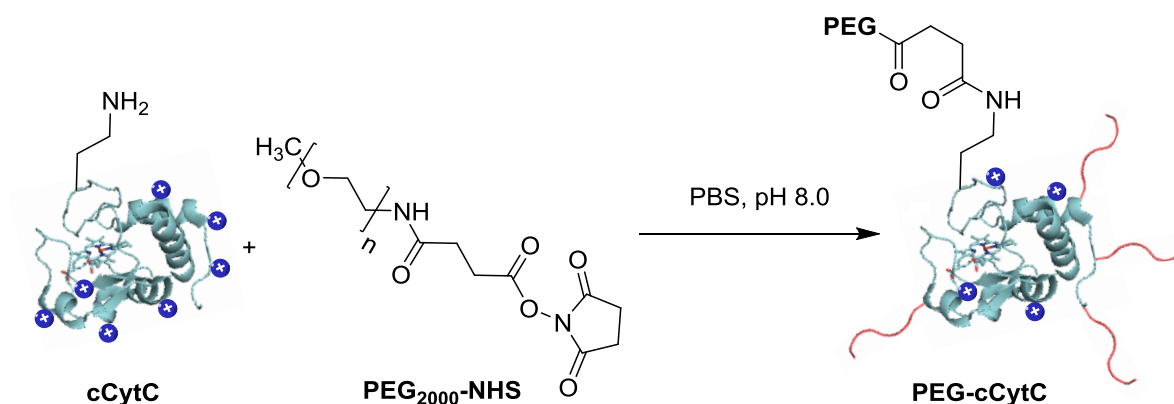
Figure 17: *Reaction of cCytC and PEG$_{2000}$-NHS to yield PEG-cCytC.*

After reaction overnight, the different reaction mixtures were purified by ultrafiltration (MWCO: 5 kDa) and analyzed by MALDI-ToF MS. Due to the relatively high molecular weight of one PEG$_{2000}$ chain, the obtained spectra allowed the identification of the different products (see ***Table 2***). According to the reaction scheme above, their mass peaks applied to:

$$MW(PEG_x - cCytC) \approx MW(cCytC) + x * 2000 \text{ g/mol}$$

Table 2: *Different stoichiometries of cCytC and PEG$_{2000}$-NHS leading to different coverages of the protein's surface with PEG$_{2000}$ chains.*

#	n(cCytC) / nmol	n(PEG-NHS) / nmol	ratio	main mass peak / kDa	# of PEGs
a	40	100	1:2.5	13.4	0 – 3
b	40	160	1:4	15.4	0 – 4
c	40	240	1:6	17.3	0 – 5
d	40	400	1:10	25.2	3 – 8
e	40	1000	1:25	41.5	12 – 19

The analysis of the obtained product can be exemplified by the following mass spectrum (***Figure 18***):
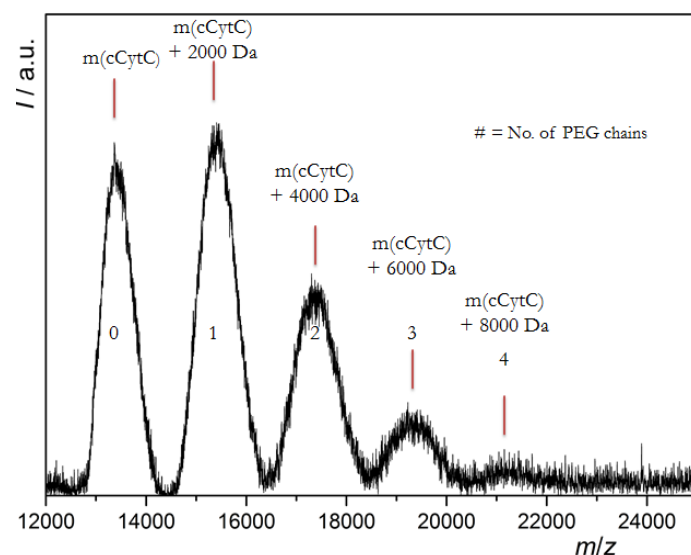
Figure 18: *MALDI-ToF MS after treating cCytC with PEG$_{2000}$-NHS in a ratio of 1:4.*

Overall, the result of this experiment can be visualized as follows (***Figure 19***):
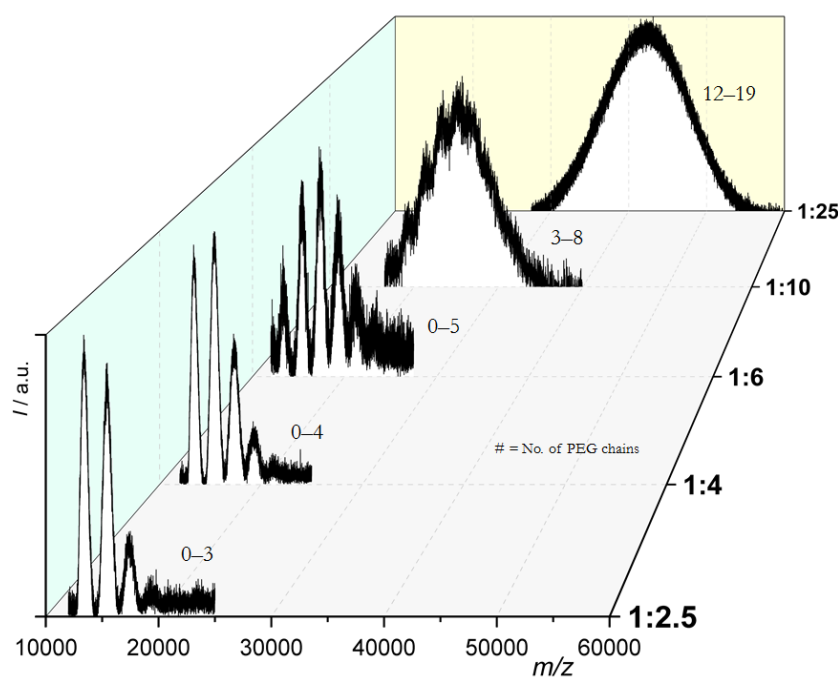
Figure 19: *Experimental outcome of treating cCytC with different ratios of PEG$_{2000}$-NHS.*

As it can be seen from the figure above, the PEGylation of cCytC does not reach a 'modest' limit if a distinct excess (like 25 eq.) of PEG$_{2000}$-NHS is added. Instead, it is obvious that grafting many PEG$_{2000}$ chains to the protein's surface leads to a significant and undesired broadening of its mass peak, most probably due to statistical reasons.

Another way to visualize the impact of different ratios of PEG$_{2000}$ chains on the protein size is gel electrophoresis. Harnessing the SDS-PAGE method, proteins are separated by their mass

while passing through a matrix of polyacrylamide.[1] As PEG chains do not have any charges, PEGylated proteins behave different in the gel than non-PEGylated proteins with similar sizes. This makes it impossible to identify the mass of the products by comparing them with protein standards of known sizes. However, the SDS-PAGE is still indicative of the effects of the covalent conjugation of PEG$_{2000}$ on the protein size (***Figure 20***):
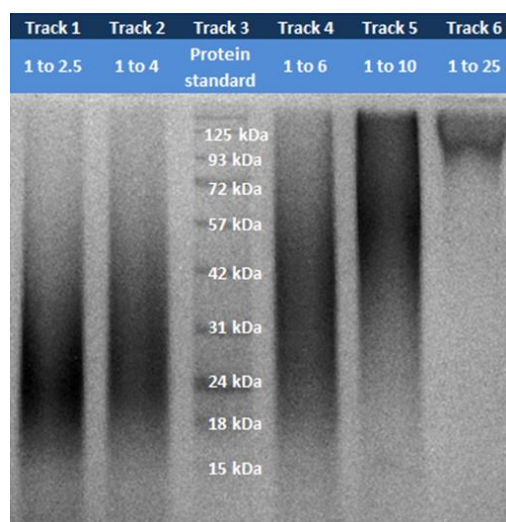
Figure 20: SDS-PAGE after cCytC was treated with different amounts of PEG$_{2000}$-NHS.

Despite the qualitative information from the SDS-PAGE, the outcome is in agreement with the results obtained by MALDI-ToF MS. Increasing the ratio of PEG$_{2000}$-NHS/cCytC leads to more grafted PEG$_{2000}$ chains. Exact analysis of protein sizes is difficult due to the spread of the protein signals. This can be explained by two major reasons: At first, the substrate cCytC already has a certain polydispersity which can also be visualized by MALDI-ToF MS. Secondly, the PEG$_{2000}$ chains contain an intrinsic distribution and are also known to give broad signals in SDS.[52] However, gel electrophoresis is a simple method to visualize the relation between the PEG$_{2000}$-NHS/cCytC stoichiometry and estimate the overall mass of the product obtained.

Considering above arguments for *grafting on* different amounts of PEG$_{2000}$, the synthesis pathway was continued with a moderate amount of $3 - 8$ PEG$_{2000}$ chains conjugated to the enzyme. This number should guarantee water solubility after denaturation while still leaving substantial capacity for the addition of other functional groups.

3.2.3: PEGylation of native cytochrome *c*

Looking from a different perspective, a direct PEGylation to the native protein without expanding the availability of amino groups might provide a stoichiometric limit and hence control over subsequent functionalization. Therefore, it would be valuable to explore differences between PEGylation of cationized cytochrome *c* (see **3.2.2**) and the native protein in parallel. Experimentally, the native cytochrome *c* was treated in the same way as the cCytC described in the chapter above (***Figure 21***):
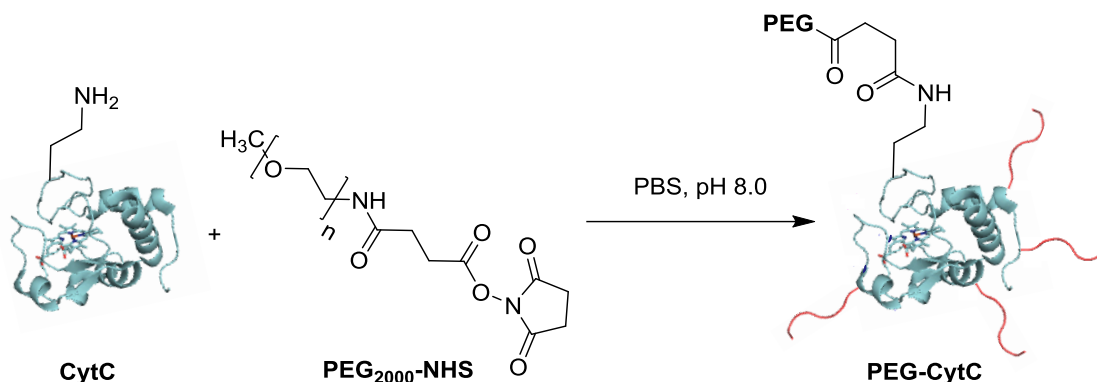
Figure 21: *PEGylation of native cytochrome c to yield PEG-CytC.*

Similarly, the different batches containing different extent of PEG$_{2000}$ modification were worked up under the same conditions described above and analyzed by MALDI-ToF MS. In this case, the resolution to match the mass peaks to different amounts of PEG$_{2000}$ on the native protein's surface was even higher than described for the cCytC counterpart (***Figure 22***):
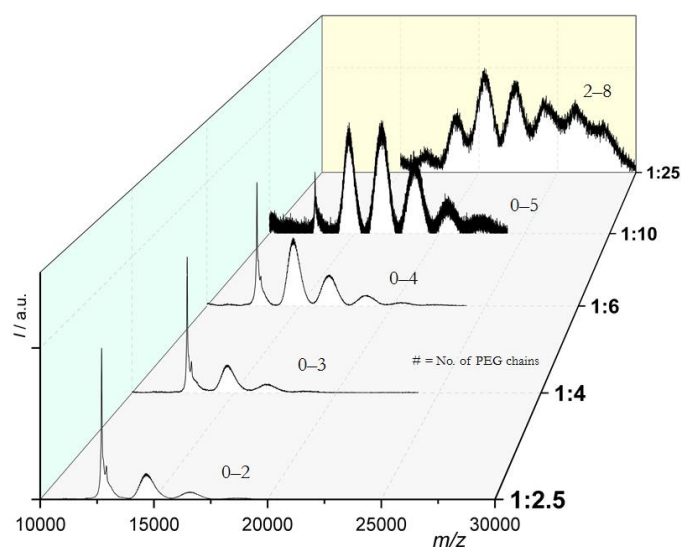
Figure 22: *Native cytochrome c treated with different ratios of PEG$_{2000}$-NHS.*

In principle, these data match with the results expected as higher amounts of PEG$_{2000}$-NHS added to fixed amounts of native cytochrome *c* resulted in higher PEGylation yields. As already seen in the cCytC case, complete PEGylation cannot be reached: 25 equivalents of PEG$_{2000}$-NHS still lead to a statistical mixture of products with different amounts of PEG$_{2000}$ chains.

However, surprising in this experiment was the very low overall coverage of the proteins with PEG$_{2000}$ in comparison to the cCytC experiment described in chapter **3.2.2**. Even with 10 equivalents of PEG$_{2000}$-NHS added to the cytochrome *c*, a distinct amount of non-PEGylated protein can still be found. Comparatively, a large excess of the PEGylating agent (25 eq.) led to molecular weights of around 23 kDa only instead of 42 kDa for cCytC. This level of impact of the cationization can be explained by the increased number of amines and also indicates that the cationization of the protein allows the PEGylation of lysines that were not accessible before.

These experimental results were also supported by gel electrophoresis. As the starting material (CytC) was monodisperse, the bands of the PEGylated protein were more defined. Even the assignment to the different products with different amounts of PEG$_{2000}$ was partly possible. In comparison to the SDS-PAGE for cCytC-PEGylation (see ***Figure 20***), it is again confirmed that the molecular sizes are much smaller using native cytochrome *c* (***Figure 23***):
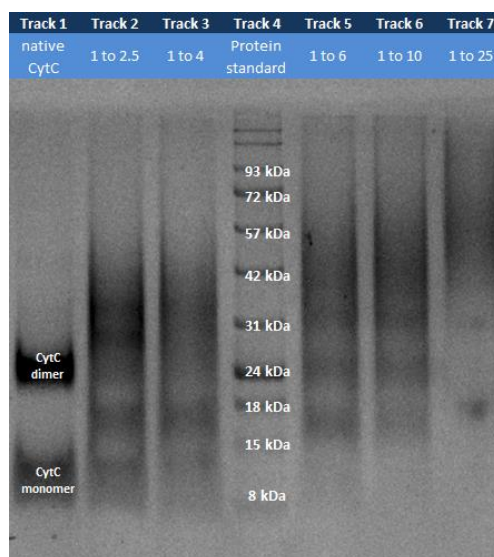
Figure 23: *SDS-PAGE after cytochrome c was treated with different amounts of PEG$_{2000}$-NHS.*

Further analysis of PEG-CytC with CD spectroscopy revealed that the impact of PEGylation on the structural integrity of the compound was relatively low. In contrast to the cationization,

the amount of α-helices and β-sheets of PEG-CytC seemed not to differ significantly from the native cytochrome C after PEGylation (see appendix, *Figure 61*).

3.2.4: Labeling and denaturation of PEG-cCytC

The primary structure of the employed cytochrome *c* contains a single cysteine at position 108 allowing monofunctionalization by maleimide/thiol chemistry.
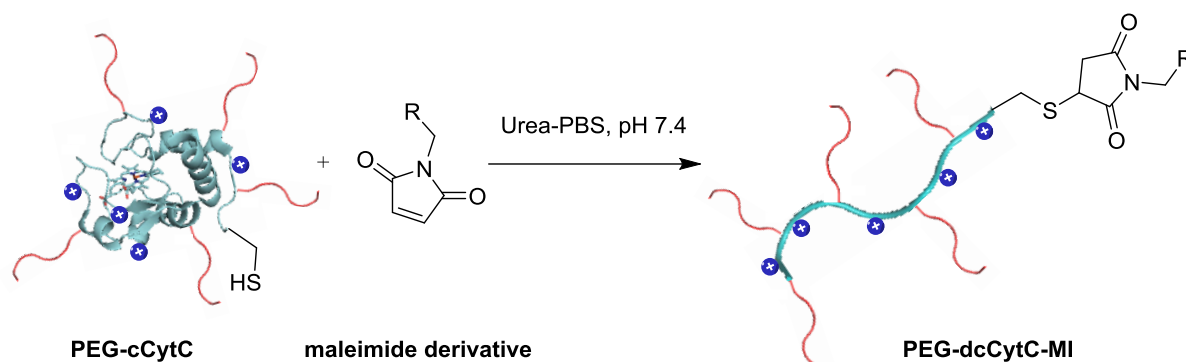
Figure 24: *Denaturation and labeling of PEG-cCytC to yield PEG-dcCytC-MI.*

At the same time, the denaturation of the protein was performed in conjunction to the monofunctionalization since the presence of the denaturation agent urea has been shown previously not to hinder the maleimide/thiol chemistry.[36] The protein was dissolved in phosphate buffer containing 5 M urea and 2 mM EDTA. This condition primarily disrupts the tertiary interaction (van der Waals, hydrogen bonds) of proteins causing its structure to open into a strand-like protein brush with a polypeptide backbone and covalently bound PEG$_{2000}$ chains. In an ideal model, the PEG$_{2000}$ chains would now be able to sterically stabilize the brush-like structure by mediating the interaction of solvent molecules to the brush. In this case, removal of the urea by ultrafiltration would not lead to a re-collapse of the architecture. However, it can be reasonable speculated that a partial refolding of the polymer-protein brush can be expected due to the non-extensive coverage of the PEG$_{2000}$ chains. For visualization purposes, figure representations of denatured protein conjugates are depicted in the idealized fashion (see *Figure 24*).

As described above, a variety of commercially available maleimide compounds can be linked to the protein. All of these molecules contain the typical $C_4H_2O_2N$ maleimide structure, but differ regarding their moieties being bound to it. In the course of this thesis, the following molecules have been linked to the protein (*Figure 25*):
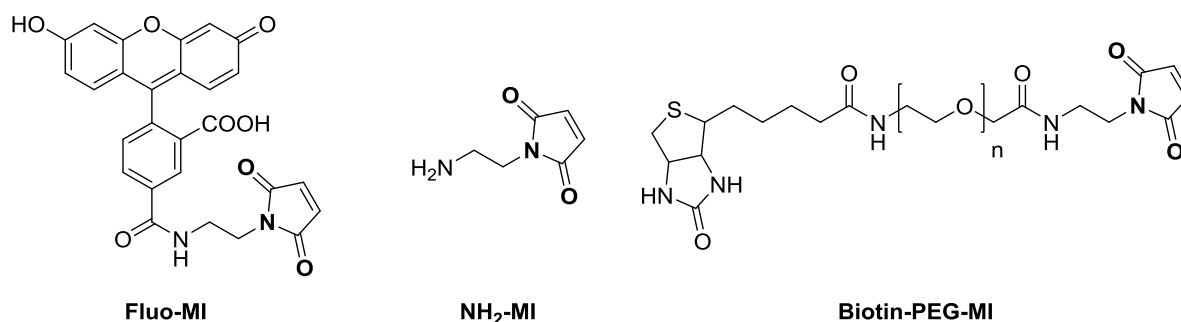
Figure 25: *Maleimide derivatives that have been linked to the protein.*

In most of the cases, fluorescein maleimide (**Fluo-MI**) was used. Fluorescence labeling of the protein brushes enhances the possibilities to further analyze the product and their subsequent derivatives. Fluorescein is a highly fluorescent compound with an excitation maximum at λ_{ex} = 492 nm and an emission maximum at λ_{em} = 520 nm. Beside its wide availability, fluorescein maleimide has the advantage that its excitation and emission do not overlap with the heme absorbance of cytochrome c (λ_{abs} = 410 nm, ***Figure 26***):
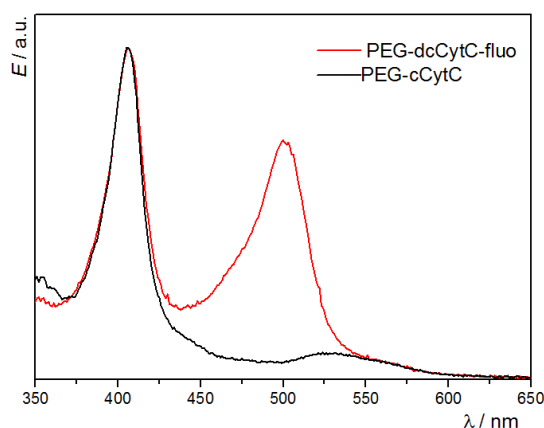
Figure 26: *UV-VIS spectra of PEG-dcCytC-fluo and its substrate PEG-cCytC.*

Similar to the PEGylation of cCytC (see **3.2.2**), the right stoichiometry between fluorescein maleimide and PEG-cCytC had to be determined. A high conversion of the cysteine is preferable, as substrate and product cannot be separated and a homogenous product is desirable. On the other hand, a large excess of the maleimide compound might also promote side reactions like amine coupling. To find a suitable stoichiometry, a fixed amount of PEG-cCytC was treated with different amounts of fluorescein maleimide and analyzed with UV-VIS spectroscopy after workup. Conversions can be calculated by entering the excitation coefficients of cytochrome c ($\varepsilon_{CytC} = 1.06 * 10^5 \frac{L}{mol*cm}$)[53] and fluorescein maleimide

$(\varepsilon_{\text{Fluo}-\text{MI}} = 0.68 * 10^5 \frac{\text{L}}{\text{mol}*\text{cm}})^{[54]}$ into the BEER's law equation (***Figure 27***):
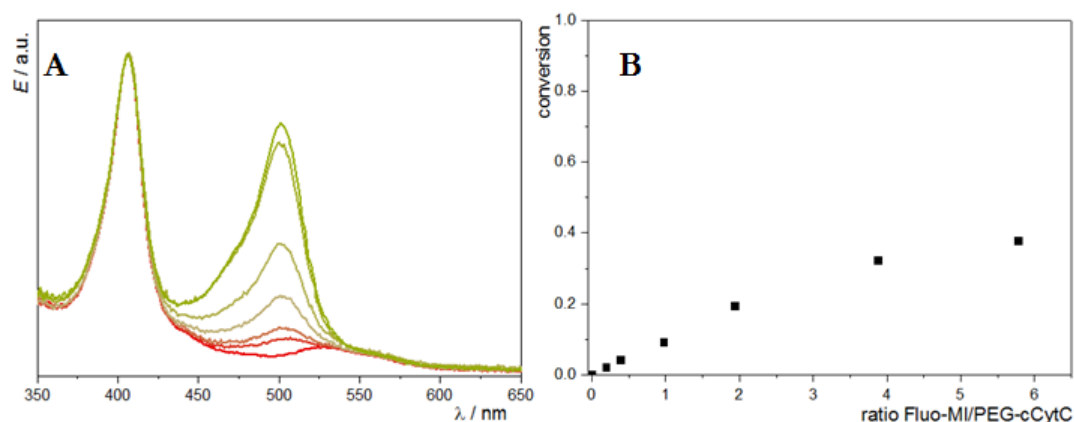
Figure 27: (***A***): *UV-VIS spectra: treating PEG-cCytC with increasing amounts of fluorescein-MI. (**B**): Increasing conversion with increasing ratio of fluorescein-MI.*

As it can be seen from the values above, conversion rates after overnight reaction are relatively low. Low conversion yields for this reaction type might be explained by steric hindrance, cysteine oxidation or the reversibility of the reaction. Regarding low overall conversion, it was decided to proceed with a mixture of converted and non-converted substrate. Characterization of the product and further steps was straightforward, as fluorescence has a significantly lower detection level than other methods like UV-VIS spectroscopy. This fact can be visualized by gel electrophoresis (***Figure 28***):

Figure 28: *SDS-PAGE with different products of the reaction scheme. Low detection level of fluorescence labeled proteins is visualized by comparing the imaging of the same gel with Coomassie staining (left) or fluorescence detection (right).*

Gel electrophoresis was able to show both, successful labeling of the protein brush and the high detection level of fluorescence-labeled proteins. In addition, by stopping the electrophoresis prematurely, complete removal of non-reacted fluorescent substrate was shown due to the absence of free molecular fluorescein at the electrophoretic front.

In a slightly altered reaction scheme, maleimide NH$_2$-MI was used instead of fluorescein maleimide. The aim was to maximize the number of potential reaction sites for further NHS modification. Introduction of the macromolecule Biotin-PEG-MI to native cytochrome C to prove monofunctionalization is described in chapter **3.4.3**. With biotin having a very high binding constant with streptavidin, introduction of this affinity tag can also be seen an example of introducing functional platforms other than fluorescent labels to the protein's surface.

3.2.5: Addition of ATRP initiators to yield the macroinitiator PEG-dcCytC-fluo-Br

While the *grafting to* strategy provides a straightforward platform for polymer-protein conjugation, the sterical demand and reactivity to connect at a macromolecular level can be a limiting factor. This becomes prominent if greater customization of the polypeptide backbone is required as we have shown that adding a large excess of PEG$_{2000}$-NHS to cCytC does not seem to push the reaction beyond a certain limit even though there are more than enough amino groups present. Hence, an alternative would be to functionalize the backbone using the *grafting to* strategy, where the amino groups can be accessed easily by small molecule initiators to yield a macroinitiator.

A macroinitiator is a macromolecule that is able to initiate polymerizations. The initiation step in ATRP reactions is the homolytic bond breaking of a C-Br bond (see **1.2.1**). For this reason, a bromine-containing molecule has to be introduced to the protein's surface.

The initiator of choice was α-bromoisobutyrate, which is a standard initiator for ATRP reactions.[55] Introduction to the protein's surface was achieved by treating PEG-dcCytC-fluo with the 2-bromoisobutanoic acid *N*-hydroxysuccinimide activated ester (see ***Figure 29***).

In contrast to other modification steps described earlier, the highest possible coverage of the protein with initiators subsequently leading to a high density of polymers growing from the protein backbone was desired.
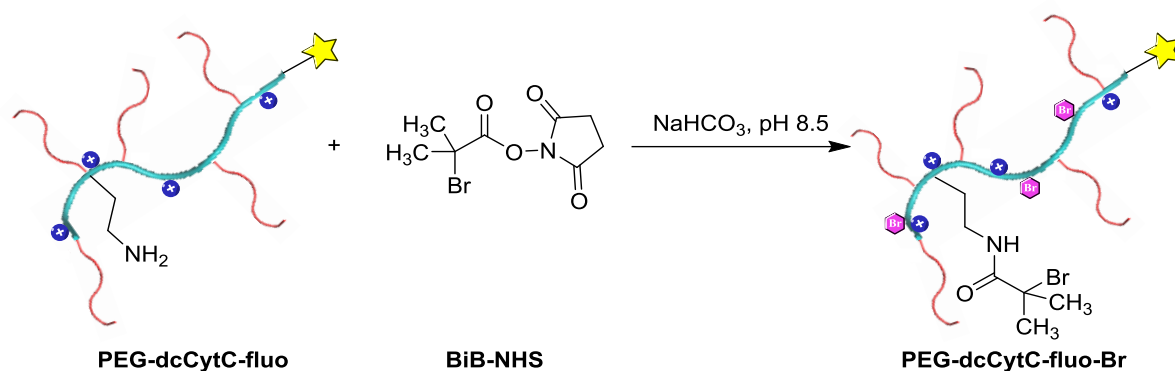
Figure 29: *ATRP initiator α-bromoisobutyrate is linked to the protein's surface.*

Quantification of the initiators that were transferred to the protein revealed to be difficult. The α-bromoisobutyrate unit contributes to the whole mass (~25 kDa) with only 150 Da. For this reason, statements on the exact number of initiators can't be made based on MALDI-ToF MS. On the other hand, if 10 initiators were transferred, the mass increase of 1.5 kDa should be visualizable. However, MALDI-ToF MS spectra did not show the expected mass increase. In contrast, many of the experiments revealed lower molecular weights for the macroinitiator PEG-dcCytC-fluo-Br than for its substrate PEG-dcCytC-fluo (***Figure 30***):
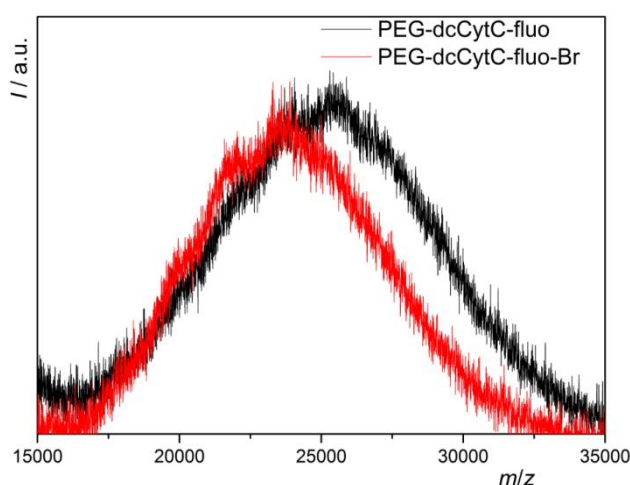
Figure 30: *The macroinitiator PEG-dcCytC-fluo-Br shows lower m/z values in MALDI-ToF MS analysis then its substrate PEG-dcCytC-fluo.*

While the observation is unexpectedly surprising, a possible explanation for this observation lies in the principle of the MALDI-ToF MS measurements. For being detected by the mass detector, the molecules need to be ionized first. The ionization potential varies a lot between charged macromolecules (like cCytC and other derivatives) and uncharged ones. If most of

the cationic amines of PEG-dcCytC-fluo were transferred to amides, the product PEG-dcCytC-fluo-Br would have a net charge close to zero. This way, it might show different behavior in MALDI-ToF MS measurements than the polycationic macromolecules did before.

To prove that α-bromoisobutyrate functionalization was successful, an alternative characterization *via* the fluorescamine assay was used instead in order to qualitatively determine the extent of free primary amines within the system.

3.2.6: Characterization of functional groups (fluorescamine assay)

The spiro compound fluorescamine was introduced by *Weigele et al*. in 1972 as a new fluorogenic compound 'for the detection of primary amines in the picomole range'. Reaction with amines 'almost instantaneous at room temperature in aqueous media' were emphasized and it was pointed out, that the 'products are highly fluorescent, whereas the reagent and its degradation products are nonfluorescent'.[56] The fluorescamine assay can be used for protein quantification as an alternative to the BRADFORD assay or the LOWRY assay.[57-58] Its selective reaction with primary amines can also be used to 'count' lysines and those ones that arose from the cationization of glutamate and aspartate. In the context of this work, this allows conclusions to be drawn on the extent of protein modification. The reaction of fluorescamine with primary amines can be illustrated as follows (***Figure 31***):
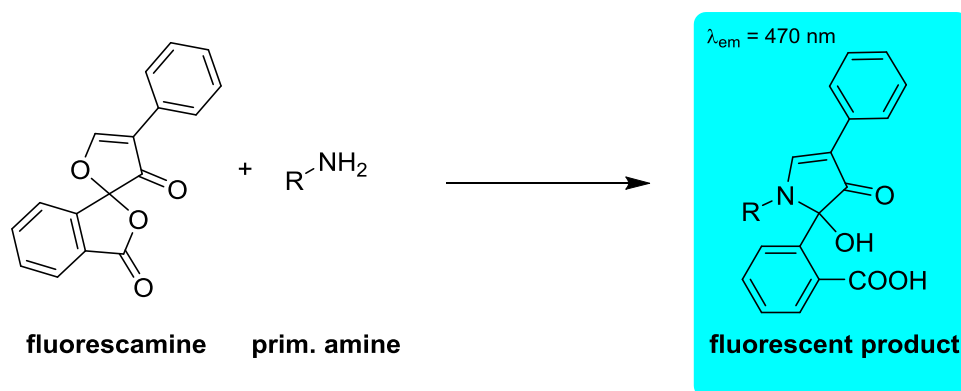
Figure 31: *Reaction of fluorescamine with a primary amine to yield a fluorescent product.*

Results of the fluorescamine assay for different cytochrome *c* derivatives are illustrated in ***Figure 32***. Experimental setup, data basis and calculation are demonstrated in chapter **5.6.1**.
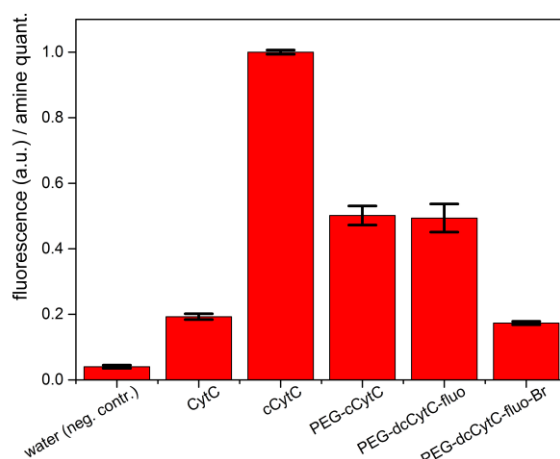
Figure 32: *Results of the fluorescamine assay for different cytochrome c derivatives.*

The results displayed above generally match with the expectations. As described by *Weigele et al.*, aqueous hydrolysis of fluorescamine does not lead to a fluorescent product. Still, a negative control with water only was conducted to determine the basic emission at 470 nm. Cytochrome *c* can be used as a reference as it contains 17 lysines plus its N-terminus. The increase in fluorescence for cCytC is surprisingly high. As this is highly reproducible, this might indicate the limitation of the fluorescamine assay. A possible explanation is that the polycationic properties of cCytC might accelerate the assay reaction or that the specific protein environment may enhance the emissive properties of the reaction product. Regardless, a significant increase of amines is definitely expected and shown. PEGylation leads to a decrease in fluorescence, as many formerly available primary amines were converted into amides. Denaturation of the protein alone does not change the number of amines, which is also displayed in ***Figure 32*** with no significant difference in fluorescence between PEG-cCytC and PEG-dcCytC-fluo. In the end, the addition of the initiator affects the number of amines in the same way as PEGylation does. The expected decrease in fluorescence is confirmed in the assay.

In summary, the fluorescamine assay is a suitable tool to show relative changes in the amount of amines during the different modification steps. The trend of fluorescence/number of amines matches the expectations. However, statements of the exact quantity of amines can't be made, as the polycationic cCytC seems to behave differently than the native cytochrome *c*.

3.3 Brush synthesis by Cu-catalyzed AGET ATRP

3.3.1: Idea/Introduction of the chosen system

PEG-dcCytC-fluo-Br was subsequently used as a macroinitiator in an AGET ATRP. Analogously to previous studies in the WEIL group on HSA-based macroinitiators, the α-bromoisobutyrate building blocks allow *grafting* polymers *from* the protein surface.
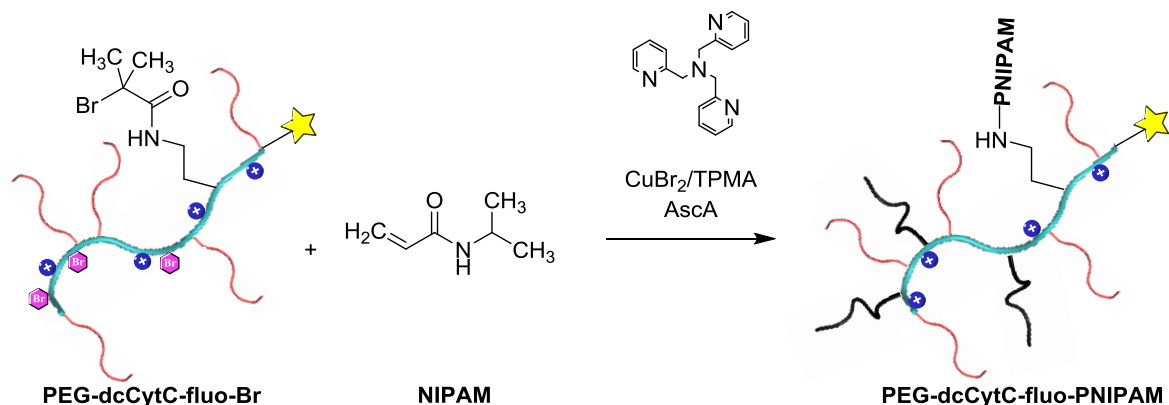
Figure 33: *AGET ATRP on the surface of the protein to yield PEG-dcCytC-fluo-PNIPAM.*

Growing polymers under biologically relevant conditions has emerged growing interest (see **1.2.3**). ATRP requires transition metals, in most cases copper compounds with organic ligands, as catalysts. In this present work, $CuBr_2$/TPMA was used as the catalytic system (see ***Figure 33***). TPMA, tris(2-pyridylmethyl)amine has the advantage of promoting fast ATRP reactions (high K_{ATRP}, see **1.2.1**) on the one hand, while still providing elevated level of control on the other hand (high K_{deact}).[59] Water is known to be one of the 'fastest' ATRP solvents and to accelerate ATRP.[60] As future studies might aim for introducing substrates into living systems and to polymerize brushes in biological environments, an additional aim is to conduct the polymerization at room temperature.

3.3.2: Setup, reaction control and monomer scope

Before starting the reaction, different requirements had to be fulfilled to enable reaction control and further analysis of the polymer-protein hybrid. ^{1}H NMR spectroscopy was chosen as the method of choice to monitor the reaction process. For this reason, all reactions were performed in D_2O. As oxygen would lead to radical quenching, air had to be removed from all flasks and solvents by repetitive freeze-pump-thaw cycles.

In a standard experimental setup, the macroinitiator, the catalyst and the monomer were

dissolved in D$_2$O and oxygen was removed. A typical ratio of monomer/protein/ catalyst/ascorbic acid was 532/1/5/46 calculated per protein. If an equal number of initiators per protein is assumed, that ratio can also be displayed as monomer/initiator/catalyst/ascorbic acid 106/1/1.2/9. The reaction was started by dropwise addition of ascorbic acid (in aqueous solution). At time intervals, samples were taken out by means of a syringe and monomer conversion was analyzed by ^{1}H NMR spectroscopy. Determination of conversion did not demand external NMR standards: spectra were normalized using the sharp CH$_2$ singlet of the PEG$_{2000}$ chains ($\delta = 3.70$ in D$_2$O) as the constant NMR peak.

When the desired polymer brush size was achieved, the reaction was quenched by exposing it to air. In theory, by non-ATRP caused radical formation, growth of polymers could have occurred in solution instead of polymers being covalently bound to the protein. This had to be excluded. After determining final conversion with ^{1}H NMR, the raw material was applied to a *Sephadex* column (G50 or G75). By collecting the sharp red protein fraction only and repeating ^{1}H NMR measurements, covalent binding of polymer and protein was shown.

Surprisingly, the polymer-protein hybrids gave prominent signals in MALDI-ToF MS. This finding was in contrast to earlier studies in the WEIL group on HSA brushes, where brush size analysis harnessing this method was not possible. This way of proving covalent polymer-protein conjugation can be exemplified by comparing the MALDI-ToF MS spectra of the macroinitiator and the product, a PNIPAM-protein hybrid (***Figure 34***):

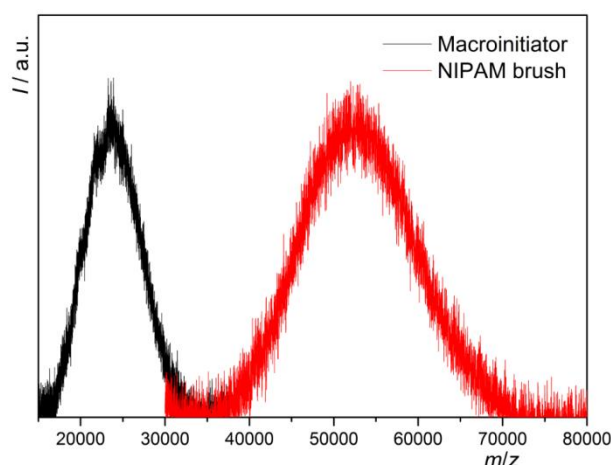***Figure 34:*** *MALDI-ToF MS spectra of the macroinitiator PEG-dcCytC-fluo-Br and a synthesized PNIPAM-protein brush with an average size of 53 kDa.*

Due to this attractive way to analyze and prove polymer growth, NIPAM was chosen as the standard monomer in subsequent *grafting from* polymerizations.

As it can be seen from ***Figure 34***, the full width at half maximum of the brush is enhanced in

comparison to the macroinitiator. Still, that difference was lower than expected and based on the dispersity levels displayed in those MALDI-ToF MS results, one could still speculate that there is a certain level of control over the polymerization.

To enable the engineering of the nanoscale architecture, the capability to control the size of the resulting brush by optimizing reaction setup is a fundamental issue. Possible variables were reaction time, monomer concentration and the amount of ascorbic acid. Altering the amount of ascorbic acid in the range from 4.0 to >15 equivalents did not result in a significant acceleration of the reaction. This indicated that the amount of reducing agent does not play a key role regarding reaction kinetics. Meanwhile, doubling the concentration of NIPAM which, in principle, doubles the monomer/initiator ratio resulted in faster brush formation and larger brush sizes. The results of different experiment setups are summarized in **_Table 3_**:

Table 3: Synthesis of Cu-catalyzed PNIPAM-protein brushes. NIPAM/protein ratios are calculated based on NMR conversion or on MALDI-ToF MS analysis results.

JG	molar ratio NIPAM:prot.	reaction time	conversion (NMR)	NIPAM/prot. (NMR)	m/z (MALDI)	NIPAM/prot. (MALDI)
126	532:1	o.n.	57%	300:1	55 kDa	275:1
133	532:1	2.5 h	34%	180:1	49 kDa	220:1
137	1064:1	2.5 h	51%	540:1	86 kDa	550:1
144	1064:1	2 h	48%	510:1	73 kDa	430:1
154	532:1	0.5 h	29%	150:1	41 kDa	150:1
203	1187:1	1.5 h	35 %	420:1	66 kDa	380:1

As it can be seen from the table above, sizes calculated based on NMR and those measured by MALDI-ToF MS were in good agreement. This indicates the low degree of 'free polymer' side product in solution.

After having synthesized PNIPAM-protein brushes of different sizes in the range from 40 to 90 kDa, the attention was focused on monomer scope. As the water solubility remains a critical part of the project, the range of possible monomers was limited to a small selection.

Figure 35 shows the most relevant monomers for radical polymerization in aqueous solution. Examples from the different monomer subclasses methacrylates, acrylates, acrylamides and styrenes are shown.

DMAA, which is structurally closely related to NIPAM, gave similar results as observed before. On average, the synthesized brushes had lower molecular weights than for NIPAM, even if longer reaction times or higher monomer concentrations were applied.
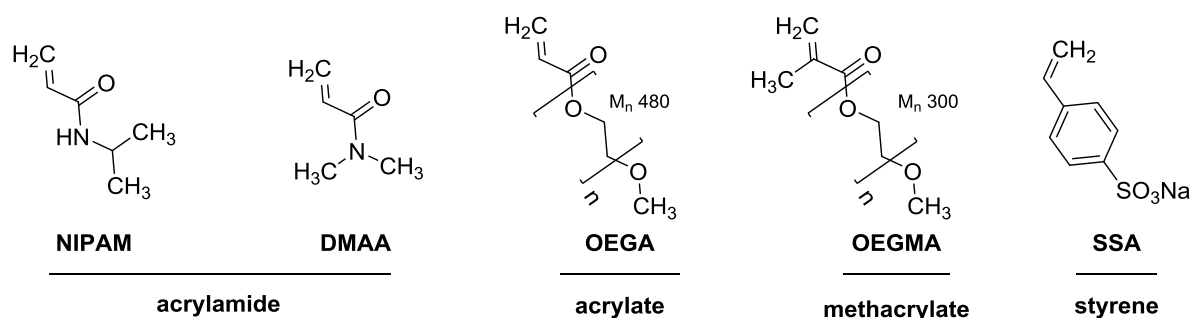
Figure 35: *Examples for water-soluble ATRP monomers from different subclasses.*

Monomers of other subclasses, in this case oligo(ethylene glycol) methyl ether methacrylate (OEGMA) and oligo(ethylene glycol) methyl ether acrylate (OEGA), were also polymerized on the surface of the macroinitiator. As their NMR peaks overlapped with the PEG$_{2000}$ peak, DSS (sodium 3-sulfopropyltrimethylsilane) was used as an external, water-soluble conversion standard. In contrast to the acrylamides described above, MALDI-ToF MS peaks of these bottle brush polymers could not be obtained. This finding was in agreement with earlier studies on these monomers in the WEIL group. In addition, it was found that – under similar reaction conditions – POEGA- or POEGMA-brushes formed with similar or even higher reaction speed than in the PNIPAM or PDMAA case. This was unexpected regarding their bulkiness and seems to be in contrast to the principle mechanism of ATRP (see **1.2.1**). Here, one would expect that better stabilization of the carbon radical species should decelerate the polymerization.[61] That way, for ATRP monomers can be ordered according to the expected reaction speed: acrylamides > acrylates > methacrylates > styrenes. As this was not the case for the synthesized brushes, it has to be questioned whether AGET ATRP mechanisms apply for this brush synthesis.

Reaction conditions and results are summarized in ***Table 4***:

Table 4: *Synthesis of CuBr$_2$-catalyzed polymer-protein brushes with different monomers. Polymer/protein ratios are calculated based on NMR conversion or based on MALDI-ToF MS analysis results (if mass peaks were available).*

JG	molar ratio monomer:prot.	reaction time	conversion (NMR)	monomer/prot. (NMR)	m/z (MALDI)	monomer/prot. (MALDI)
			DMAA			
210a	1000:1	1 h	15%	150:1	**31 kDa**	80:1
			OEGA			
210b	1000:1	1 h	46%	460:1	-	-
			OEGMA			
210c	1000:1	1 h	86%	860:1	-	-

3.3.3: Brush analysis

After the workup of the crude material by *Sephadex* chromatography and ultrafiltration, the physical properties of the brushes were investigated.

DOSY (diffusion-ordered spectroscopy) NMR allows the interpretation on the hydrodynamic size of the brushes. In this two-dimensional NMR technique, the diffusion coefficient D of the analyte is plotted against its ^{1}H NMR spectrum. As reported, addition of a water-soluble NMR standard with a reference size (1,4-dioxane: 0.212 nm) allows the translation of the diffusion coefficient to the hydrodynamic radius R_0 using the Stokes-Einstein equation.[62] Simply put, the R_0 of a PNIPAM-protein brush with a size of 55 kDa at room temperature was calculated as follows (for DOSY NMR see appendix, ***Figure 58***):

$$R_{0,\text{brush,r.t.}} = \frac{D_{\text{dioxane}}}{D_{\text{brush}}} \cdot R_{0,\text{dioxane}} = \frac{10^{-8.914}}{10^{-10.495}} \cdot 0.212 \text{ nm} = 8.1 \text{ nm}$$

As such, the hydrodynamic diameter of the polymer-protein hybrids was determined to be around 16 nm in average. Particles of this size are big enough to be visualized harnessing microscopy methods like atomic force microscopy (AFM) or transmission electron microscopy (TEM, ***Figure 36***):
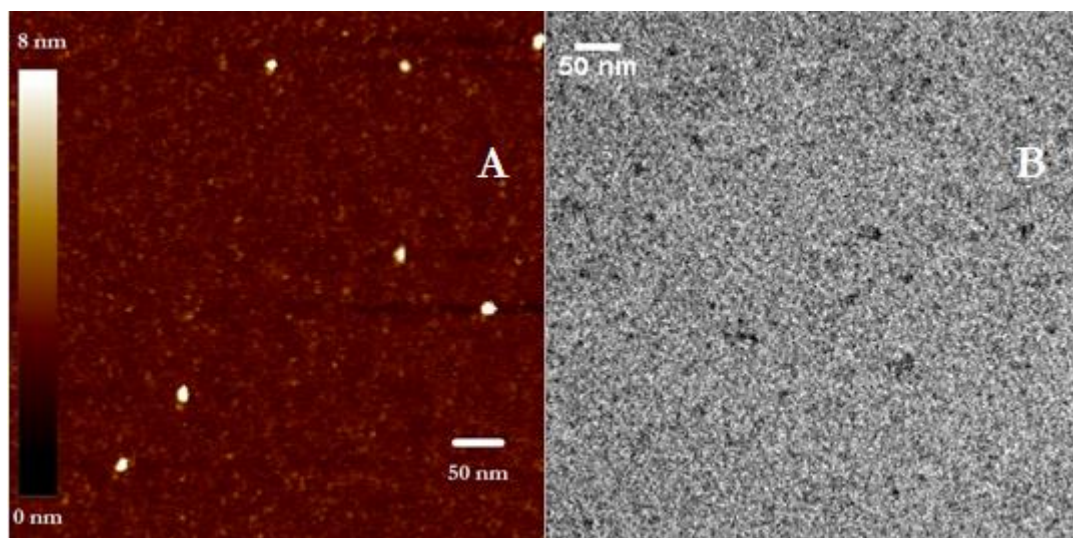
Figure 36: *AFM (**A**) and TEM (**B**) images of a PNIPAM-protein brush of ~55 kDa. Average molecular sizes were determined to be in the range of 10 – 15 nm.*

Further studies on the size of those PNIPAM-protein hybrids were done harnessing dynamic light scattering (DLS). However, because of protein aggregate formation, reproducible results of tested derivatives – native cytochrome *c*, macroinitiator or polymer-protein brushes – could not be obtained within the time frame of this thesis.

3.4 Tailoring functional protein brushes into precision nanosystems

3.4.1: Potential use of synthesized protein derivatives in redox catalysis: ABTS assay

In previous chapters, the chemical modification of cytochrome *c* was described. A building block with a polymer-protein hybrid material as a scaffold and a catalytic core containing a heme was obtained. In following experiments, the aim was to prove that the metalloprotein scaffold has conserved its intrinsic biological function.

As described above (see **1.1.2**), nature has exploited the electronic properties of iron in metalloproteins for catalyzing different reactions. Moreover, organic chemists have recognized and shown the potential of iron as a redox catalyst for functional group transformation as well as even radical polymerizations.[22] For this reason, the introduction of the brushes in redox systems was an evident choice. ABTS is the abbreviation for the diammonium salt of 2,2'-azino-bis(3-ethylbenzothiazoline-6-sulphonic acid) and is displayed in *Figure 37*:
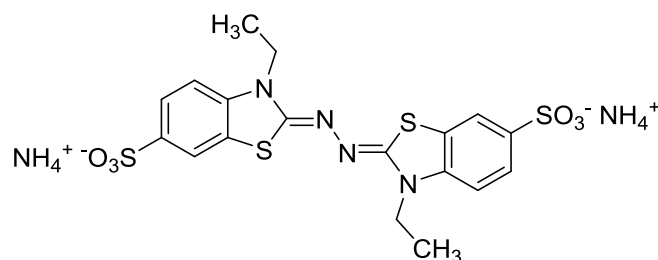
Figure 37: *Structural formula of ABTS.*

The ABTS assay was introduced by *Milner et al.* in 1993.[63] Exploiting an adjusted protocol by *Seidler et al.* from 2017, this assay allows investigating the ability of metalloproteins to catalyze hydrogen peroxide's oxidation of ABTS to form a blue-green radical cation.[64]

The basic reaction of the ABTS assay is displayed in *38*. The ability of activating hydrogen peroxide should correlate with the versatility of those metalloproteins to catalyze redox reactions in other chemical systems.
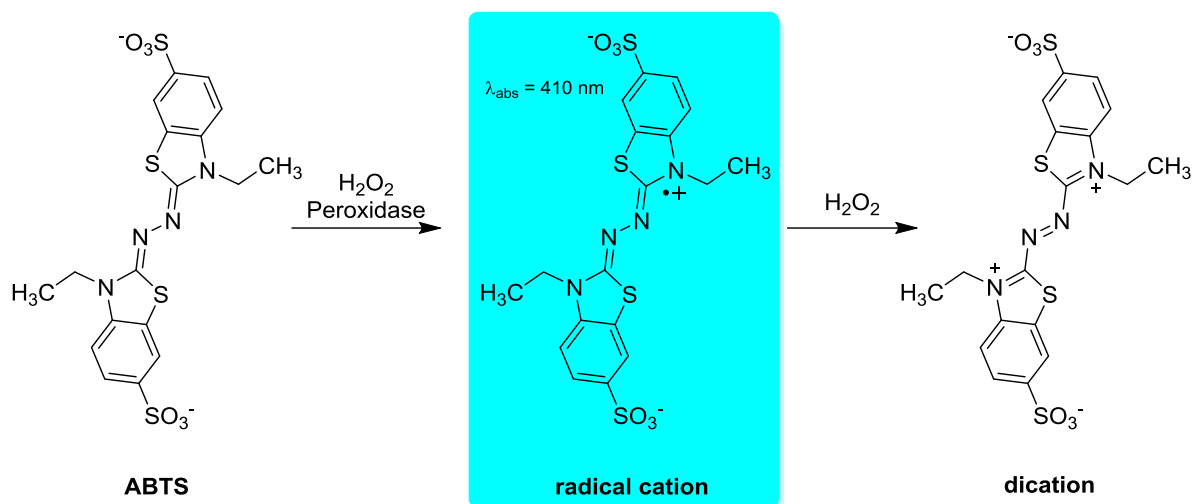
Figure 38: *Principle of the ABTS assay.*

In first experiments, native cytochrome *c* and synthesized derivatives were analyzed to answer the question, whether peroxidase properties are preserved after protein modification. After addition of ABTS and hydrogen peroxide to the protein solution, the absorption at $\lambda = 410$ nm was determined over a course of 45 min.
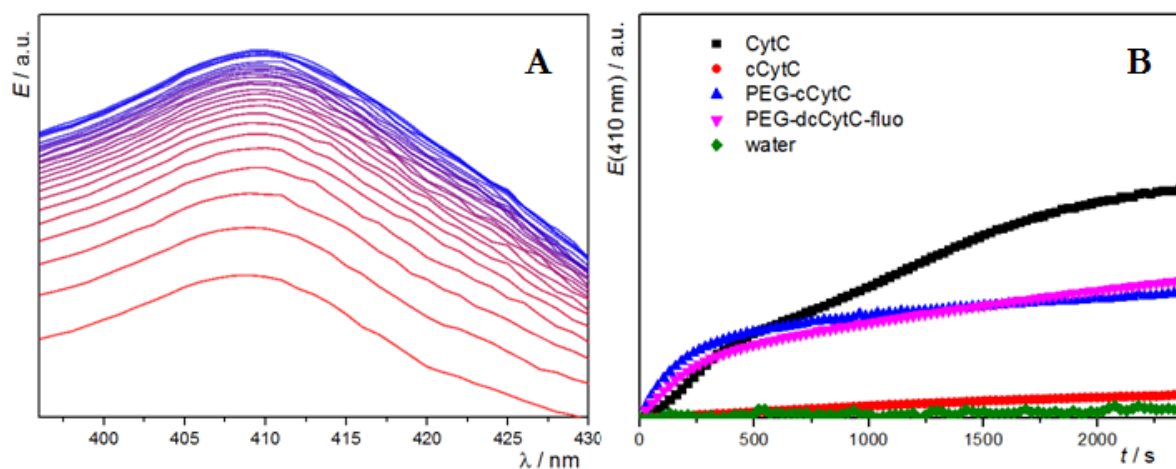
Figure 39: *(**A**): UV-VIS spectra around $\lambda = 410$ nm during the course of the ABTS assay with PEG-cCytC. Spectra were measured periodically after 52 seconds. (**B**): Absorption at $\lambda = 410$ nm for different catalysts during the ABTS assay.*

As it can be seen from ***Figure 39***, peroxidase activity of cytochrome *c* is preserved after functionalization for the PEGylated and cationized metalloprotein before (PEG-cCytC) and after denaturation (PEG-dcCytC-fluo). Both of the derivatives show the expected hyperbolic trend. In comparison the native cytochrome *c*, they seem to have a lower peroxidase activity, as this graph shows a higher slope. Still, peroxidase activity was shown to be present for both of the modified metalloproteins. It is important to note that the addition of ABTS to a solution

of cCytC instantly resulted in a turbid solution. An interaction between the polycation cCytC and the anionic ABTS was assumed, which made the analysis of enzyme activity impossible.

In summary, the preservation of the capability of the protein to catalyze redox reaction after modification was shown. Further ABTS assay analysis of the polymer-protein brushes will be part of chapter **3.4.2**, where temperature effects are included.

3.4.2: PNIPAM-protein brushes: potential temperature-controllable biocatalysts?

Ideally, the synthesized protein-PNIPAM brushes can be integrated in nanosystems as precise building blocks with properties switchable upon temperature. Temperature-dependency was supposed to be incorporated into the system by growing polymers on the protein's surface that possess LCST properties at moderate temperatures. The polymer-of-choice in this context was poly(*N*-isopropylacrylamide), showing LCST properties in water at 32 °C. An interesting model of an intelligent and self-limiting catalyst that might be realized by follow-up works of this thesis is displayed in the following graphic (***Figure 40***):
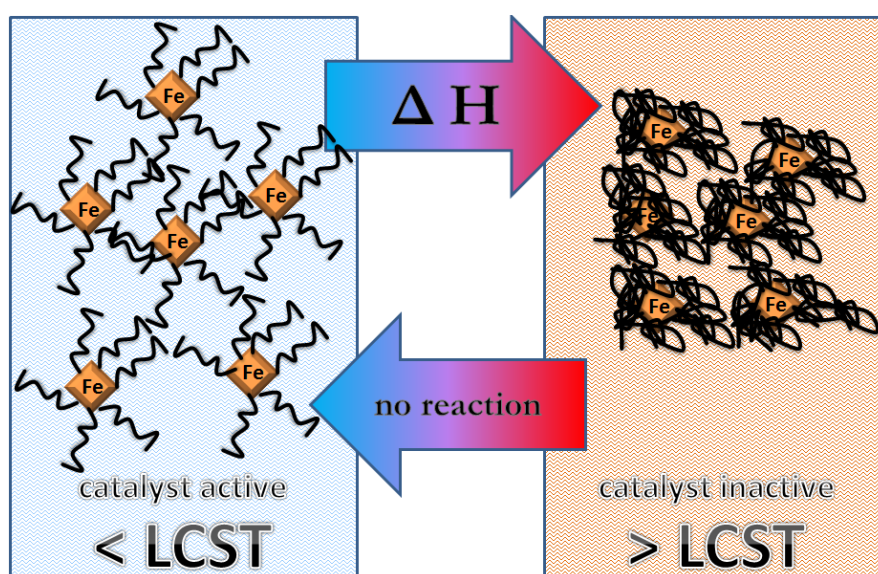
Figure 40: *Idea of an intelligent catalytic system using PNIPAM-protein brushes.*

A given exothermic reaction converts the substrates A + B to their products C + D; the heme groups of the polymer-protein brushes serve as catalysts. This equilibrium is far on the side of C + D and the reaction produces heat. If the solution warms up above the LCST temperature in the course of the reaction, the catalytic capacity of the brush drastically decreases as the heme is out of range for the substrates. When the reaction is slowed down, the temperature acclimatizes and the brushes redissolve to restart the cycle.

3 RESULTS AND DISCUSSION

If a solution of PNIPAM in water is warmed above 35 °C, precipitation is visible by naked eye (see **3.5.2**). In an aqueous solution of the PNIPAM-protein brush, precipitation was not observed within the tested temperature range (r.t. – 60 °C). This finding was in agreement with different examples in literature, where no sharp LCST behavior was found when PNIPAM brush systems were heated above expected LCST temperatures.[65-67]

A first approach to test temperature-dependency on a molecular level is an ABTS assay (see **3.4.1**) under alternating temperature conditions. A PNIPAM-protein brush with an overall size of 55 kDa served as a catalyst. A PDMAA-protein brush which should not show LCST behavior at the temperatures applied was synthesized to serve as a negative control. Reactions were conducted at 28 °C (<LCST) and respectively at 40 °C (>LCST).
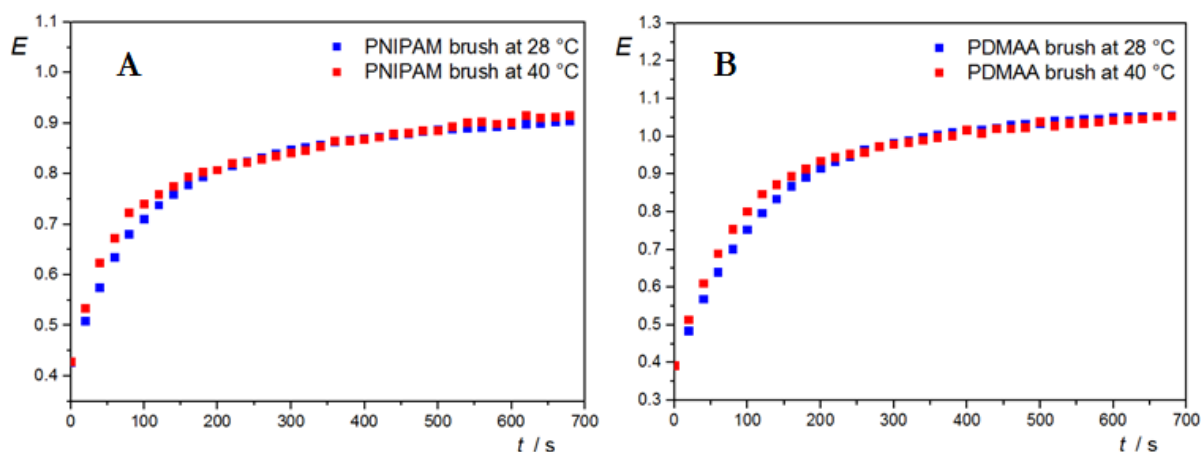
Figure 41: *ABTS assay catalyzed by a PNIPAM- (**A**) or a PDMAA-protein brush (**B**) at elevated temperatures.*

As those data in ***Figure 41*** reveal, the experimental results did not indicate a collapse of the polymer-protein hybrids at 40 °C. The velocity of the reaction was not slowed down, but accelerated a little bit for both cases, PDMAA and PNIPAM. Acceleration of the reaction might be explained by the RGT rule/van't-Hoff equation.

In summary, the ABTS assay at elevated temperature did not allow the conclusion that the catalytic capacity of the brush can be controlled by the LCST.

Afterwards, the temperature-dependent behavior of the 55 kDa protein brush was investigated harnessing ^{1}H NMR spectroscopy. Spectra of the sample were recorded sequentially at room temperature, at 40 °C and again at room temperature. Here, elevated temperature did not change the shape of the spectra; peak broadness was not significantly increased. This supported the results described above, that there was no macroscopic LCST-caused precipitation at 40 °C.

Still, brush collapse on an intramolecular level was possible. To investigate this issue, temperature-dependent DOSY NMR measurements (see **3.3.3**) were performed. This allowed comparing the hydrodynamic radius at room temperature and 40 °C: If a collapse of the PNIPAM chains of the brushes occurs, the hydrodynamic radius should decrease in comparison to the size of 8.1 nm calculated above.

$$R_{0,\text{brush},40\,°C} = \frac{D_{\text{dioxane}}}{D_{\text{brush}}} \cdot R_{0,\text{dioxane}} = \frac{10^{-8.591}}{10^{-9.966}} \cdot 0.212 \text{ nm} = 5.0 \text{ nm}$$

While heating of the system led to certain distortion of the DOSY spectra, a significant decrease of the brush size of can be seen indeed (for DOSY NMR see appendix, ***Figure 59***). After cooling down, the size radius of the brush was determined to be around 7.6 nm, indicating a partly reversible switching of the polymer-protein brush size by temperature effects (for DOSY NMR see appendix, ***Figure 60***).

Further investigation of the brush sizes using temperature-dependent light scattering experiments was again complicated by the formation of aggregates to a minor amount, still interfering with the measurements.

3.4.3: Monofunctionalization of C-108 in the protein's primary structure

As described in chapter **3.1.1**, cytochrome *c* from *Saccharomyces cerevisiae* was chosen as the protein scaffold, where the amino acid C-108 is of special interest. Both of the other cysteines in the protein's primary structure, C-20 and C-23, are covalently blocked due to their binding of the heme as the protein's prosthetic group. This way, C-108 allows the introduction and linkage of functional molecules at a single and defined position.

In the course of this thesis, the potential of monofunctionalization by maleimide chemistry (see **3.2.4**) was investigated. Thus, native cytochrome *c* was linked to molecule that allowed drawing conclusions on reaction parameters like yield or specificity during the course of the reaction. The maleimide linker of choice was Biotin-PEG-MI (***Figure 42***):

$M_n \sim 5000$ g/mol
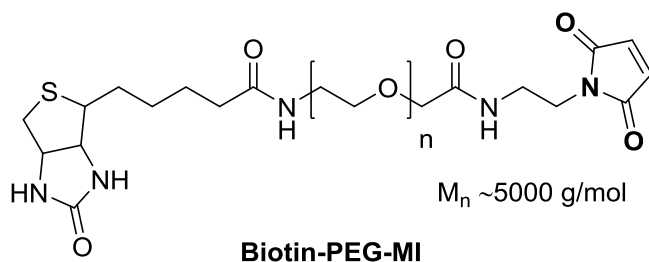
Biotin-PEG-MI

Figure 42: *Chemical structure of the maleimide compound Biotin-PEG-MI.*

With its average molecular size of ~5 kDa, linkage of this macromolecule with native cytochrome *c* (12.6 kDa) leads to a significant increase of the protein's molecular mass.

A tenfold excess of the maleimide linker was mixed with the protein. The course of the reaction was monitored by MALDI-ToF MS with special interest in possible appearance of *m/z* peaks with the size of ~17.6 kDa (monofunctionalization) or ~22.6 kDa (reaction with amines). It turned out that the reaction of these two macromolecules was very slow. The peak proving monofunctionalization was visible after one hour and kept growing during the course of the reaction. After three days, also a second, very small peak at 22.5 kDa, indicating the existence of protein reacted with two building blocks, was visible (***Figure 43***):
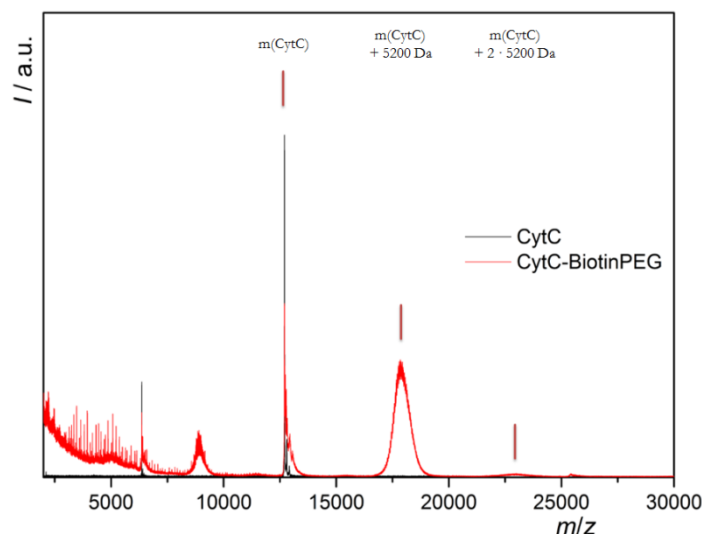
Figure 43: *MALDI-ToF MS spectra of native cytochrome c (black)
and after one week of reaction with Biotin-PEG-MI (red).*

All MALDI-ToF MS experiments were conducted under the same conditions. Since the outcome of every experiment depends a lot on sample preparation and ionization, a kinetic profile of the reaction is not achievable.

As the observed peak at 22.5 kDa indicating bifunctionalization is more or less negligible, monofunctionalization of the compound can be shown in principle. As expected, non-reacted

cytochrome *c* was still visible. This might partly be explained by back reaction during the harsh conditions of the MALDI-ToF MS measurements. Due to biotin's affinity towards streptavidin, affinity purification against a streptavidin loaded stationary phase has been widely shown to be a reliable methodology to isolate the monofunctionalized product.

3.5 Cytochrome *c* and derivatives as ATRPases: linear polymer synthesis

3.5.1: ATRPases and polymerization experiments with native cytochrome *c*

In nature, metalloproteins – many of them with enzymatic functions – are very diverse and undertake a broad range of tasks (see **1.1.2**). However, enzymes can also be applied in synthetic chemistry should their mechanism fit within the framework of a designated chemical reaction. In a representative example, *Bruns et al.* (2011) took horseradish peroxidase (HRP) completely out of its biological context and exploited it to catalyze ARGET ATRP.[24] In nature, peroxidases catalyze the reduction of peroxides. In the context of ATRP, the iron-containing heme was harnessed for the initiation of the bond breakage between carbon and bromine (see **1.2.1**).

Supported by a series of studies, Bruns discovered this biodegradable ATRP catalyst and coined the term 'ATRPase'. Since then, different iron-containing enzymes with catalytic potential for ATRP have been described. In subsequent work, *Bruns et al.* showed ATRP catalysis by hemoglobin or even by human blood (2013).[26] *Matyjaszewski et al.* simplified the system and exploited a modified heme without a protein scaffold to yield polymers with narrow distribution.[27] However, it is intriguing that cytochrome *c* has not been described to show catalytic behavior in ATRP even though it possesses a heme that demonstrates peroxidase type activity.

In a first approach, we attempted to polymerize NIPAM with cytochrome *c* analogously to a protocol from *Bruns et al.* for catalysis with HRP (***Figure 44***):[24]
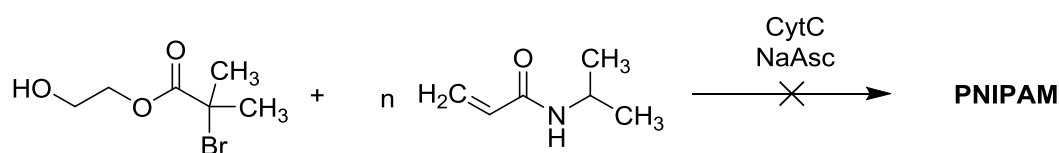
Figure 44: *PNIPAM synthesis catalyzed by cytochrome c based on a protocol by Bruns et al. No conversion was observed.*

Bruns et al. harnessed the water-soluble ATRP initiator 2-hydroxyethyl 2-bromoisobutyrate for growing linear polymers in buffer solution. A special feature of these polymerizations is the very low amount of catalyst (3.4 mol% with reference to the initiator). The reaction was started upon the addition of sodium ascorbate. In this present work, cytochrome *c* was applied in the same way as HRP to yield PNIPAM. Upon the addition of sodium ascorbate, the solution color turned from deep red to pink. That was in contrast to the brown color that *Bruns et al.* had observed for the HRP or hemoglobin catalytic system. In addition, ^{1}H NMR monitoring of the reaction did not show any polymer formation.

In the next step, reactions with HRP were used as a positive control and performed alongside cytochrome *c*. Here, the color change from deep red to brown for HRP in contrast to the pink coloration of cytochrome *c* became obvious (***Figure 45***):
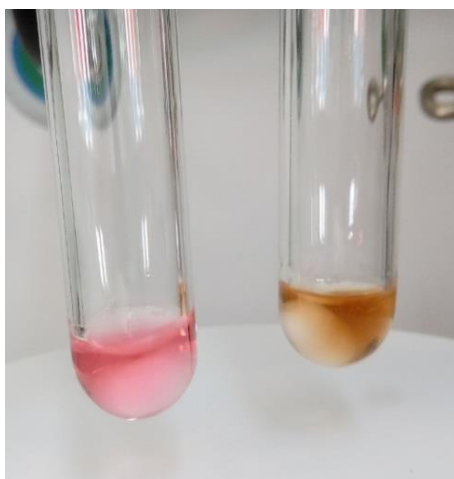
Figure 45: *Cytochrome c (left, pink) and horseradish peroxidase (right, brown) after addition of sodium ascorbate.*

The experiment supported the first results, polymer formation was only observed in the (brown) HRP containing reaction vessel. Based on these results, native cytochrome *c* did not seem to be able to catalyze ATRP under the applied conditions. The next attempts followed another protocol published by *Bruns et al.* in 2013 in which hemoglobin was described as an ATRP catalyst with MQ water as a solvent and ascorbic acid as reducing agent.[26] Nonetheless, polymerization did not take place upon these conditions.

The aforementioned results are perplexing since, for all the proteins investigated by *Bruns et al.*, the heme that is directly participating in the ATRP mechanism is largely similar among them. Nonetheless, the observation of the apparent difference in color upon treatment with sodium ascorbate led us to investigate the heme in greater detail.

3.5.2: Impact of cationization on cytochrome *c*'s catalytic behavior

By analyzing the heme complex among the aforementioned proteins, the axial ligands of cytochrome *c*'s heme constitute the main difference. As described in **1.1.3**, these ligands are primarily tailoring iron's electron density and therefore enable the metalloproteins to fulfill their specific biological tasks. To be able to catalyze reactions and convert substrates, the iron cations of metalloenzymes (like hemoglobin or HRP) are situated in a high-spin and five-coordinate state with an open coordination site. In contrast, cytochrome *c*, having no enzymatic function, has no intrinsic biological interaction with substrates and is situated in a low-spin, six-coordinate state without further coordination possibilities (***Figure 46***):
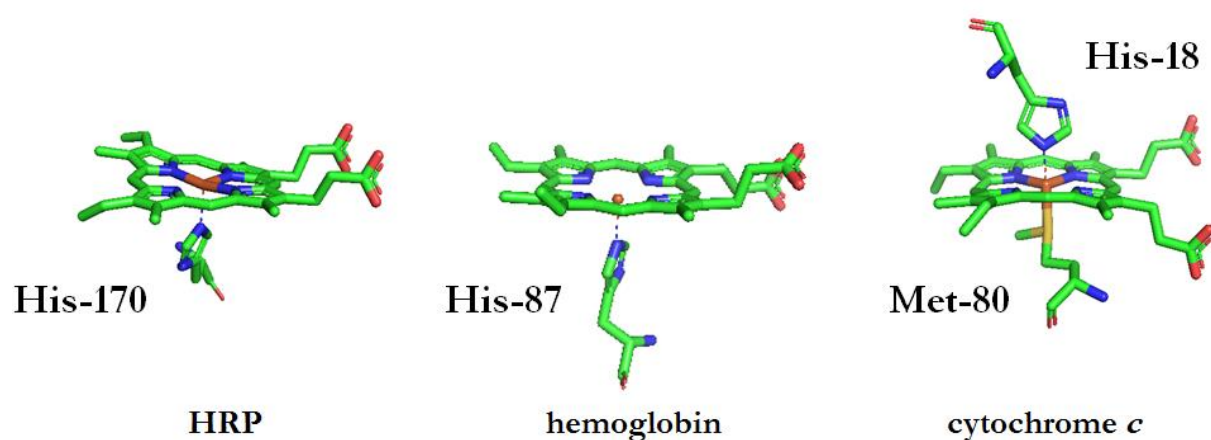
Figure 46 : *Heme ligation in horseradish peroxidase [1ATJ], hemoglobin [1A00] and cytochrome c [1CHH].*

Lack of coordination possibilities might be the reason for the lack of ATRPase functionality for cytochrome *c*. As the protein structure is the integral part of the ligand environment, we hypothesized that the earlier observed changes in secondary structure of the protein upon chemical modification (see **3.2.1**) should have an impact on the heme complex.

In a preliminary experiment, we relied on the colorimetric observation and tested against all the chemically modified cytochrome *c* proteins synthesized before. Surprisingly, when PEG-cCytC was treated with ascorbic acid, the solution turned positively brown instead of pink and that same color change was also observed for cCytC. This finding can be seen by naked eye or can be visualized by measuring UV-VIS spectra ***Figure 47***:
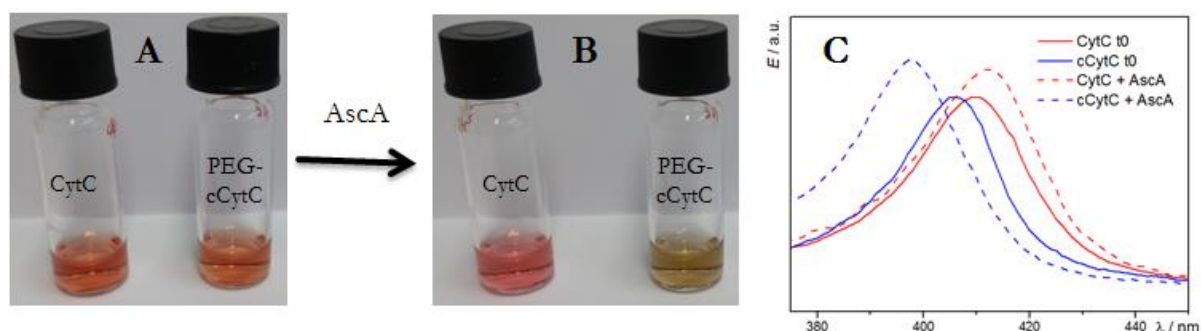
Figure 47: *Photo of native cytochrome c and PEG-cCytC before (**A**) and after (**B**) addition of ascorbic acid. (**C**): UV-VIS spectra of CytC (red) and PEG-cCytC (blue). Spectra are shown before (continuous) and after (dashed) addition of ascorbic acid.*

By performing different experiments that allowed deeper insight into the system, the red shift (turning pink) of native cytochrome *c* was shown to be a reductive process. When this solution was exposed to oxygen, it rapidly turned red again. This finding was repeatable for many reduction-oxidation cycles. In contrast, the blue shift (turning brown) of PEG-cCytC was found to derive from the acidic properties of ascorbic acid. Addition of acetic acid – an acid of similar pK_a – also gave a brown solution. A red solution could then be regained by addition of 1 M NaOH solution.

A high impact of cationization on the structural integrity was shown in chapter **3.2.1**. This distortion of the protein structure by cationization, proven by CD spectroscopy, leads to the different optical behavior upon treatment with reducing agents. This finding leads to the assumption that the ligand field of the iron core changes upon cationization of the protein. For this reason, PEG-cCytC was tested as a potential ATRP catalyst for the polymerization of NIPAM (**Figure 48**):
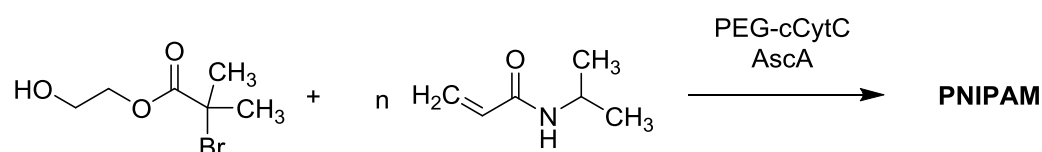
Figure 48: *PEG-cCytC catalyzes the ARGET ATRP of NIPAM.*

Interestingly, successful polymer formation was observed indeed. The reaction was monitored by ^{1}H NMR spectroscopy (**Figure 49**):
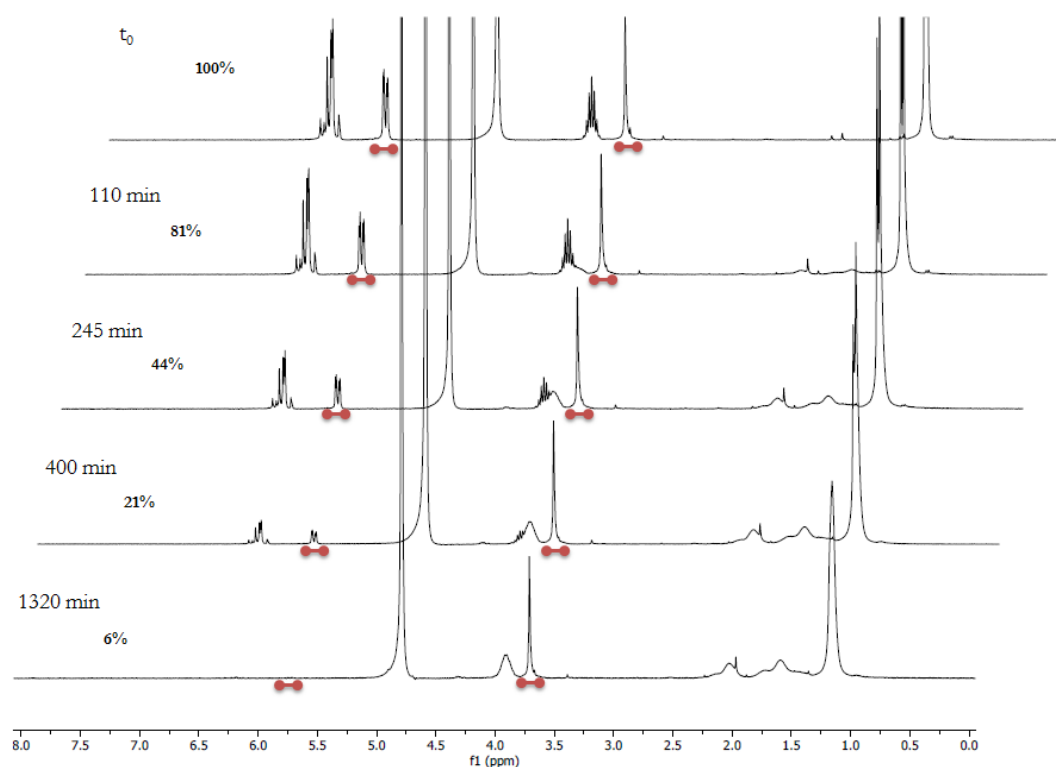
Figure 49: *NMR studies on the formation of PNIPAM catalyzed by PEG-cCytC. Conversions are calculated based on the dd peak at 5.73 ppm referenced to the PEG peak at 3.72 ppm.*

Similar to the brush synthesis described in chapter **3.3.1**, the PEG_{2000} chain peaks of the catalyst were used as an internal NMR standard to characterize monomer conversion.

Since PNIPAM exhibits LCST behavior, the polymer formation could also be qualitatively observed when the reaction mixture was warmed up to 35 °C (***Figure 50***):
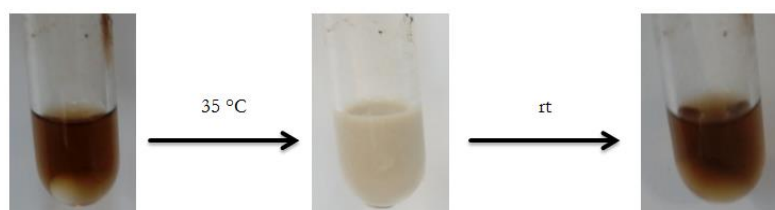
Figure 50: *LCST behavior of the synthesized PNIPAM: warming to 35 °C leads to precipitation of the polymer from the aqueous solution.*

The precursor cCytC was likewise successfully exploited as an ATRP catalyst with results similar to those of PEG-cCytC. Still, usage of PEG-cCytC instead brought two major advantages: Firstly and as described above, the PEG_{2000} chains can be used as internal conversion standard in NMR spectroscopy. This simplifies the system because external,

water-soluble NMR standards are therefore not required. Secondly, PEGylation is known to increase protein stability and may help to increase the reusability of the catalyst.

PEG-dcCytC-fluo (see chapter **3.2.4**) also showed ATRPase activity. But as there was no obvious benefit of the denaturation step, harnessing PEG-cCytC was continued.

No impact was found on the amount of PEG_{2000} chains on the surface on catalytic behavior. As such, highly PEGylated protein (~41.5 kDa) was synthesized and used as ATRP catalyst to intensify aforementioned advantages.

3.5.3: Reaction parameters, analysis of polymers, control reactions and monomer scope

To further explore the catalytic behavior of PEG-cCytC, polymerizations with different reaction parameters (ratio of reagents, pH, salt concentration, temperature) were conducted.

To gain further insights into reaction kinetics, a hemoglobin control was conducted in parallel to the polymerization catalyzed by PEG-cCytC. Samples were taken periodically and analyzed by both NMR spectroscopy and gel permeation chromatography (GPC).
Both of the reactions showed a similar reaction speed with conversion around 80% after 6.5 h. After reacting overnight, hardly any monomer was left in both cases. Exact calculation of conversion is only possible for PEG-cCytC as the NMR spectra of hemoglobin does not show reference peaks. For PEG-cCytC, the initial conversion of monomers seems to proceed linearly with time (***Figure 51***):
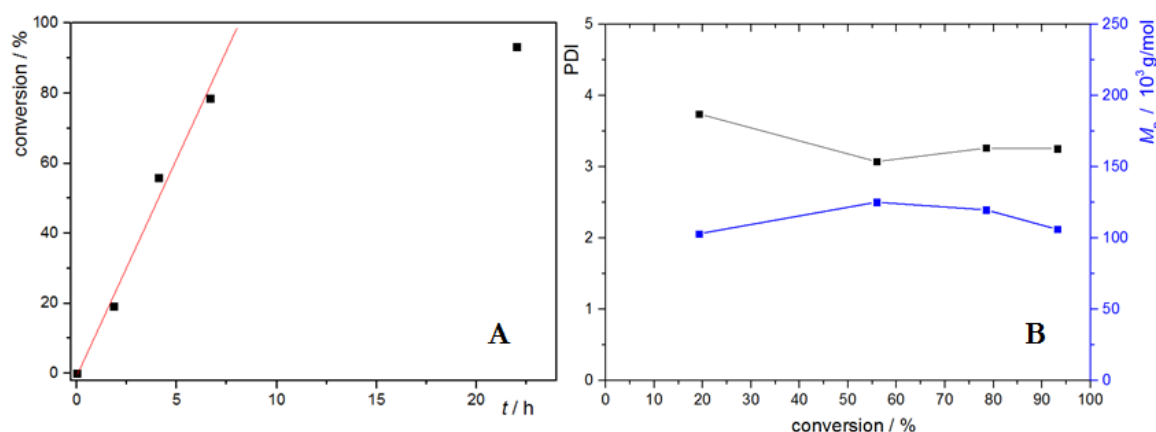
Figure 51: *Time-conversion plot (**A**) and further kinetic data (**B**) for the first successful polymerization of NIPAM using PEG-cCytC as a catalyst.*

However, it was observed that the molecular weight of the polymers did not increase with higher conversion. At first glance, this seems to be counterintuitive. In this respect, *Bruns et*

al. hypothesized that this can be explained by the rapid formation of polymer 'of rather high molecular weight […] at the beginning of the reaction'. Later on, 'also shorter chains that caused the average molecular weight to drop' were formed. The afforded PDIs for the HRP and hemoglobin system fall between 1.7 and 2.6, indicating low level of control. It is also important to note that while ATRP is generally tolerant towards unprotected nucleophiles, narrowly dispersed polymers are almost always produced in the absence of these possible interferences. With these findings and support from the literature, it raises the question whether the conventional ARGET ATRP mechanism holds true for these enzyme catalyzed polymerizations. While the exact mechanism is challenging to be determined at this point, we proceed to systematically test the influence of pH, solvents and temperature on the catalytic system. These factors are widely known parameters to exert a distinct effect upon protein conformation and architecture. We speculate that by varying these parameters, a greater understanding can be achieved from the protein perspective.

In agreement with *Bruns'* protocol, D_2O without any buffer salts was used as a solvent. In order to work oxygen-free, ascorbic acid (pK_a 4.1) was added by means of a syringe in small volumes without controlling the final pH value. After successful polymerizations, final pH values between 2.8 and 3.5 were determined. *Bruns et al.* describe a distinct impact of the pH value on the catalytic behavior for both HRP and hemoglobin. To analyze the impact of the pH for PEG-cCytC, two parallel NIPAM polymerizations were conducted. One of the polymerizations was started with ascorbic acid, whereas in the other case sodium ascorbate was used as the reducing agent. Both reactions were monitored using NMR:

Table 5: *Reaction progress for NIPAM polymerizations under different pH conditions.*

time	0 h	1 h	3 h	7 h
conversion pH 3.0 / %	-	8	34	65
conversion pH 7.3 / %	-	4	8	15

As it can be seen from ***Table 5***, the results support Bruns' statement on the effect of pH, where the pH optimum for hemoglobin's ATRPase activity was reported to be in the acidic region (around pH 3).[26]

Different control experiments were performed to support suggested ATRP mechanism. If no ascorbic acid was added or if the reducing agent was replaced by acetic acid, no conversion was observed within 24 h. If no catalyst was added to the reaction mixture, also no polymer

formation was observed. In experiments where HEBIB, the ATRP initiator, was excluded, still some polymer formation was visible overnight (5% – 10% conversion). This indicates a certain degree of non-ATRP (free radical polymerization) polymer formation during the course of the reaction. This can most probably be explained by re-oxidation of the reduced Fe^{2+} by minimal quantities of oxygen and subsequent radical formation.

During the present work, different monomers were polymerized. Similar to the brush synthesis described in chapter **3.3.1**, the monomer range was limited as solubility in water was necessary. Overall, the following polymers have been synthesized by PEG-cCytC catalysis (***Figure 52***):
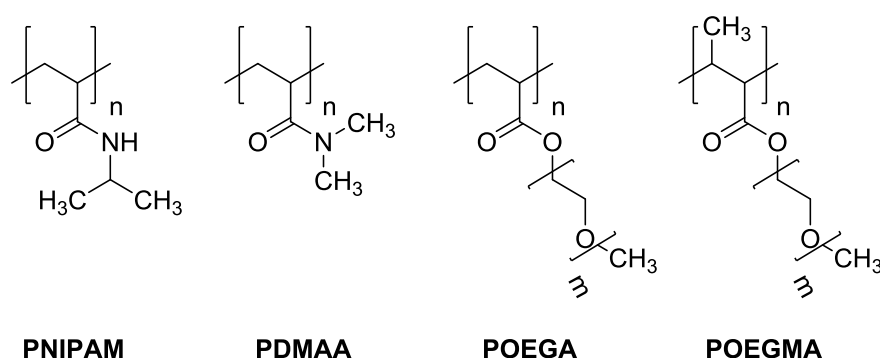
Figure 52: Polymer structures of PNIPAM, PDMAA, POEGA and POEGMA.

For POEGA and POEGMA synthesis, DSS was used as an NMR standard to determine conversions (see **3.3.2**). In principle, the observations and experimental outcome were similar as for NIPAM. GPC analysis revealed similar PDIs for acrylamides (lowest for PDMAA: 2.4) and for (meth)acrylates (lowest for POEGA: 2.2).

As these polymers do not show LCST behavior at moderate temperatures, polymerization at elevated temperatures was investigated. For DMAA, it was found that warming the reaction solution to 40 °C significantly accelerates polymer formation (see ***Table 6***). At room temperature, polymerization of this monomer often proceeded at very low reaction rate only. Importantly, the opportunity to tailor polymerization kinetics by heating the reaction solution is a special feature of the use of PEG-cCytC as an ATRPase and a major advantage over other protein catalysts described before. For those non-modified metalloproteins, heating of the aqueous solutions might rapidly result in precipitation of the protein due to denaturation. However, as PEG-cCytC has several PEG_{2000} chains on its surface, it is conferred higher stability and solubility at elevated temperatures.

Table 6: *Reaction progress for DMAA polymerization at different temperatures.*

time	0 h	1 h	2 h	4 h	6 h
conversion r.t. / %	-	-	2	7	14
conversion 40 °C / %	-	55	71	84	91

In summary, the ability of PEG-cCytC to serve as an ATRPase was shown. Exploiting metalloproteins for polymer synthesis is a promising example for potential future plastic production (see **1.2.3**). To the best of the author's knowledge, PEG-cCytC is the first example in literature for a modified enzyme showing ATRPase properties while the native enzyme does not.

3.5.4: Limitations of PEG-cCytC-catalyzed ATRP

However, in comparison to 'traditional' ATRP with copper catalysts, ATRP with PEG-cCytC has certain drawbacks. Most of the following disadvantages are also described by *Bruns et al.*[24, 26]

Polymer quality: ATRP is a controlled radical polymerization technique; the level of control can be evaluated by polymer analysis. Under optimized conditions, polymer chemists are able to tailor polymer sizes and keep PDIs close to 1.0. For PEG-cCytC and other ATRPases, level of control seems to be low. PDIs higher than 2.0 indicate a distinct degree of free radical mechanisms (see **3.5.3**) and in many cases, polymer weights were higher than expected.

Reproducibility: In principle, all of the above polymerizations are reproducible. However, the speed of the different polymerization reactions fluctuated between different batches. In some cases, also a lag time was observed. Here, polymerizations did not start for some time (~1 h) and then proceeded normally with a linear monomer conversion. In other cases, polymerizations stopped after a certain amount of conversion. This also was in agreement with results from *Bruns et al.* They explained this finding by side reactions with protein side residues or consumption of ascorbic acid.[24]

Solvent: Highly PEGylated PEG-cCytC is well-soluble in polar organic solvents like DMF or DMSO. Polymerization in these solvents would highly increase the monomer range as also less polar molecules could be polymerized. Somehow, monomer conversion was always low in these solvents and polymerizations could not be performed successfully. This might be explainable upon collapsing of the enzyme in organic solvents. Successful polymerizations were conducted in MQ water only. Experiments in buffer solution (PBS, glycine buffer,

acetate buffer, brine, sodium bromide solution) did not result in significant conversion of NIPAM. Here, a possible explanation is a lowered catalytic activity or accessibility of the heme due to complexation with anionic ligands.

Efforts and costs: Due to the value of the native enzyme, high catalyst amounts are not desirable and application in large batches does not come into question. The cheap copper complexes from traditional AGET ATRP can often be applied with high excess and reaction control is achieved by slow addition of reducing agent. The very low concentration of the PEG-cCytC might explain several of the drawbacks described above.

3.6 Self-catalyzed synthesis of protein brushes

3.6.1: Idea: self-catalyzed protein brushes

Harnessing ATRP as a *grafting from* method to grow polymers from biological macromolecules is known in literature since many years.[68-69] Chapter **3.3.1** describes an example for this reaction type: catalyzed by CuBr$_2$/TPMA, different monomers were grown on the protein's surface. Also the possibility to exploit metalloproteins as catalysts for polymer synthesis is well-known and was introduced by *Bruns et al.* in 2011.[24] This present work shows, that cationized cytochrome *c* derivatives are – just like other examples like HRP or hemoglobin – able to catalyze the formation of water-soluble polymers.

We hypothesized that a connection of both of these topics is possible: Self-catalyzed synthesis of polymer-protein hybrids can be achieved if the heme of PEG-dcCytC-fluo-Br is able to initiate the ATRP on its own surface (***Figure 53***):
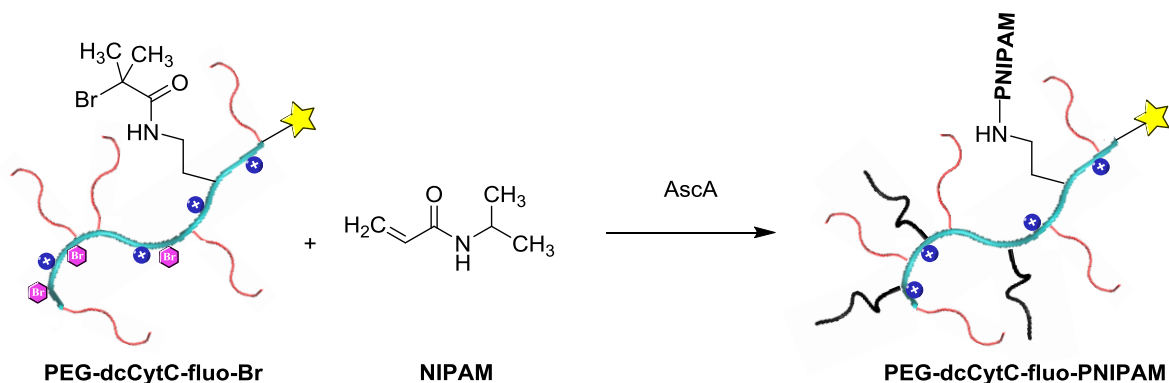
Figure 53: *Self-catalyzed ARGET ATRP of NIPAM on the surface of the macroinitiator.*

In this case, polymers could grow in a *grafting from* procedure without applying any external catalyst (like CuBr$_2$, see **3.3.1**). The question, whether the catalysis would run intra- or

intermolecular, is hard to answer. Intramolecular self-catalysis would imply that the reactive iron center is flexible enough to initiate the reaction on its own surface. On the other hand, intermolecular self-catalysis would imply that macroinitiator A initiates the polymerization on the surface of macroinitiator B. Both ways might underlie substantial steric hindrance. However, this methodology has, to the best of the author's knowledge, not been described in literature yet. Still, the system would be very straightforward. Addition of ascorbic acid to an aqueous solution of monomer and macroinitiator should already yield brush-like polymers.

3.6.2: Different approaches to yield self-catalyzed brushes

In agreement with **3.5.3**, NIPAM was chosen as a standard monomer to investigate possibilities of self-catalyzed synthesis of polymer-protein hybrids. In a first approach, the macroinitiator PEG-dcCytC-fluo-Br was mixed with 580 equivalents of NIPAM in D_2O and ascorbic acid (50 eq.) was added. Monitoring the reaction by ^{1}H NMR did not indicate successful growth of polymers on the protein's surface.

Further attempts to grow protein brushes without external catalyst were performed by varying the monomer concentration, the amount of ascorbic acid and the temperature. Still, MALDI-ToF MS analysis of the reaction did not indicate self-catalyzed surface polymerization.

As most of the polymerizations described in **3.5.3** were catalyzed by PEG-cCytC, which has not been denatured in urea buffer, it was questioned whether the globular macroinitiator PEG-cCytC-Br (see ***Figure 16***) would allow self-catalyzed brush synthesis instead (***Figure 54***):
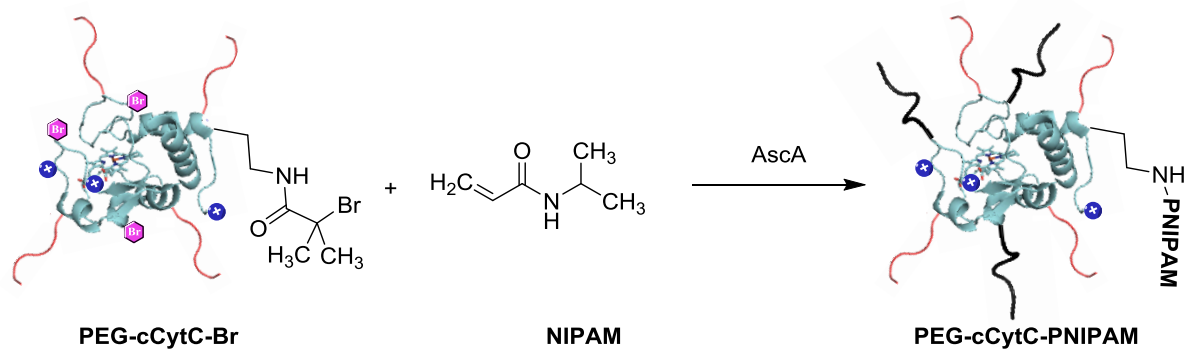
Figure 54: *Self-catalyzed PNIPAM growth from the surface of PEG-cCytC-Br.*

Here, formation of a brush with 45 kDa was observed in a first test experiment when PEG-cCytC-Br was mixed with 500 equivalents of NIPAM and 25 equivalents of ascorbic acid and the reaction was stirred for three days.

However, it was not possible to reproduce this very promising first result with other batches of PEG-cCytC-Br. If long reaction times, high monomer concentrations or slightly elevated temperatures (28 °C) were applied, polymer formation was observed in ^{1}H NMR spectra. Nevertheless, MALDI-ToF MS spectra did not support the calculated mass increase based on NMR results: sometimes no MALDI-ToF MS peaks were visible, whereas in other cases no or only marginal molecular weight increase in respective to the macroinitiator was observed. Two explanations are possible: it might be the case that the polymer-protein hybrids that were formed do not give MALDI-ToF MS signals to the same extent the substrate PEG-dcCytC-Br does. This way, eventually formed brushes would not be detectable by MALDI-ToF MS because of the much stronger signal of the globular macroinitiator. More probable, instead of polymer growth on the macroinitiator's surface, polymerization actually occurred in solution. Non-ATRP caused side reactions, possibly explainable by interactions between the redox-active iron and minimal quantities of oxygen, might result in free polymer formation. To a minor extent, this has also been observed and described when PEG-cCytC was exploited as an ATRPase (see **3.5.3**).

Hence, we tried to overcome potential kinetic hindrance by adjusting the polymerization setup: Performing the reaction in urea buffer should result in a strand-like conformation of the macroinitiator and therefore keep both, catalytic heme and initiators, more accessible. At the same time, urea should not interfere with the ATRP mechanism. However, successful polymerization was not observed. In another approach, addition of an external ligand, in this case TPMA (see **3.3.1**), was thought to enable polymerization by reversibly binding the iron cation from the heme and thus facilitating a higher flexibility of the catalytic core. Also in this case, a positive effect of the additive was not observed. As reported by *von Werne et al.,* additional and free small molecule initiators can be used in surface-initiated ATRP to ensure living polymerization mechanisms at very high monomer concentrations (sacrificial initiator).[70] Thus, HEBIB (see **3.5.3**) was added to the reaction to allow growth of polymers in both solution and on the surface under ATRP control. But also in this case, no significant size increase was found for the protein component. As it was shown in **3.4.2** that there is no LCST behavior for PEG-dcCytC-fluo-PNIPAM in the observed area, also a polymerization above PNIPAM's LCST (40 °C) was conducted. But also under these conditions, no peak was visible in the MALDI-ToF MS spectra of the raw material.

As it was not possible to reproduce positive results with NIPAM as a monomer, other water-soluble monomers were employed. In agreement with **3.3.2**, DMAA, OEGA and OEGMA were chosen. However, for these monomers ^{1}H NMR spectroscopy indicated much faster polymer formation than for NIPAM. While – in agreement with **3.3.2** – no MALDI-ToF MS peaks were achievable for the (meth)acrylates, results for DMAA as a monomer were similar to NIPAM and brush sizes did not or only marginally increase.

Table 7: *Summary of all approaches to yield a self-catalyzed polymer-protein brush.*

A	B	C	D	E	F	G	H	I
JG	catalyst	monomer	ratio C:B	AscA	t	note	NMR conv.	MALDI m/z
124	PEG-dcCytC-fluo-Br	NIPAM	580:1	50 eq.	22 h	-	< 5%	-
137b	PEG-dcCytC-fluo-Br	NIPAM	1180:1	25 eq.	o.n.	-	< 5%	-
137c	PEG-dcCytC-fluo-Br	NIPAM	1180:1	25 eq.	o.n.	+ TPMA	58%	-
141	PEG-dcCytC-fluo-Br	NIPAM	1125:1	25 eq.	2 d	+ TPMA	< 5%	-
142	PEG-dcCytC-fluo-Br	NIPAM	1180:1	25 eq.	o.n.	+ TPMA	< 5%	-
160	PEG-cCytC-Br	NIPAM	500:1	25 eq.	3 d	**successful**	70%	**45 kDa**
165	PEG-dcCytC-fluo-Br	NIPAM	800:1	25 eq.	o.n.	-	< 5%	-
170	PEG-dcCytC-fluo-Br	NIPAM	7500:1	50 eq.	o.n.	-	< 5%	-
171	PEG-cCytC-Br	NIPAM	2800:1	25 eq.	o.n.	-	< 5%	-
173	PEG-cCytC-Br	DMAA	5000:1	50 eq.	o.n.	-	21%	-
175	PEG-cCytC-Br	DMAA	2500:1	50 eq.	1 h	gel	-	-
178a	PEG-cCytC-Br	DMAA	2200:1	50 eq.	2 h	gel	-	-
178b	PEG-cCytC-Br	OEGMA	2200:1	50 eq.	1 h	gel	-	-
179a	PEG-cCytC-Br	OEGA	2500:1	50 eq.	4 h	gel	-	-
179b	PEG-cCytC-Br	OEGMA	2500:1	50 eq.	3 h	gel	-	-
181	PEG-cCytC-Br	DMAA	2200:1	50 eq.	1.5 h	-	14%	-
182a	PEG-cCytC-Br	OEGA	2500:1	50 eq.	2 h	-	-	-
182b	PEG-cCytC-Br	OEGMA	2500:1	50 eq.	2 h	-	-	-
185	PEG-cCytC-Br	NIPAM	2200:1	50 eq.	2 d	-	16%	
190	PEG-cCytC-Br	NIPAM	500:1	25 eq.	3 d	gel	-	-
195	PEG-cCytC-Br	NIPAM	500:1	50 eq.	2 d	-	24%	-
198	PEG-cCytC-Br	NIPAM	500:1	50 eq.	1 d	urea buffer	< 5%	-
215a	PEG-cCytC-Br	DMAA	1200:1	50 eq.	o.n.	+ HEBIB	70%	-
215b	PEG-cCytC-Br	DMAA	1200:1	50 eq.	o.n.	-	60%	-
217a	PEG-cCytC-Br	NIPAM	1000:1	25 eq.	o.n.	28 °C	20%	-
217b	PEG-cCytC-Br	NIPAM	1000:1	25 eq.	o.n.	40 °C	74%	-

Instead, for experiments with DMAA, OEGA and OEGMA, gel formation was often observed even at monomer conversions <50%. As such gel formation was never observed while synthesizing linear polymers catalyzed by PEG-cCytC, it is estimated that a crosslinking of polymers and proteins plays a role in the formation of these structures.

Table 7 summarizes all experiments that were conducted to yield self-catalyzed polymer-protein brushes. As it was possible in only one out of many experiments to proof covalent polymer growth on the surface of the protein, it has to be summarized that the desired methodology of self-catalyzed polymer-protein brushes could not be implemented successfully. While it was possible to enable polymer formation under these ARGET ATRP conditions, a proof of covalent linkage between polymer and protein harnessing MALDI-ToF MS (like in **3.3.2**) was not achievable. MALDI-ToF MS did not show any peaks or that the mass of the peaks obtained did not differ significantly from the mass of the macroinitiator.

A possible explanation for these unsuccessful experiments might be the slow reaction rate. Reactions between two macromolecules – like in the case of intermolecular catalysis (see **3.6.1**) – are known to proceed very slowly. This might promote side reactions like free radical polymerization in solution, which have a far higher reaction rate.

However, implementation of this method is part of follow-up works of this thesis.

4 Conclusion and Outlook

In the course of this thesis, the hemeprotein cytochrome *c* from *Saccharomyces cerevisiae* (see **3.1**) was chemically modified to serve as the polypeptide backbone of functional polymer-protein brushes. Based on this highly-defined structure, different brushes with tailorable sizes and built-up from variant monomers were synthesized and analyzed regarding physical and chemical properties. Demonstrated conservation of heme activity within the designed thermoresponsive scaffold of PEG-dcCytC-fluo-PNIPAM indicates successful combination of catalytic function and tailorable architecture within one macromolecule. In addition, ATRPase activity of cationized cytochrome *c* derivatives was shown and investigated as a promising example for catalytic function of these hybrid materials.

Cytochrome *c* was converted into the strand-like macroinitiator PEG-dcCytC-fluo-Br harnessing four subsequent modification steps: *cationization – PEGylation – denaturation and labeling – initiator addition* (see **3.2**). Different experiments to optimize stoichiometry between the protein component and different reactants were performed to control the nanoscale composition of the resulting material. The synthesized protein derivatives were analyzed using MALDI-ToF MS, gel electrophoresis or fluorescamine assay. Especially the possibility to monofunctionalize the protein backbone at amino acid C-108 and thus to link functional moieties at predetermined and precise positions was intensively studied and shown.

Growing polymers from the macroinitiator harnessing AGET ATRP with $CuBr_2$/TPMA as a catalyst in a *grafting from* procedure yielded polymer-protein brushes with sizes adjustable by reaction time and monomer concentration (see **3.3**). Reaction kinetics were monitored harnessing ^{1}H NMR spectroscopy and GPC, brush sizes were determined by MALDI-ToF MS. Additional analysis methods allowed further characterization and imaging of the hybrid material. Different water-soluble monomers have been polymerized on the protein's surface, with emphasis in the thermoresponsive PNIPAM polymer.

Following, conservation of catalytic activity of the metalloprotein after modification and its desired thermoresponsiveness were investigated (see **3.4**). Exploiting the oxidation of ABTS by hydrogen peroxide as a standard model, it was shown that the designed protein derivatives were still able to catalyze redox reactions. However, temperature-dependent ABTS assays of the polymer-protein brushes did not show the desired control over catalytic activity due to the collapse of the material upon warming of the solution above PNIPAM's LCST in water (~32 °C). While DOSY NMR experiments did indicate a decrease of size of the brushes upon heating to 40°C, further studies are needed to investigate whether the functionality

of these building blocks can be tailored by temperature. Analyzing and comparing PNIPAM-protein hybrids with different ratios of polymer and protein might allow further insights into the possibilities of switching the protein's catalytic activity upon heating and cooling.

In another section of this work, the potential of cytochrome *c* and synthesized derivatives to serve as ATRP catalysts was investigated (see **3.5**). While native cytochrome *c* did not catalyze the polymerization of NIPAM, it was shown that cationized derivatives of the protein can be exploited as ATRPases. Supported by different optical behavior, we speculate that a change in the ligand field of the iron cation in the heme upon cationization enables the modified protein to catalyze the polymerization. While this hypothesis needs stronger support by further insights into the ligand structure of the modified proteins, we observe a switch in catalytic activity upon cationization. However, the polydispersity of the resulting polymers indicated a low level of control over the polymerization. Subsequently, we studied the effect of reaction parameters like temperature, pH or salt concentration on the system. In addition to NIPAM, also water-soluble monomers of other subclasses were shown to be able to be polymerized by PEG-cCytC.

After ATRPase activity was shown for synthesized cytochrome *c* derivatives, we envisioned a system where a macroinitiator bearing a heme can catalyze polymerizations on its own surface (see **3.6**). To facilitate that, different conditions were employed to enable self-catalyzed surface polymerization by the macroinitiators PEG-dcCytC-fluo-Br and PEG-cCytC-Br. Despite extensive efforts, it was not possible to find conditions where reproducible and tailorable synthesis of the desired hybrid material was possible.

While this work describes the synthesis of defined metalloprotein-based hybrid materials, future studies might aim to further exploit their functionality within catalytic systems. As it was shown for cytochrome *c* that natural macromolecules can be engineered with nanoscale precision, it is part of ongoing work to make use of its conserved redox activity within a more complex environment.

5 Experimental part

5.1 Materials

5.1.1: Commercially available chemicals

Cytochrome *c* from *Saccharomyces cerevisiae* (≥ 85%) was purchased from *Sigma-Aldrich*. *N*-Isopropylacrylamide was purchased from *TCI* and recrystallized in toluene/cyclohexane before usage. *N,N*-Dimethylacrylamide, oligo(ethylene glycol) methyl ether methacrylate (OEGMA, M_n 300 g/mol) and oligo(ethylene glycol) methyl ether acrylate (OEGA, M_n 480 g/mol) were purchased from *Sigma-Aldrich* and passed through a short column of basic alumina and stored at 4 °C prior to use. Other chemicals for protein modification and assays were purchased from different suppliers and – if not stated otherwise – used as received.

5.1.2: Preparation of (buffer) solutions

In the course of this present work, different buffers and other solutions were prepared:

Ethylenediamine solution (2.5 M, pH 4.75)

Ethylenediamine (167 mL, 2.5 mol) was added to 600 mL of MQ H_2O. pH was adjusted to 4.75 by dropwise addition of conc. HCl solution. More MQ H_2O was added to yield 1000 mL of a 2.5 M ethylenediamine solution with pH 4.75.

Phosphate buffer solution (50 mM, pH 8.0)

Anhydrous sodium dihydrogen phosphate (NaH_2PO_4, 3.0 g, 25 mmol) was dissolved in 480 mL of MQ H_2O. NaOH solution (1 M) was added to yield a solution with pH of 8.0. Addition of more MQ H_2O gave 500 mL of a 50 mM phosphate buffer solution.

Urea phosphate buffer solution (5 M urea, 50 mM PBS, 2 mM EDTA, pH 7.4)

Urea (300.3 g, 5 mol), disodium hydrogen phosphate ($Na_2HPO_4 \cdot 7H_2O$, 10.54 g, 39 mmol), anhydrous sodium dihydrogen phosphate (NaH_2PO_4, 1.32 g, 11 mmol) and EDTA (584.48 mg, 2 mmol) were dissolved in 800 mL of MQ H_2O. The pH was adjusted to pH 7.4 by addition of HCl (1 M) respectively NaOH (1 M). More MQ H_2O was added to yield 1000 mL of the urea phosphate buffer solution.

Sodium hydrogen carbonate solution (100 mM, pH 8.5)

Sodium hydrogen carbonate (NaHCO$_3$, 1.68 g, 20 mmol) was dissolved in 180 mL of MQ water. pH was adjusted to 8.5 by addition of HCl (1 M). Additional MQ H$_2$O was added to yield 200 mL of a 100 mM of sodium hydrogen carbonate solution.

Phosphate EDTA buffer solution (50 mM phosphate Buffer, 2 mM EDTA, pH 6.8)

Anhydrous sodium dihydrogen phosphate (NaH$_2$PO$_4$, 0.60 g, 5 mmol) and EDTA (58.45 mg, 0.2 mmol) were dissolved in 90 mL of MQ H$_2$O. NaOH solution (1 M) was added to yield a solution with pH of 6.8. Addition of more MQ H$_2$O gave 100 mL of a 50 mM phosphate EDTA buffer solution.

5.2 Characterization methods

5.2.1: ^{1}H NMR and DOSY NMR spectroscopy

NMR spectroscopy was performed on the instruments *Avance III 700*, *Avance 300* or *Avance III 250* by *Bruker*. Deuterium oxide (set to $\delta = 4.79$ ppm) purchased from *Sigma Aldrich* was used as a solvent and all signals were referred to TMS (tetramethylsilane). Obtained spectra were analyzed and processed using the software *MestReNova* by *Mestrelab Research*.

5.2.2: Matrix-assisted laser desorption/ionization (MALDI) mass spectrometry

MALDI time-of-flight (MALDI-ToF) mass spectrometry was performed on the instrument *Daltonics Reflex III* by *Bruker*. Saturated solution of sinapinic acid dissolved in a 1:1 water:acetonitrile mixture with 0.2% TFA (trifluoroacetic acid) was used as the matrix solution. Data were processed with *Origin 9.1*.

5.2.3: UV-VIS and fluorescence spectroscopy

UV-VIS and fluorescence spectra were recorded on a *Spark 20M* from *Tecan Group Ltd* using a 384 respectively 96 well UV-Star microplate. Data were processed with *Origin 9.1*.

5.2.4: Gel permeation chromatography (GPC)

GPC experiments were conducted on a PSS SECcurity instrument with autosampler, column oven with three GRAM columns and a RI as well as an UV detector (*Agilent Technologies 1260 Infinity*). DMF containing 1 g/L lithium bromide was used as the eluent at a flowrate of

1 mL/min. Poly(methyl methacrylate) was used as a standard for molecular weight determination. Samples were prepared at with concentrations ~1 mg/mL.

5.2.5: Transmission electron microscopy (TEM)

TEM samples were prepared by adding 4 µL of the polymer-protein brush solution onto a carbon-coated copper grid. After drying for 10 min, the remaining solution was removed from the grid by means of a filter paper. The samples were stained with 2% uranyl formate and dried. Measurements were performed on a *JEOL JEM-1400 TEM* operating at an accelerating voltage of 120 kV. *ImageJ* was used as software for size analysis.

5.2.6: Atomic force microscopy (AFM)

AFM imaging was conducted on a *Dimension FastScan Bio AFM* by *Bruker* equipped with the ScanAsyst mode. The sample solution was deposited onto a freshly cleaved mica surface and left for 30 min at room temperature allowing adsorption of the sample. The samples were scanned with scan rates between 1 and 3 Hz. Several AFM images were acquired for every sample to ensure reproducibility. Images were analyzed by using *Gwyddion 2.38* software.

5.3 Procedures: Brush synthesis

5.3.1: cCytC

$$\text{CytC} \quad + \quad \text{EDA} \quad \xrightarrow{\text{EDC·HCl, pH 4.75}} \quad \text{cCytC}$$

Cytochrome *c* from *Saccharomyces cerevisiae* (36.0 mg, 2.86 µmol, 1.0 eq.) was dissolved in degassed ethylenediamine solution (5 mL, 2.5 M, pH 4.75). Insoluble parts were removed by means of a syringe filter. EDC·HCl (193.0 mg, 1.01 mmol, 25 eq. per COOH function) was added subsequently as a solid. After complete addition, the reaction mixture was stirred overnight at room temperature. The reaction was quenched by addition of sodium acetate solution (1 mL, 4 M, pH 4.75). The raw reaction mixture was purified twice with sodium acetate solution (100 mM, pH 4.75) and five times with MQ water using a Vivaspin 20 concentrator (MWCO 5000 Da) and lyophilized afterwards to yield a pale red fluffy solid (32.5 mg, 85%, MALDI-ToF MS: 13.4 kDa).

Table 8: Synthesis of cCytC starting from native cytochrome c.

	CytC			EDC			EDA	t	yield	mass	note
JG	mg	µmol	eq.	mg	µmol	eq.	mL	-	mg	kDa	-
100a	14.0	1.11	1.0	45.4	237	15	1.0	2 h	-	13.1	incomp. conv.
100b	14.0	1.11	1.0	90.8	474	30	1.0	o.n.	11.3	13.5	comp. conv.
104	3.0	0.24	1.0	16.0	83	25	0.5	o.n.	3.6	13.4	comp. conv.
110	36.0	2.86	1.0	193	1007	25	5.0	o.n.	32.5	13.4	comp. conv.
114	36.0	2.86	1.0	193	1007	25	5.0	o.n.	29.2	13.5	comp. conv.
127	41.3	3.28	1.0	222	1158	25	6.0	o.n.	35.8	13.6	comp. conv.
147	30.0	2.38	1.0	162	841	25	6.0	o.n.	28.1	-	-
157	26.3	2.09	1.0	141	738	25	6.0	o.n.	26.5	-	-
161	28.6	2.27	1.0	154	803	25	6.0	o.n.	28.5	-	-
167	16.0	1.27	1.0	86.3	449	25	3.0	o.n.	15.3	-	-
186	26.8	2.13	1.0	144	751	25	5.0	o.n.	25.9	-	-
204	25.0	1.99	1.0	135	704	25	5.0	o.n.	24.7	-	-

5.3.2: PEG-cCytC

$$\text{cCytC} \quad + \quad \textbf{PEG}_{2000}\textbf{-NHS} \quad \xrightarrow{\text{PBS, pH 8.0}} \quad \textbf{PEG-cCytC}$$
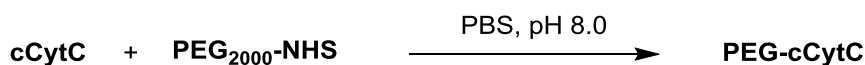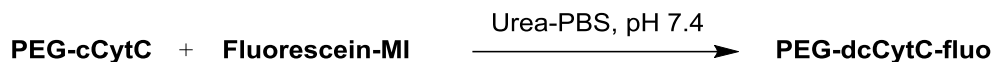
cCytC (30.8 mg, 2.30 µmol, 1.0 eq.) was dissolved in degassed phosphate buffer solution (10 mL, 50 mM, pH 8.0). PEG$_{2000}$-NHS (20.3 mg, 10.15 µmol, 4.4 eq.) dissolved in DMSO (200 µL) was added dropwise to the cCytC solution. After stirring overnight at room temperature, the reaction mixture was purified seven times with MQ water using a Vivaspin 20 concentrator (MWCO 5000 Da) and lyophilized afterwards to yield a pale red fluffy solid (45.2 mg, 77%). MALDI-ToF MS showed a main product peak at 25.5 kDa, which indicates a sixfold protein conjugation with PEG$_{2000}$.

Table 9: Synthesis of PEG-cCytC starting from cCytC.

	cCytC			PEG$_{2000}$-NHS			*t*	yield	mass*	# of PEGs
JG	mg	µmol	eq.	mg	µmol	eq.	-	mg	kDa	-
101	9.5	0.71	1.0	3.5	1.75	2.5	o.n.	11.2	21.5	1 − 5
111	33.5	2.50	1.0	60.0	30.00	12.0	o.n.	84.7	41.5	7 − 18
116	30.8	2.30	1.0	20.3	10.15	4.4	o.n.	45.2	25.5	3 − 8
132	27.7	2.07	1.0	18.3	9.15	4.4	o.n.	42.0	25.5	3 − 8
158	31.4	2.34	1.0	56.2	28.10	12.0	o.n.	68.4	41.5	7 − 18
162	26.2	1.96	1.0	17.3	8.65	4.4	o.n.	38.5	-	-
168	28.2	2.10	1.0	18.6	9.30	4.4	o.n.	23.2	23.5	3 − 7
187	17.1	1.28	1.0	11.3	5.65	4.4	o.n.	25.4	-	-
191	33.0	2.46	1.0	21.8	10.90	4.4	o.n.	47.3	-	-
**m/z* peak with maximum intensity										

5.3.3: PEG-dcCytC-fluo

$$\text{PEG-cCytC} \quad + \quad \text{Fluorescein-MI} \xrightarrow{\text{Urea-PBS, pH 7.4}} \text{PEG-dcCytC-fluo}$$

PEG-cCytC (15.2 mg, 0.60 µmol, 1.0 eq.) was dissolved in degassed urea phosphate buffer (4 mL, 5 M urea, 50 mM PBS, 2 mM EDTA, pH 7.4). Fluorescein maleimide was dissolved in DMSO to yield a stock solution of 20.8 mg/mL (42 mM). From that stock solution, a volume of 14.4 µL (equals 0.30 mg, 0.60 µmol, 1.0 eq.) was diluted in additional 30 µL of DMSO. This solution was added dropwise to the PEG-cCytC solution. After stirring under dark conditions overnight at room temperature, the reaction mixture was purified seven times with MQ water using a Vivaspin 6 concentrator (MWCO 5000 Da). After lyophilization, a pale red-orange fluffy solid (14.1 mg, 92%) was obtained. UV-VIS analysis revealed low conversion rates (see **3.2.4**). MALDI-ToF MS showed a main product peak at 26.1 kDa.

**Table 10:** _Synthesis of PEG-dcCytC-fluo starting from PEG-cCytC._

JG	PEG-cCytC			Fluorescein-MI			t	yield	mass
	mg	**µmol**	**eq.**	**mg**	**µmol**	**eq.**	**-**	**mg**	**kDa**
108	3.1	0.14	1.0	0.52	1.04	7.2	o.n.	2.1	21.6
119	30.0	1.18	1.0	0.59	1.18	1.0	o.n.	30.1	26.1
138	15.2	0.60	1.0	0.30	0.60	1.0	o.n.	14.1	26.1
205	47.0	1.84	1.0	0.94	1.89	1.0	o.n.	45.9	-

5.3.4: PEG-dcCytC-fluo-Br (macroinitiator)

$$\text{PEG-dcCytC-fluo} \quad + \quad \text{BiB-NHS} \quad \xrightarrow{\text{NaHCO}_3,\ \text{pH 8.5}} \quad \text{PEG-dcCytC-fluo-Br}$$
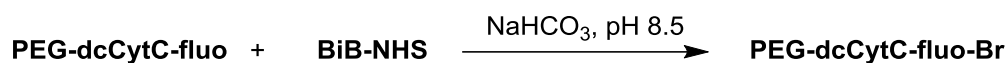
PEG-dcCytC-fluo (4.7 mg, 0.18 µmol, 1.0 eq.) was dissolved in NaHCO$_3$ solution (5 mL, 0.1 M, pH 8.5). 2-Bromoisobutanoic acid N-hydroxysuccinimide ester (2.7 mg, 10.2 µmol, 57 eq.) dissolved in DMSO (400 µL) was added dropwise to the PEG-dcCytC-fluo solution. After stirring under dark conditions overnight at room temperature, the product was purified with MQ water seven times using a Vivaspin 6 concentrator (MWCO 5000 Da). After lyophilization, a pale red-orange fluffy solid (4.3 mg, 88%) was obtained. MALDI-ToF MS showed a main product peak at 24.1 kDa.

Table 11: *Synthesis of PEG-dcCytC-fluo-Br starting from PEG-cCytC.*
*MALDI results were not in agreement with expectations (see **3.2.5**).*

	PEG-dcCytC-fluo			BiB-NHS			t	yield	mass
JG	mg	µmol	eq.	mg	µmol	eq.	-	mg	kDa
109	2.2	0.10	1.0	2.4	8.94	88	o.n.	0.9	21.6
121	4.7	0.18	1.0	2.7	10.22	55	o.n.	4.3	24.1
128	10.3	0.40	1.0	6.4	24.24	60	o.n.	9.9	24.1
139	13.8	0.54	1.0	8.6	32.57	60	o.n.	13.2	-
207	47.0	1.84	1.1	29.3	111.0	60	o.n.	46.5	-

<u>5.3.5: PEG-dcCytC-fluo-PNIPAM (protein-polymer brush)</u>

$$\text{PEG-dcCytC-fluo-Br} \quad + \quad \text{NIPAM} \xrightarrow[\text{AscA}]{\text{CuBr}_2/\text{TPMA}} \text{PEG-dcCytC-fluo-PNIPAM}$$
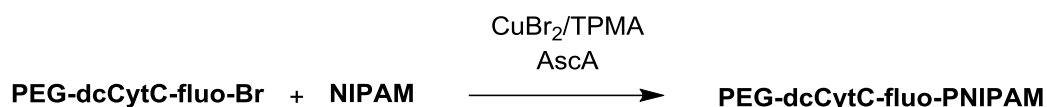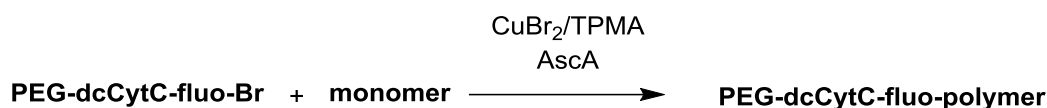
Macroinitiator PEG-dcCytC-fluo-Br (2.0 mg, 83 nmol, 1.0 eq.) and *N*-isopropylacrylamide (5.0 mg, 44.2 µmol, 532 eq.) were dissolved in D_2O (200 µL) in a Schlenk flask. $CuBr_2$ (1.56 mg, 7 µmol) and tris(2-pyridylmethyl)amine (16.22 mg, 56 µmol) were dissolved in 1:1 mixture of DMF:D_2O (v:v, 350 µL). 22.5 µL of this solution (5 eq. of Cu) were added to the protein solution. The flask and the solution were degassed through freeze-pump-thaw cycles (3 x) and then refilled with argon. Ascorbic acid (5.0 mg, 30 µmol) was dissolved in D_2O (500 µL). This solution was degassed by bubbling argon for 15 minutes. The polymerization was started by dropwise addition of ascorbic acid solution (100 µL, equals 69 eq.) to the reaction mixture by means of a syringe. After 2.5 hours and ~30% of conversion, the reaction was quenched by exposing the system to air. The raw material was purified by applying it to a *Sephadex* column. Afterwards, the solution was ultrafiltrated using a Vivaspin 6 concentrator (MWCO 5000 Da). MALDI-ToF MS showed a main product peak at 49 kDa, indicating covalent binding of ~220 NIPAM molecules at the brush.

Table 12: *Synthesis of PNIPAM-protein brushes with different sizes.*

JG	Macroinitiator	NIPAM	CuBr₂/TPMA	AscA	*t*	size	Protein:NIPAM
126	2.0 mg / 83 nmol / 1.0 eq.	5.0 mg / 44.2 µmol / 532 eq.	0.10 mg / 450 nmol / 5 eq.	0.67 mg / 3.8 µmol / 46 eq.	o.n.	55 kDa	1:275
133	2.0 mg / 83 nmol / 1.0 eq.	5.0 mg / 44.2 µmol / 532 eq.	0.10 mg / 450 nmol / 5 eq.	1.0 mg / 5.9 µmol / 69 eq.	2.5 h	49 kDa	1:220
137	2.0 mg / 83 nmol / 1.0 eq.	10.0 mg / 88.4 µmol / 1064 eq.	0.10 mg / 450 nmol / 5 eq.	0.34 mg / 1.9 µmol / 23 eq.	2.5 h	86 kDa	1:550
144	2.0 mg / 83 nmol / 1.0 eq.	10.0 mg / 88.4 µmol / 1064 eq.	0.10 mg / 450 nmol / 5 eq.	0.34 mg / 1.9 µmol / 23 eq.	2.0 h	73 kDa	1:430
154	2.0 mg / 83 nmol / 1.0 eq.	5.0 mg / 44.2 µmol / 532 eq.	0.10 mg / 450 nmol / 5 eq.	0.34 mg / 1.9 µmol / 23 eq.	0.5 h	41 kDa	1:150
203	4.0 mg / 166 nmol / 1.0 eq.	21.2 mg / 197 µmol / 1187 eq.	0.20 mg / 900 nmol / 5 eq.	0.67 mg / 3.8 µmol / 23 eq.	1.5 h	67 kDa	1:380

5.3.6: Synthesis of brushes with other monomers

$$\text{PEG-dcCytC-fluo-Br} \quad + \quad \text{monomer} \xrightarrow[\text{AscA}]{\text{CuBr}_2/\text{TPMA}} \text{PEG-dcCytC-fluo-polymer}$$

Synthesis of polymer-protein brushes with the monomers DMAA, OEGA and OEGMA were conducted in the same way as for NIPAM (see **5.3.5**). For POEGA and POEGMA brushes, no MALDI-ToF MS peaks could be obtained. Therefore, monomer conversion according to ^{1}H NMR spectra is displayed in ***Table 14***.

Table 13: *Synthesis of protein brushes with different monomers. In experiment 194,*
due to lack of NMR conversion standard no exact conversion can be determined.

JG	Macroinitiator	Monomer	CuBr$_2$/TPMA	AscA	t	NMR conv.	Protein:NIPAM
DMAA							
194a	1.3 mg	5.6 mg	0.10 mg	0.23 mg	2 h	20%	233:1
	48 nmol	56 µmol	450 nmol	1.3 µmol			
	1.0 eq.	1166 eq.	9 eq.	27 eq.			
210a	3.0 mg	13.3 mg	0.15 mg	0.51 mg	1 h	15%	150:1
	133 nmol	133 µmol	675 nmol	2.9 µmol			
	1.0 eq	1000 eq.	5 eq.	22 eq.			
OEGA							
194b	1.3 mg	26.9 mg	0.10 mg	0.23 mg	2 h	~50%	-
	48 nmol	56 µmol	450 nmol	1.3 µmol			
	1.0 eq.	1166 eq.	9 eq.	27 eq.			
210b	3.0 mg	63.8 mg	0.15 mg	0.51 mg	1 h	46%	460:1
	133 nmol	133 µmol	675 nmol	2.9 µmol			
	1.0 eq	1000 eq.	5 eq.	22 eq.			
OEGMA							
194c	1.3 mg	16.8 mg	0.10 mg	0.23 mg	2 h	~80%	-
	48 nmol	56 µmol	450 nmol	1.3 µmol			
	1.0 eq.	1166 eq.	9 eq.	27 eq.			
210c	3.0 mg	39.9 mg	0.15 mg	0.51 mg	1 h	86%	860:1
	133 nmol	133 µmol	675 nmol	2.9 µmol			
	1.0 eq	1000 eq.	5 eq.	22 eq.			

5.4 Procedures: Further cytochrome *c* modifications

5.4.1: PEG-CytC

$$\text{CytC} \quad + \quad \text{PEG}_{2000}\text{-NHS} \xrightarrow{\text{PBS, pH 8.0}} \text{PEG-CytC}$$
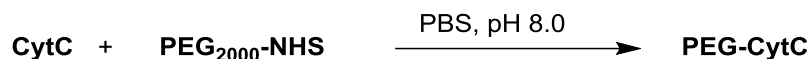
Cytochrome *c* (9.5 mg, 0.75 µmol, 1.0 eq.) was dissolved in degassed phosphate buffer solution (3 mL, 50 mM, pH 8.0). PEG_{2000}-NHS (3.5 mg, 1.75 µmol, 2.5 eq.) was dissolved in DMSO (50 µL) and added dropwise to the protein solution. After stirring overnight at room temperature, the reaction mixture was purified seven times with MQ water using a Vivaspin 6 concentrator (MWCO 5000 Da) and lyophilized afterwards to yield a red fluffy solid (10.5 mg, 88%). MALDI-ToF MS showed a main product peak at 16.5 kDa, which indicates a twofold protein conjugation with PEG_{2000}.

5.4.2: PEG-cCytC-Br (globular macroinitiator)

$$\text{PEG-cCytC} \quad + \quad \text{BiB-NHS} \xrightarrow{\text{NaHCO}_3, \text{ pH 8.5}} \text{PEG-cCytC-Br}$$
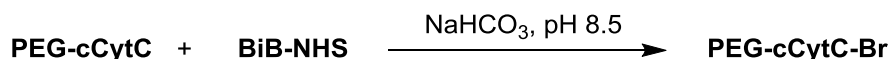
PEG-cCytC (38.3 mg, 1.51 µmol, 1.0 eq.) was dissolved in degassed $NaHCO_3$ solution (7 mL, 0.1 M, pH 8.5). 2-Bromoisobutanoic acid *N*-hydroxysuccinimide ester (23.0 mg, 87 µmol, 57 eq.) was dissolved in DMSO (400 µL) and added dropwise to the protein solution. After overnight reaction at room temperature, the product was purified with MQ water seven times using a Vivaspin 20 concentrator (MWCO 5000 Da). After lyophilization, a pale red-orange fluffy solid (40.1 mg, 87%) was obtained. MALDI-ToF MS showed a main product peak at 24 kDa.

Table 14: *Synthesis of PEG-dcCytC-fluo-Br starting from PEG-cCytC.*

	PEG-dcCytC-fluo			BiB-NHS			time	yield	mass
JG	mg	µmol	eq.	mg	µmol	eq.	-	mg	kDa
147b	8.0	0.32	1.0	5.0	18.8	60	o.n.	7.3	-
169	38.3	1.50	1.0	23.0	87.1	58	o.n.	37.0	24.0
188	40.8	1.60	1.0	24.5	92.8	58	o.n.	44.1	-

5.4.3: CytC-BiotinPEG

$$\text{CytC} \quad + \quad \text{Biotin-PEG-NHS} \xrightarrow{\text{EDTA-PBS, pH 6.8}} \text{CytC-BiotinPEG}$$

Cytochrome *c* (2.5 mg, 198 nmol, 1.0 eq.) was dissolved in degassed phosphate EDTA buffer solution (5 mL, 50 mM, pH 6.8, 2 mM EDTA). Biotin-PEG maleimide (11 mg, 2.0 µmol, 10 eq.), dissolved in the same buffer (250 µL), was dropwise added to the protein solution. The reaction mixture was allowed to stir for seven days. MALDI-ToF MS samples were taken periodically. MALDI-ToF MS measurement showed the main peak at 17.7 kDa indicating monofunctionalization.

5 EXPERIMENTAL PART

5.5 Procedures: Polymerizations

5.5.1: PNIPAM synthesis harnessing PEG-cCytC as an ARGET ATRPase
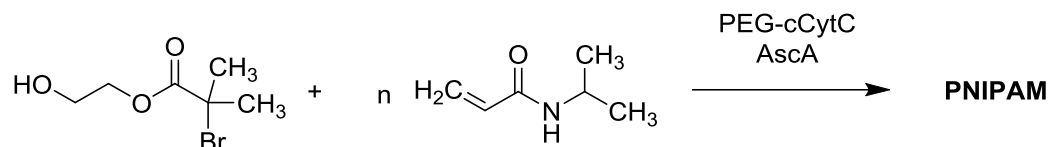
PEG-cCytC (17.2 mg, 414 nmol, 0.037 eq.), *N*-isopropylacrylamide (101.6 mg, 898 µmol, 80 eq.) and 2-hydroxyethyl 2-bromoisobutyrate (2.37 mg, 11.3 µmol, 1.0 eq.) were dissolved in D$_2$O (500 µL) in a Schlenk flask. The flask and the solution were degassed through freeze-pump-thaw cycles (3 x) and afterwards refilled with argon. Ascorbic acid (25.0 mg, 142 µmol) was dissolved in D$_2$O (500 µL). This solution was degassed by bubbling argon for 15 minutes. The polymerization was started by dropwise addition of ascorbic acid solution (100 µL, equals 2.5 eq.) to the reaction mixture by means of a syringe. Polymerization was monitored using ^{1}H NMR and GPC.

Table 15: Synthesis of PNIPAM using PEG-cCytC as a catalyst.

JG	HEBIB	NIPAM	PEG-cCytC	AscA	*T*
120	2.37 mg	101.6 mg	17.2 mg	5.0 mg	rt
	11.3 µmol	898 µmol	414 nmol	28.4 µmol	
	1.0 eq.	80 eq.	0.037 eq.	2.5 eq.	
122	1.21 mg	50.1 mg	13.0 mg	6.0 mg	rt
	5.7 µmol	443 µmol	313 nmol	34.0 µmol	
	1.0 eq.	78 eq.	0.055 eq.	6 eq.	
130	0.48 mg	30.0 mg	7 mg	0.73 mg	rt
	3.3 µmol	264 µmol	169 nmol	4.1 µmol	
	1.0 eq.	80 eq.	0.051 eq.	1.25 eq.	
159	0.52 mg	21.7 mg	6 mg	2.1 mg	28 °C
	2.4 µmol	192 µmol	235 nmol	12.0 µmol	
	1.0 eq.	80 eq.	0.098 eq.	5 eq.	

5.5.2: ARGET ATRP of DMAA, OEGA and OEGMA
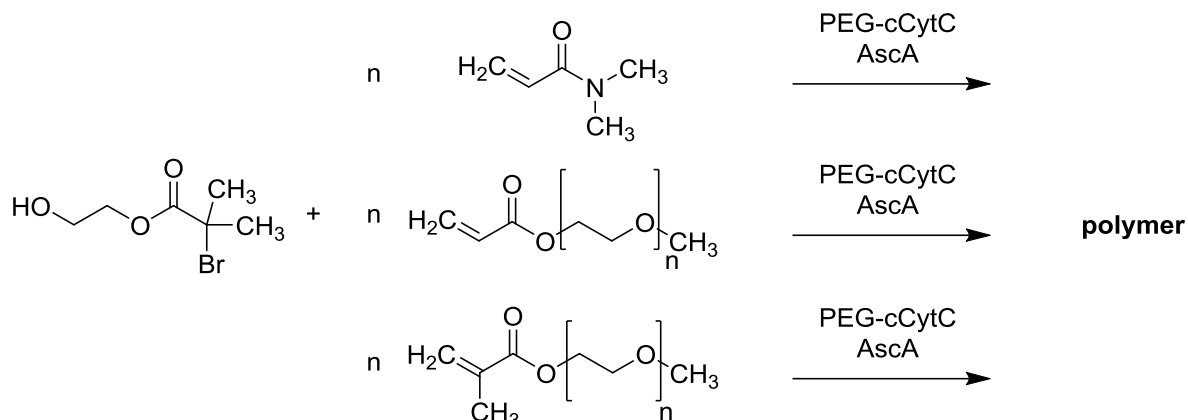
PEG-cCytC, monomer and 2-hydroxyethyl 2-bromoisobutyrate were dissolved in D_2O (200 µL) in a Schlenk flask (amounts: see **_Table 16_**). The flask and the solution were degassed through freeze-pump-thaw cycles (3 x) and afterwards refilled with argon. The solution was warmed to 28 °C in a water bath. Ascorbic acid was dissolved in D_2O (500 µL). This solution was degassed by bubbling argon for 15 minutes. The polymerization was started by dropwise addition of ascorbic acid solution (100 µL) to the reaction mixture by means of a syringe. Polymerization was monitored harnessing ^1H NMR and GPC.

Table 16: _Synthesis of PDMAA, POEGA and POEGMA using PEG-cCytC as a catalyst._

JG	HEBIB	Monomer	PEG-cCytC	DSS*	AscA	*T*
	DMAA					
	0.25 mg	19.2 mg	5.0 mg	-	1.0 mg	
120	1.18 µmol	194 µmol	120 nmol	-	5.7 µmol	28 °C
	1.0 eq.	164 eq.	0.1 eq.	-	5 eq.	
	OEGA					
	0.21 mg	37.6 mg	4.0 mg	4.0 mg	0.87 mg	
122	0.98 µmol	78 µmol	96 nmol	18.3 µmol	4.9 µmol	28 °C
	1.0 eq.	80 eq.	0.1 eq.	19 eq.	5 eq.	
	OEGMA**					
	0.21 mg	23.5 mg	4.0 mg	4.0 mg	0.87 mg	
130	0.98 µmol	78 µmol	96 nmol	18.3 µmol	4.9 µmol	28 °C
	1.0 eq.	80 eq.	0.1 eq.	19 eq.	5 eq.	
* used as NMR standard for (meth)acrylates.						
** observation: 50 % conversion only.						

5.6 Procedures: Assays

5.6.1: Fluorescamine assay

Analyzed protein derivatives were dissolved in MQ water with a concentration of 80 µM. In wells of a 384 well plate, 20 µL of the protein solutions were diluted with another 20 µL of MQ water (three wells/protein). Equal concentration in every well was achieved by further addition of protein solution aiming for equal absorption at $\lambda = 410$ nm (heme) in every well.

Fluorescamine (1.0 mg, 3.6 µmol) was dissolved in DMSO (3 mL). 5 µL of this solution were added to each well. After shaking for 25 minutes under dark conditions, fluorescence emission at $\lambda_{em} = 470$ nm was determined (excitation at $\lambda_{ex} = 365$ nm). These values (except the water control) were adjusted regarding their concentration determined above. Following values are received:

Table 17: *Fluorescence emission for each well. Results are displayed in* ***Figure 31***.

well	water	CytC	cCytC	PEG-cCytC	PEG-dcCytC-fluo	macroinitiator
1	2721	11406	60004	28898	27185	10019
2	2325	12083	59794	28988	32262	10618
3	2164	11043	59255	31955	29002	10415
Ø	2403	11511	59684	29947	29483	10350
σ	287	528	386	1739	2572	305

5.6.2: ABTS assay

A modified protocol by *Seidler et al.* was followed.

Analyzed proteins were dissolved in MQ water with a concentration of 1 mg/mL. In wells of a 96 well plate, 40 µL of the protein solutions were diluted with another 40 µL of MQ water. Equal concentration in every well was achieved by further addition of protein solution aiming for equal absorption at $\lambda = 410$ nm (heme) in every well. ABTS solution (100 µL, 0.5 mg/mL) was added. Subsequently, H_2O_2 solution (100 µL, 1 mM) was added and absorption at $\lambda = 410$ nm was determined over a course of 45 min.

For investigation of thermoresponsivity, above protocol was followed at room temperature. Subsequently, the spectrometer was warmed to 40 °C and the experiment was repeated with equal amounts of all components.

6 Additional experimental data

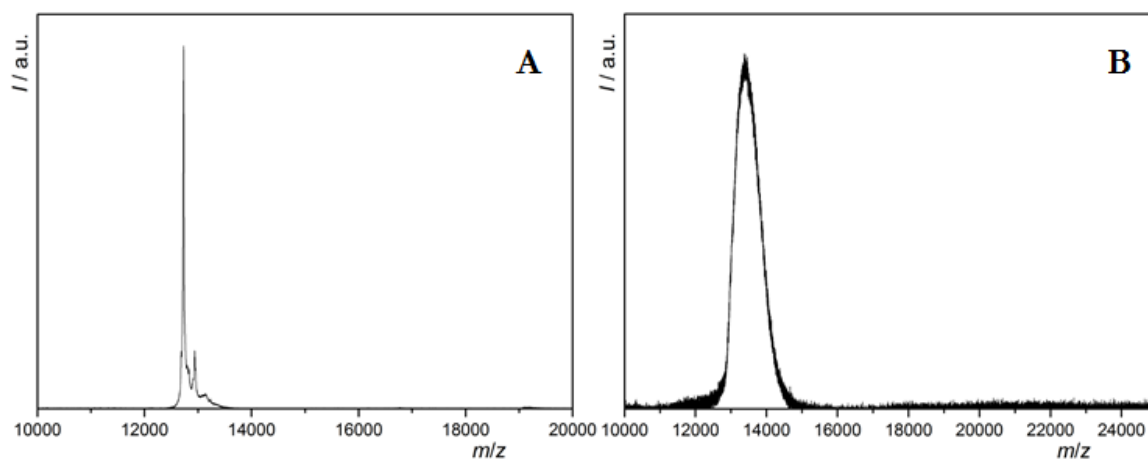## 6.1 Representative MALDI spectra of synthesized protein derivatives

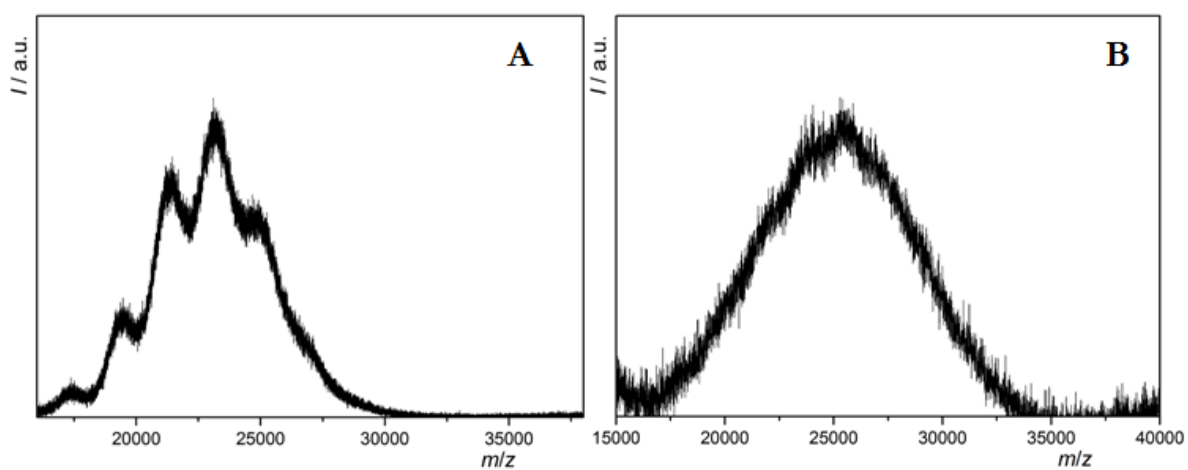***Figure 55:*** *MALDI-ToF spectra of native cytochrome c (**A**) and cCytC (**B**).*

Figure 56: *MALDI-ToF spectra of PEG-cCytC (**A**) and PEG-dcCytC-fluo (**B**).*
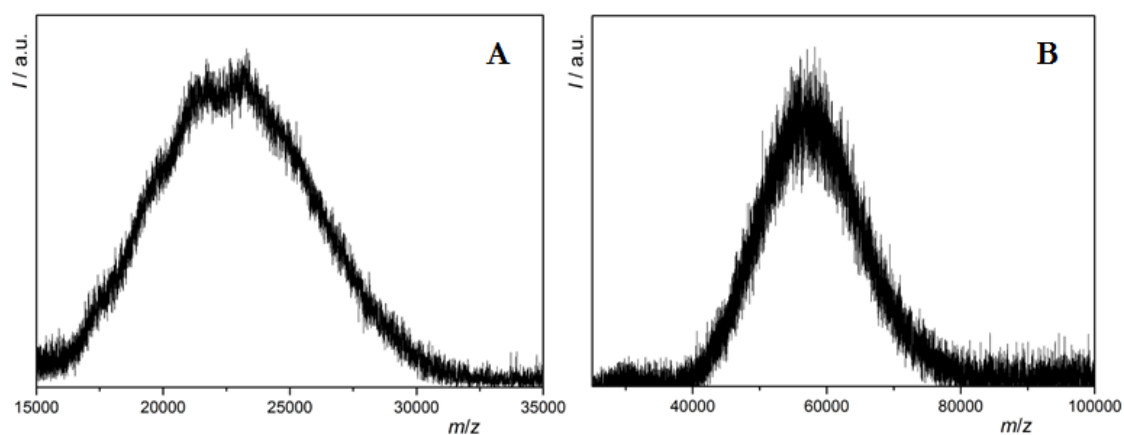
Figure 57: *MALDI-ToF spectra of PEG-dcCytC-fluo-Br (**A**) and*
*PEG-dcCytC-fluo-PNIPAM (55 kDa) (**B**).*
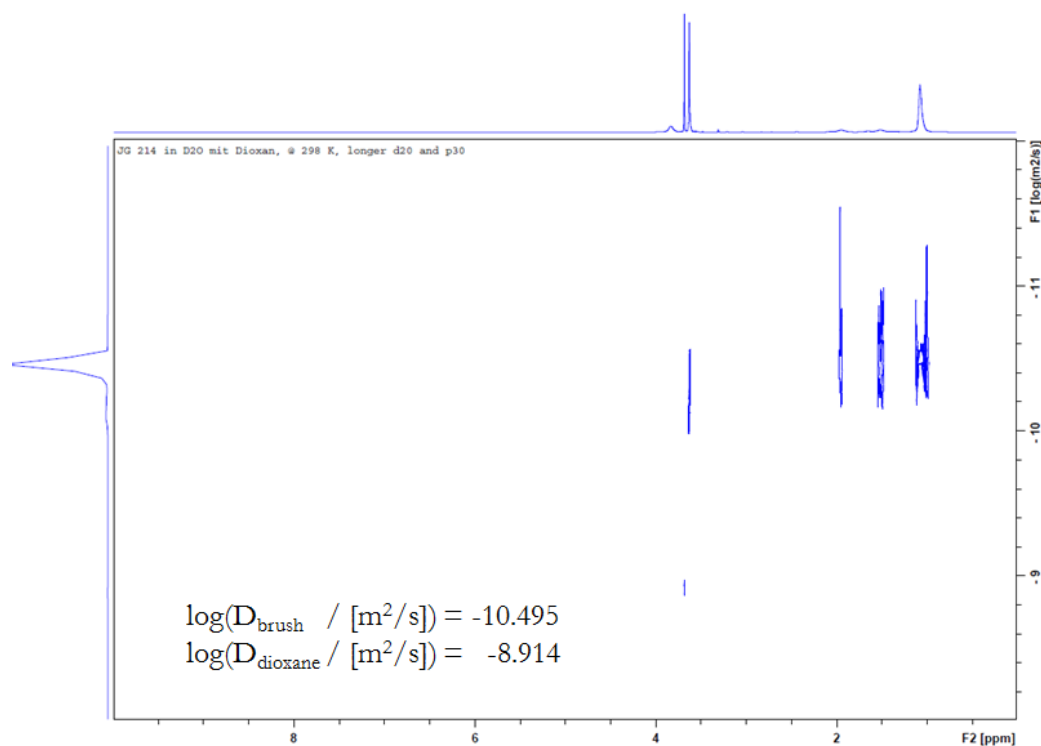
6.2 Brush size determination by DOSY NMR

$$\log(D_{brush} \ / \ [m^2/s]) = -10.495$$
$$\log(D_{dioxane} \ / \ [m^2/s]) = \ -8.914$$

Figure 58: *DOSY NMR of a PNIPAM-protein brush (55 kDa). Spectra*
were recorded at room temperature. R_0 was calculated to be 8.1 nm.

JG 214 in D2O mit Dioxan, @ 313 K, longer d20 and p30

$\log(D_{brush} \ / \ [m^2/s]) = -9.966$
$\log(D_{dioxane} / \ [m^2/s]) = -8.591$
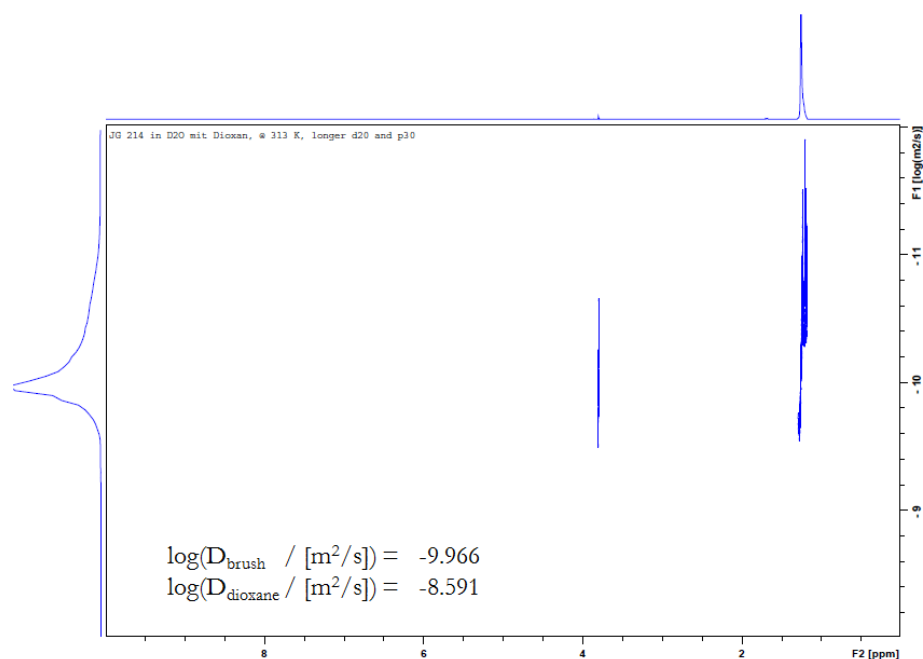
Figure 59: *DOSY NMR of a PNIPAM-protein brush (55 kDa).*
Spectra were recorded at 40 °C. R_0 was calculated to be 5.0 nm.

JG 214 in D2O mit Dioxan, @ 298 K, longer d20 and p30

$\log(D_{brush} \ / [m^2/s]) = -10.367$
$\log(D_{dioxane} / [m^2/s]) = -8.814$
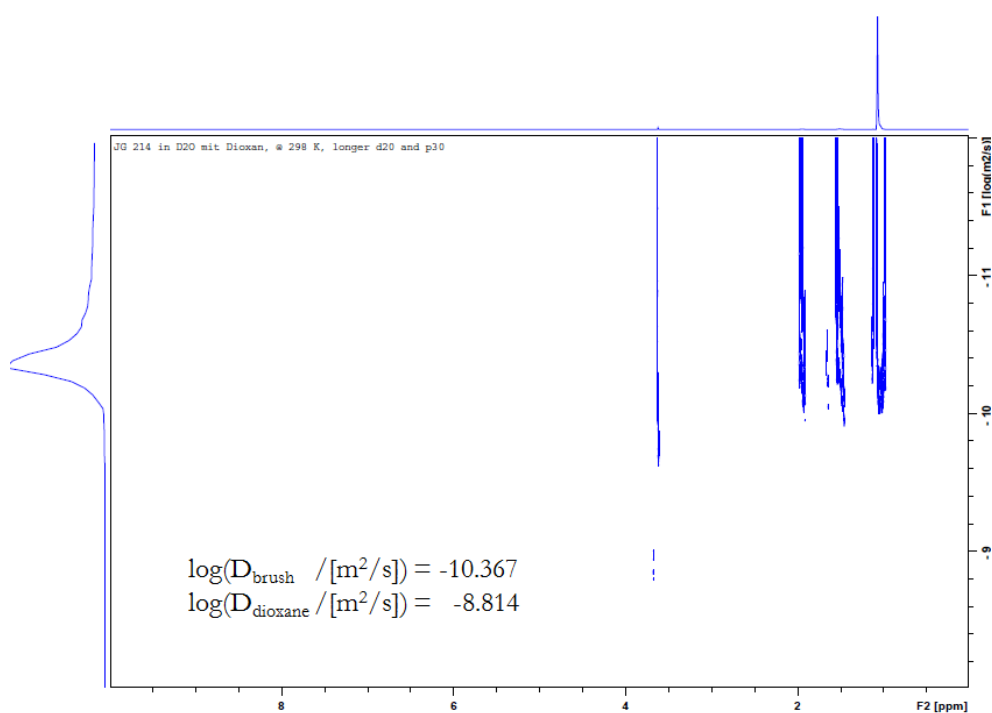
Figure 60: *DOSY NMR of a PNIPAM-protein brush (55 kDa). Spectra*
were recorded after heating to 40 °C and subsequent cooling
down to room temperature. R_0 was calculated to be 7.6 nm.

6.3 Circular dichroism spectra
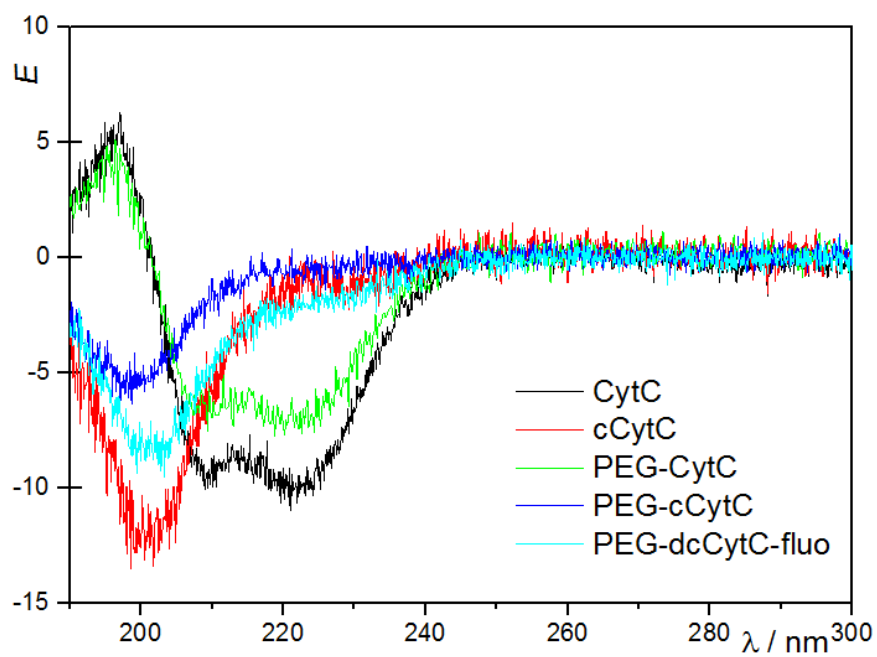
Figure 61: *CD spectra of different synthesized cytochrome c derivatives.*

7 Literature

[1.]   Stryer, L. et al., *Biochemistry*. Springer Spektrum: 2013; Vol. 7.

[2.]   Voet, D. et al., *Biochemistry*. Wiley Int-Ed: 2004; Vol. 3.

[3.]   Nelson, D. L. et al., *Lehninger principles of biochemistry*. Macmillan: 2008.

[4.]   Thomson, A. J. et al., *Curr. Opin. Chem. Biol.* **1998,** *2* (2), 155-8.

[5.]   Herres-Pawlis, S. et al., *Bioanorganische Chemie*. John Wiley & Sons: 2017.

[6.]   Stevens, J. M. et al., *The FEBS Journal* **2011,** *278* (22), 4170-4178.

[7.]   Bustin, S., *Molecular Biology of the Cell, Sixth Edition*. MDPI: 2015; Vol. 6.

[8.]   Lin, Y.-W. et al., *J. Inorg. Biochem.* **2013,** *129*, 162-171.

[9.]   Lu, Y. et al., *Chem. Rev.* **2001,** *101* (10), 3047-3080.

[10.]   Sligar, S. G. et al., *J. Am. Chem. Soc.* **1987,** *109* (25), 7896-7897.

[11.]   Bren, K. L. et al., *J. Am. Chem. Soc.* **1993,** *115* (22), 10382-10383.

[12.]   Plastics–the Facts: Analysis of European plastics production. In *Plastic Europe*, 2017.

[13.]   Nesvadba, P., *Encyclopedia of Radicals in Chemistry* **2012**.

[14.]   Matyjaszewski, K. et al., *Mater. Today* **2005,** *8* (3), 26-33.

[15.]   Matyjaszewski, K. et al., *Chem. Rev.* **2001,** *101* (9), 2921-2990.

[16.]   Kato, M. et al., *Macromolecules* **1995,** *28* (5), 1721-1723.

[17.]   Wang, J.-S. et al., *J. Am. Chem. Soc.* **1995,** *117* (20), 5614-5615.

[18.]   Jakubowski, W. et al., *Macromolecules* **2005,** *38* (10), 4139-4146.

[19.]   Min, K. et al., *J. Am. Chem. Soc.* **2005,** *127* (11), 3825-3830.

[20.]   Xue, Z. et al., *Polymer Chemistry* **2015,** *6* (10), 1660-1687.

[21.]   Papanikolaou, G. et al., *Toxicol. Appl. Pharmacol.* **2005,** *202* (2), 199-211.

[22.]   Bauer, I. et al., *Chem. Rev.* **2015,** *115* (9), 3170-3387.

[23.]   He, W. et al., *Macromol. Rapid Commun.* **2012,** *33* (12), 1067-1073.

[24.]   Sigg, S. J. et al., *Macromol. Rapid Commun.* **2011,** *32* (21), 1710-1715.

[25.]   Ng, Y.-H. et al., *Polymer Chemistry* **2011,** *2* (3), 589-594.

[26.]   Silva, T. B. et al., *Biomacromolecules* **2013,** *14* (8), 2703-2712.

[27.]   Simakova, A. et al., *Angew. Chem.* **2013,** *125* (46), 12370-12373.

[28.]   Giri, J. et al., *ACS Nano* **2011,** *5* (5), 3456-3468.

[29.]   Rothemund, P. W., *Nature* **2006,** *440* (7082), 297.

[30.]   Petrov, A. et al., *WIREs Nanomed Nanobiotechnol* **2012,** *4* (5), 575-585.

[31.]   Lee, L. A. et al., *Nano Research* **2009,** *2* (5), 349-364.

[32.]   Pesce, D. et al., *Biomaterials* **2013,** *34* (17), 4360-4367.

[33.]   Miyazaki, K. et al., *Journal of Molecular Evolution* **1999,** *49* (6), 716-720.

[34.]   Wu, Y. et al., *Biomacromolecules* **2012,** *13* (6), 1890-1898.

[35.]   Eisele, K. et al., *Biomaterials* **2010,** *31* (33), 8789-8801.

[36.]   Wu, Y. et al., *J. Am. Chem. Soc.* **2010,** *132* (14), 5012-5014.

[37.]   Ng, D. Y. W. et al., *Angew. Chem.* **2014,** *53* (1), 324-328.

[38.]   Gauthier, M. A. et al., *Polymer Chemistry* **2010,** *1* (9), 1352-1373.

[39.]   Ding, Z. et al., *Journal of Biomedical Materials Research* **1998,** *39* (3), 498-505.

[40.]   Ding, Z. et al., *Nature* **2001,** *411*, 59.

[41.]   Shimoboji, T. et al., *PNAS* **2002,** *99* (26), 16592-16596.

[42.]   Kulkarni, S. et al., *Biomacromolecules* **2006,** *7* (10), 2736-2741.

[43.]   Wu, Y. et al., *Biomacromolecules* **2015,** *3* (2), 214-230.

[44.]   Alconcel, S. N. et al., *Polymer Chemistry* **2011,** *2* (7), 1442-1448.

[45.]   Thordarson, P. et al., *Applied Microbiology* **2006,** *73* (2), 243.

[46.]   Ghosh, S. S. et al., *Bioconjugate Chem.* **1990,** *1* (1), 71-76.

[47.]   Lo, T. P. et al., *Biochemistry* **1995,** *34* (1), 163-171.

[48.]   Thöny-Meyer, L., *Biochimica et Biophysica Acta (BBA) - Bioenergetics* **2000,** *1459* (2), 316-324.

[49.]   Berova, N. et al., *Circular dichroism: principles and applications*. John Wiley & Sons: 2000.

[50.]   Chou, P. Y. et al., *Biochemistry* **1974,** *13* (2), 222-245.

[51.]   Akdogan, Y. et al., *Soft Matter* **2012,** *8* (43), 11106-11114.

[52.]   Yu, D. et al., *J. Pharm. Sci.* **2010,** *99* (8), 3326-3333.

[53.]   Colón, W. et al., *Biochemistry* **1997,** *36* (41), 12535-12541.

[54.]   ThermoFisherScientific User Guide: Fluorescein-5-Maleimide 62245. (accessed 25.02.2019).

[55.]   Tang, W. et al., *Macromolecules* **2007,** *40* (6), 1858-1863.

[56.]   Udenfriend, S. et al., *Science* **1972,** *178* (4063), 871-872.

[57.]   Bradford, M., *Anal. Biochem.* **1976,** *72* (1-2), 248-254.

[58.]   Lowry, O. H. et al., *J. Biol. Chem.* **1951,** *193*, 265-275.

[59.]   Tang, W. et al., *J. Am. Chem. Soc.* **2008,** *130* (32), 10702-10713.

[60.]   Matyjaszewski, K., *Macromolecules* **2012,** *45* (10), 4015-4039.

[61.]   Gillies, M. B. et al., *Macromolecules* **2003,** *36* (22), 8551-8559.

[62.]   Wilkins, D. K. et al., *Biochemistry* **1999,** *38* (50), 16424-16431.

[63.]   Miller, N. J. et al., *Clinical Science* **1993,** *84* (4), 407-412.

[64.]   Seidler, C. et al., *Tetrahedron* **2017,** *73* (33), 4979-4987.

[65.]   Balamurugan, S. et al., *Langmuir* **2003,** *19* (7), 2545-2549.

[66.]   Zhu, P. W. et al., *J. Phys. Chem. B* **1997,** *101* (16), 3155-3160.

[67.]   Kizhakkedathu, J. N. et al., *Macromolecules* **2004,** *37* (3), 734-743.

[68.]   Averick, S. et al., *ACS Macro Letters* **2011,** *1* (1), 6-10.

[69.]   Averick, S. et al., *Angew. Chem. Int. Ed.* **2014,** *126* (10), 2777-2782.

[70.]   Von Werne, T. A. et al., *J. Am. Chem. Soc.* **2003,** *125* (13), 3831-3838.